MEASUREMENT AND PREDICTION OF AEROSOL FORMATION FOR THE SAFE UTILIZATION OF INDUSTRIAL FLUIDS

A Dissertation

by

KIRAN KRISHNA

Submitted to the Office of Graduate Studies of
Texas A&M University
in partial fulfillment of the requirements for the degree of

DOCTOR OF PHILOSOPHY

December 2003

Major Subject: Chemical Engineering

MEASUREMENT AND PREDICTION OF AEROSOL FORMATION FOR THE SAFE UTILIZATION OF INDUSTRIAL FLUIDS

A Dissertation

by

KIRAN KRISHNA

Submitted to Texas A&M University
in partial fulfillment of the requirements
for the degree of

DOCTOR OF PHILOSOPHY

Approved as to style and content by:

M. Sam Mannan (Chair of Committee)	Kenneth D. Kihm (Member)
Kenneth R. Hall (Member)	Harry H. West (Member)

Kenneth R. Hall
(Head of Department)

December 2003

Major Subject: Chemical Engineering

ABSTRACT

Measurement and Prediction of Aerosol Formation for the

Safe Utilization of Industrial Fluids. (December 2003)

Kiran Krishna, B.E., Bangalore University;

M.S., Texas A&M University

Chair of Advisory Committee: Dr. M. Sam Mannan

Mist or aerosol explosions present a serious hazard to process industries. Heat transfer fluids are widely used in the chemical process industry, are flammable above their flash points, and can cause aerosol explosions. Though the possibility of aerosol explosions has been widely documented, knowledge about their explosive potential is limited. Studying the formation of such aerosols by emulating leaks in process equipment will help define a source term for aerosol dispersions and aid in characterizing their explosion hazards.

Analysis of the problem of aerosol explosions reveals three major steps: source term calculations, dispersion modeling, and explosion analysis. The explosion analysis, consisting of ignition and combustion, is largely affected by the droplet size distribution of the dispersed aerosol. The droplet size distribution of the dispersed aerosol is a function of the droplet size distribution of the aerosol formed from the leak. Existing methods of dealing with the problem of aerosol explosions are limited to enhancing the dispersion to prevent flammable concentrations and use of explosion suppression

mechanisms. Insufficient data and theory on the flammability limits of aerosols renders such method speculative at best. Preventing the formation of aerosol upon leaking will provide an inherently safer solution to the problem.

The research involves the non-intrusive measurement of heat transfer fluid aerosol sprays using a Malvern Diffraction Particle Analyzer. The aerosol is generated by plain orifice atomization to simulate the formation and dispersion of heat transfer fluid aerosols through leaks in process equipment. Predictive correlations relating aerosol droplet sizes to bulk liquid pressures, temperatures, thermal and fluid properties, leak sizes, and ambient conditions are presented. These correlations will be used to predict the conditions under which leaks will result in the formation of aerosols and will ultimately help in estimating the explosion hazards of heat transfer fluid aerosols. Heat transfer fluid selection can be based on liquids that are less likely to form aerosols. Design criteria also can incorporate the data to arrive at operating conditions that are less likely to produce aerosols. The goal is to provide information that will reduce the hazards of aerosol explosions thereby improving safety in process industries.

DEDICATION

To my parents, Christine and E.R. Krishna and my sister Radhika,

for all their love, encouragement and support.

ACKNOWLEDGEMENTS

Right now I feel like a thespian going up to receive an Oscar or a Tony. So many people to thank and so little time and space. When I look back at all the people who have contributed, in various degrees, to the success of my graduate school career, it is truly humbling.

I owe a deep debt of gratitude to my advisor, mentor and guide, Professor Sam Mannan, for his unflagging confidence in me throughout these last five years. From the first time that I met him, there has always been something reassuring about his booming voice and commanding presence. As an adviser he has helped me with difficult decisions, made critical and creative suggestions, and stuck his neck out for me, and many others, when we most needed it.

Professor Ken Kihm, my virtual committee co-chair, helped me develop and formalize many of my half baked ideas on the modeling of aerosols. He really forced me to think for myself, but always reigned me in when I got too far off track. His casual hints and musings, that later helped me figure out solutions to problems and concerns, now seem almost prophetic.

It has been an undiluted pleasure to work with Dr. Bill Rogers. None of this would have been possible without his patience and hard work in helping set up and maintain my experimental apparatus. He has been the magician who managed to transform my clumsiest of sentences into eloquent, meaningful discourse. Thank you

for helping me come up with a title, and yes, it is definitely far more apt then any of my attempts.

I would also like to thank Professors Ken Hall and Harry West for serving on my doctoral committee, patiently perusing my manuscript, and providing corrections and criticisms that have really enhanced this dissertation. I also appreciate all the discussions and advice on modeling aerosols, provided by Dr. John Woodward at Baker Risk & Engineering Consultants, San Antonio, Texas, where I interned during the fall of 2001, and Professor Tom Spicer of the University of Arkansas at Fayetteville.

Throughout my research I have been blessed to have brilliant lab mates: Passaporn Sukmarg (Ning) and Tae-Kyun Kim (TK). There is no doubt that their diligence and ability to put up with me has been a critical factor in my success. The long hours in the lab, the days when nothing seemed to work, and the intellectual battles, are all now happy memories because of their support, persistence and encouragement.

Nathan Okonski and Randy Marek deserve special mention for all their efforts in fabricating and repairing numerous widgets and gizmos in the laboratory. Thanks also to Dr Sang Young Son and Jae Sung Park or Dr. Kihm's Group for teaching me the nuances of good digital photography, and Dr. Sumit Chandra and Mustafa Chowdhury for their help with the orifice characterization.

I am extremely fortunate to have been part of the Mary Kay O'Connor Process Safety Center. At the Center, you are encouraged to think deeply, to go further, and to look at concepts in a new and critical way. When I reflect on how I have acquired the

skills I need to shape my own future, and make so many close friends, I feel very lucky and grateful to be part of the Center. The intellectual environment and people at the Center are phenomenal. You learn a ton from the students, the staff, and the professors. The greatest outcome from working at the Center is that on graduation you gain credibility with and access to an amazing network of people. All told, it has been an extremely inspirational experience.

The Department of Chemical Engineering has been my home away from home for these last five years. I am grateful to the Department for providing me with the opportunity to pursue my doctorate, and to the administrative staff, in particular, for easing all of my bureaucratic hassles. Apart from the Department and the Process Safety Center, my research was also funded by the State of Texas through the Texas Higher Education Coordinating Board.

Paramount among the many reasons for my amazing time at Texas A&M University has been my equally amazing friends. To all of them thank you for bearing with my semi-edible cooking, capricious sense of humor, and bullheadedness.

Finally, I would like to thank my large family for always being there for me. This journey would never have started without their inspiration, encouragement, and support. To my cousins Ramji and Anu, this endeavour started when, as a kid, I saw you guys get your doctorates; thanks for the inspiration and for being such great role models for me to emulate.

TABLE OF CONTENTS

Page

CHAPTER

Page

LIST OF TABLES

LIST OF FIGURES

FIGURE Page

FIGURE Page

LIST OF SYMBOLS

Π	Dimensionless group
σ	Surface tension, kg/s^2
ν	Kinematic viscosity, m^2/s
δ	Spray uniformity parameter for the Rosin-Rammler distribution
ρ_G	Density of gas, kg/m^3
μ_G	Gas (air) viscosity, kg/m s
ρ_L	Density of the liquid, kg/m^3
μ_L	Dynamic viscosity of liquid, kg/m s
A	Absorbed light energy
C_D	Discharge coefficient
d	Jet or stream diameter
D	Aerosol mean droplet diameter
d_0	Orifice diameter
D_b	Diameter of the laser beam
E_s	Potential surface energy
F, f	The focal length of the lens L_2
g	Acceleration due to gravity, m/s^2
I	Light intensity
I_0	Light intensity at the center of the pattern
J_1	The first-order spherical Bessel function
J_o	The zero-order spherical Bessel function

l	Length of a stream segment, m
L	Light intensity
L_B	Break up length
Lf	Aerosol formation distence
M	Number of class sizes
m_d	Mass of a drop, kg
N	Number of droplets of diameter r
P	Pressure, N/m^2
P_a	Pressure of air, N/m^2
P_i	Pressure inside a drop, N/m^2
Q	Volumetric flow rate, m^3/s
q	Potential growth rate of the disturbance
r	Spherical droplet radius
s	Radial distance in the detection plane measured from the optical axis
S	Scattered light energy
T	Transmitted light energy
V	Velocity of the liquid stream, m/s
W	Mass of a droplet with radius r
X	Size parameter for the Rosin-Rammler distribution

LIST OF ABBREVIATIONS

AAR	Alkylated aromatic
BDO	Biphenyl/diphenyl oxide
DAA	Di-aryl alkyl
DTA	Di/tri-aryls
HHC	Heavy hydrocarbons
HTF	Heat transfer fluid
Lp	Laplace number
MTP	Modified terphenyls
Re	Reynolds number
SMD	Sauter mean diameter
We	Weber number
WMO	White mineral oil

CHAPTER I

INTRODUCTION

The chemical industry utilizes different process fluids that vary widely in their properties. These fluids do not necessarily take part in chemical reactions to form a desired product, but their specific properties are utilized for "services" as fuels, lubricants, heat transfer fluids (HTFs), or other such functions. While hazards posed by such fluids are generally well documented and either regulated by laws or by recommended best practices, there are certain misconceptions about industrial fluid handling that generally leads to hazardous situations. For example, most organic fluids are considered to be combustion hazards, which are associated with the presence of the said fluid in the vapor phase. This misleads people into assuming that under conditions, which do not produce sufficient vapor for combustion, the fluids are benign. Hence we have industrial workers who assume the fluid is "safe" as long as it is utilized under its flash point. Accidents in the chemical industry almost always result in the loss of containment. Escaping fluids are released into the surroundings in the form of a liquid or vapor or both. Liquid releases, depending on the conditions, may atomize to form an aerosol, which is a dispersion of liquid droplets in air. These droplets have the potential to be dispersed over a larger area than the bulk liquid. A potential problem arises when

---

This dissertation follows the style and format of the *Journal of Loss Prevention in the Process Industries*.

a combustible liquid is atomized. It is a common misconception that flammable liquids are safe below their flash points. Aerosols of flammable liquids at temperatures well below their flash points can be as explosive as vapor-air mixtures.

The thesis of this dissertation is that it is possible to reduce the hazard of aerosol explosions, by studying the formation of such aerosols, and applying the lessons learned to reduction of aerosol formation.

This dissertation discusses the ramifications of the concept of aerosol explosions on the safe handling of industrial fluids. Details of the process by which aerosols of industrial fluids are formed upon leaking are also discussed. The information presented in this document will hopefully help educate the industry about the hazards of industrial fluids with respect to aerosol explosions and provide guidelines for the safe handling of such fluids.

STATEMENT OF THE PROBLEM

Aerosol or mist explosions are of critical concern in the chemical process industries. Heavy hydrocarbons are particularly susceptible to such hazards, and are widely utilized in the industry under the misconception that they are benign. There is therefore a need to study the mechanical formation of aerosols of heavy hydrocarbons, below their flash points, leaking to the atmosphere. Such a study must provide an understanding of the mechanism of aerosol formation and identify factors that are important to the formation process. Knowledge gained from this study can then be used

to help guide the development of tools and techniques to curtail the formation of aerosols upon leakage, thereby reducing the hazard of aerosol explosions.

OBJECTIVES

Although descriptively the process of mechanical break-up of the liquid stream into aerosol is known, there is scarce knowledge about the formation of aerosols from leaking high flash point hydrocarbons such as heat transfer fluids (HTFs). There is a need to develop functional relationships between the operating conditions of the process, i.e., the injection conditions, and the properties of the resulting atomized liquid. The important parameters for the resulting aerosol leak are its formation distance and drop size distribution.

The objectives of this research are:

- Designing an effective system to study the formation of aerosols from leaking heat transfer fluids
- Study the variation of aerosol formation behavior under different fluid temperatures, operating pressures, fluid properties, and leak sizes
- Development of empirical correlations to relate the operating conditions and liquid properties and to characterize the atomization process of HTFs
- Validation of developed correlations

This research will establish the relationships between aerosol droplet sizes, process conditions, and fluid properties. An understanding of aerosol formation behavior will help institute design level changes to equipment and processes, which will help in managing the hazard. The ultimate goal is to reduce or eliminate such hazards thereby improving chemical process safety.

JUSTIFICATION

This research will demonstrate that there is a dependence of aerosol drop size distributions on the operating conditions and the leak size. The most important conclusion for process safety is that significant quantities of aerosol are formed from HTFs at conditions well below their flash points. However, there are threshold conditions below which significant amounts of aerosols were not formed in the tested ranges.

A study of the validity of the correlations will provide a good corroboration for observations made with respect to the experimental data. Development of the correlations will help define a source term for leaking fluids forming aerosols. Incorporating aerosol formation behavior knowledge into the design process for the selection of HTFs, and operating at conditions not conducive to aerosol formation will reduce the risk of aerosol explosions. Knowledge of aerosol formation distances will help the designer arrive at locations for obstacles and guard surfaces around potential leak zones, to prevent the formation and dispersion of aerosols. Again it is important to

state that the ultimate goal is to reduce or eliminate aerosol explosion hazards thereby improving chemical process safety.

ORGANIZATION OF THE DISSERTATION

This dissertation represents works done at the Aerosol Laboratory of the Mary Kay O'Connor Process Safety Center at Texas A&M University. Parts of this dissertation have been presented at national conferences and have been published in peer-reviewed publications. Following the introduction, problem statement, objectives, and justification sections of the first chapter are five additional chapters. In Chapter II, a literature review has been presented which presents the current state of knowledge with respect to the objectives mentioned as well as additional information that will help defend the premise of this dissertation. Some of the background information presented in Chapter II has been restated elsewhere in the dissertation as deemed appropriate by the author. Chapter III discusses the experimental aspects of the research. It elaborates on the experimental set-up, fluid characterization, data-collection methodology, and preliminary data assessment. Chapter IV describes the central concept underlying this work. It describes how the objectives have been fulfilled, including the data analysis, model development, and the development of the correlations. Chapter V describes the utility of the data and the correlations, and variations, extensions, or other applications of the central idea. A discussion and summary of results are provided in Chapter VI. It

is a compilation of conclusions that were drawn from the work presented in Chapters III through V.

CHAPTER II

BACKGROUND

The hazards of gas explosions are well documented and safety systems have been developed to mitigate these hazards. Personnel are well trained in recognizing hazardous scenarios and adopting safety systems. The problem lies in the fact that the training imparted generally recognizes that gas explosion hazards require the fuel in the vapor form and thus deal with hazardous conditions above the liquid's flash point. Most literature do not address hazards below the flash point.

Are hazardous scenarios possible below the liquid's flash point? The simple answer to this question is YES. An aerosol is a suspension of solid or liquid particles in a gas. Aerosols of heavy hydrocarbons consist of liquid droplets suspended in air. Heavy hydrocarbons are widely used in the process industry as in heat exchangers, pumps, gears, etc. Process equipment inevitably fails sometime during its lifetime, and leaks are one such consequence of failure in process equipment. Depending on the conditions, the bulk heavy hydrocarbon may be emitted from the leak in the form of a stream, aerosol, vapor or any combination of these.

The lack of thorough understanding of the mechanisms behind aerosol explosions and a paucity of experimental data has resulted in the problem being largely unrecognized. The recognition of the explosion hazards posed by combustible aerosols

is not something novel. As early as 1947, Sullivan et al. experimented on the flammability of higher boiling liquid mists and though their experiments did generate some data, the results were very specific to the test methodology and prevailing conditions and no effort was made to understand the underlying mechanics behind the results. Burgoyne and co-workers also studied the flammability of oil mists and attempted to evaluate mist flammability limits (Burgoyne and Richardson, 1949, Burgoyne and Cohen, 1954, Burgoyne, 1957). In 1955, Eichhorn, published his caution to chemical plant and industry personnel that mists (aerosols) can explode. He introduced the concept of aerosol flammability limits, similar to the vapor flammability limits that are well documented and recognized by the industry.

Eichhorn's conceptualization of the phenomenon of aerosol explosions is shown in Figure II-1. Here he draws a parallel between the concept of vapor flammability and aerosol (mist) flammability. The dew point is the temperature at which the saturated vapor begins to condense. At temperatures above the dew point the fluid exists primarily in the vapor state and hence is susceptible to gas explosions. In the vapor phase, the upper and lower flammability limits define the concentration limits of interest. The lowest temperature at which a fluid generates sufficient vapor to support a momentary flame is known as the flash point of the fluid. For the vapor region, the flash point, represents the limiting condition for a fire hazard. However, Eichhorn postulates that there exists the aerosol flammability region, and indicates the unknown limits by wavy lines, as seen in Figure II-1. While, the definition of the hazardous conditions may be more complicated than has been depicted by Eichhorn, his recognition of the

existence of an aerosol flammability region is important. Later in this chapter, some of the other factors that contribute to an aerosol explosion or flammability hazard will be revealed.

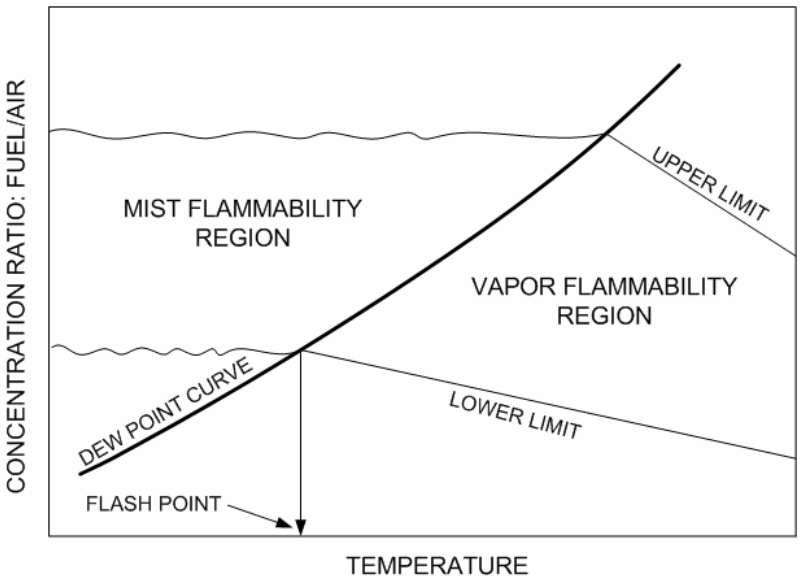

Figure II-1. Flammability diagram at a fixed pressure

While striking down the notion of the flash point as the wall between hazardous and safe conditions, Eichhorn fails to provide any anecdotal links with actual incidents. Over the years, aerosol explosions have been identified as a possible contributing cause in incident investigations but there was still a distinct lack of any definitive studies into the explosion hazards posed by aerosols. In 1995, however, Febo and Valiulis of

Factory Mutual Research Corporation, presented statistics from a then recent 10-year period. The statistics showed 54 fires and explosions involving heat transfer fluids (HTFs), which resulted in $150 million in losses. The article also highlights the scenario under which one aerosol explosion occurred. The incident involved a heater system for 2195 kW operation, containing 200 gallons of the HTF with a flash point of 232 °C. The system was located in a 60 by 100 ft. building of concrete block walls with an insulated steel deck roof. During normal operation, an expansion joint, rated at 150 psig separated and released the HTF which was stored at a pressure of 65psig. The aerosol released exploded soon after, probably ignited by the heater flame. Two of the walls were blown out and a third was bowed, but the sprinkler system was not damaged and its operation may have minimized the resulting HTF fire damage.

Febo and Valiulis (1995), also recognize the fact that the seemingly benign properties of the HTFs mislead many users and manufacturers into assuming that these fluids are not susceptible to explosions. An example provided is the rule of thumb that liquids with flash points above 300 °C, are considered incapable of indoor vapor explosions. Recognizing the phenomenon of aerosol explosions implies that use of the flash point alone to assess explosion hazards is inadequate.

While considering preventative mechanisms, Febo and Valiulis (1995), limit themselves to facility siting suggestions, in order to limit the damage from an explosion hazard. They also recommend that HTF manufacturers recognize fire and explosion hazards posed by HTF aerosols even below their flash points. They also point the way,

in terms of future work, by suggesting that fundamental studies be conducted on all aspects of the problem to provide better solutions to the problem of aerosol explosions. While liquid release below its flash point is critical in this dissertation, there is work on liquid releases of supercritical liquids (Johnson, 1991, Schmidli et al., 1990).

Bowen and Shirvill (1994) raised concerns about area classification in the Institute of Petroleum Model Code of Safe Practice (1990), which does not consider the hazardous nature of high flash point fluids with respect to the formation of a flammable aerosol hazard. They point out that insufficient information and industry ignorance are critical issues that have to be dealt with. They recommend additional understanding of aerosol explosion hazards, together with quantifiable analyses, realistic formation behavior including transient operating pressures, complex orifice configurations, influence of obstacles, among others. Additionally, information about cloud development from a spray source needs to be understood. Bowen and Shirvill also point out that aerosol mists of high flash point fluids have to be considered as flammable hazards.

Aerosol explosions have also been a problem for forensic investigators. Sehgal et al. (1999) have discussed a case where an aerosol explosion could have been the cause for an accident but a lack of data prevents any definite conclusions.

Existing elementary screening employed in heat-transfer fluid selection are flash point, fire point, and autoignition temperature. The *flash point* of a fluid is the temperature of the fluid at which it generates sufficient vapor to support momentary

combustion or a “flash”. It can be measured by the Cleveland Open Cup (COC) test (ASTM D92) or the Penske Martens Closed Cup (PMCC) test (ASTM D93). The PMCC test concentrates the vapor and hence results in a value that is 8-10 °F lower than the COC test.

Fire point is the temperature at which a fluid generates sufficient vapor to support sustained combustion and is typically 40 – 100 °F higher than the flash point. Flash and fire point tests are indicators of the volatility of a fluid, i.e., they indicate the ease with which a given liquid can vaporize, thereby generating sufficient vapor to ignite. A fluid with a lower flash/fire point, therefore, will ignite more easily.

The *autoignition temperature* is the temperature at which a fluid will ignite without any external source of ignition. It is measured by injecting the fluid into an atmosphere of heated air. The temperature of the heated air that ignites the fluid is the autoignition temperature of the fluid (ASTM D2155).

While these tests form an essential part of the selection process, merely ensuring that the fluid is below its flash point assumes that the fluids do not pose a fire hazard below their flash points. As discussed earlier, this is clearly not true. Heat transfer fluids are capable of forming aerosols/mists on leaking, and these mists are capable of being ignited and exploding at temperatures below their liquid flash points. Most hazardous situations involving heat transfer fluids occur as a result of leaks in process equipment due to mechanical failure. For major leaks caused by joint failure resulting in a substantial leakage of the heat transfer fluid, ignition sources close to the leak would be

required as the fluid would not disperse very far from the leak. Insulation fires would occur if the leaking fluid saturates the insulating material and attains its autoignition temperature. Fire and explosion risk in such situations can be considerably reduced if the fluid is maintained at a temperature well below its flash point (Fuhr, 1992, Oetinger, 2002, Albrecht and Seifert, 1971, Febo and Valiulis, 1995, 1996).

However, small leaks with sufficient operating pressure have the ability upon leaking to form aerosols, which can disperse and increase the risk of a mist explosion (Sukmarg et al, 2002).

During the design process, the factors that affect the choice of a given heat transfer fluid are the rate of heat transfer, temperature range, working pressure required, economic considerations like cost, maintenance, cleaning and replacement, limitations imposed on materials of construction and finally hazards (fire, explosion, & toxicity) (Singh, 1981, Cuthbert, 1994, Fuchs, 1997). Process engineers involved in the design process may screen for flash, fire, and auto-ignition temperatures while evaluating fire and explosion hazards but usually do not fully appreciate potential mist explosion hazards.

However, it is necessary to understand that the paucity of concrete data on the mist explosions prevents any formal design procedure from incorporating potential mist explosion hazards into the selection of heat transfer fluids. Also, mist flammability is inadequately covered in common process safety text-books such as Crowl and Louvar, 1990. In the absence of data on the flammability and explosion limits of mists, using

data for the formation of such mists is critical. Reducing the susceptibility of leaking fluids to atomization will greatly reduce the potential of mist explosion hazards. While flash points are used to identify vapor flammability hazards, a property that characterizes the mist or aerosol phase is required. The Sauter Mean Diameter (SMD) can provide an effective index to characterize the aerosol or mist, as elaborated in the following chapters.

Figure II-2. Fire triangle for aerosol explosions

In terms of fire safety, the basic approach is to consider the fire triangle. The three edges of the triangle represented by fuel, oxidizer, and ignition source are the mist, air, and any ignition source, respectively (Figure II-2). To work with each of these we must consider issues such as atomization of the mist, ignition and electrostatics, combustion of the mist, and possible fire prevention mechanisms. All aspects of the aerosol explosion phenomena have to be researched to aid in a more complete safety assessment.

OVERVIEW OF AEROSOL DOMAINS

Explosion and Combustion

The possibility of aerosols, or heterogeneous mixture explosion, leads to the understanding that all combustible fluids forming aerosols can be flammable. This is in direct contrast to the prevalent notion that only highly volatile fluids with low boiling points are explosively hazardous. Moreover, existing theory suggests that aerosol explosions may be more devastating, because of enhanced burning velocities in the heterogeneous mixture and higher enthalpy concentrations in the liquid aerosol phase, in comparison to homogenous vapor-air mixture (Polymeropoulos, 1984).

Heavy hydrocarbons, such as heat transfer fluids (HTFs), pump oils, etc., are omnipresent in the process and manufacturing industries and are capable of forming aerosols when leaked under high pressure. They are generally of low volatility and

allow the formation of heterogeneous two-phase mixtures that are prime candidates for aerosol explosions.

While it is postulated that heterogeneous aerosol mixture explosions can be more devastating than homogeneous vapor explosions, there is very limited concrete experimental evidence to support this hypothesis (Eichhorn, 1955, Vincent and Howard, 1976, Febo and Valiulis, 1995, Bowen et al., 1997). At issue is the fact that flame propagation speeds in aerosols are higher than those in vapor-air mixtures for an exclusive droplet size range. Existing theory specifies a kinetically controlled premixed combustion mode for fine droplets below 8 microns, where the aerosol behaves like a vapor, and a mass transfer controlled diffusion mode for larger drops above 15 microns, where the aerosol first vaporizes and then burns. Polymeropoulos predicted that, in the 'transition range', the flame speeds would be enhanced considerably (Polymeropoulos, 1984) (Figure II-3).

Small droplets, upstream from the flame front, evaporate quickly because of heat radiated ahead of the flame front. This results in homogeneous vapor phase combustion. The amount of radiative heat transfer depends on the surface area to volume ratio of the droplets. Smaller droplets have higher surface area per unit volume as compared to larger droplets and are thereby exposed to higher heat transfer flux. On the other hand, evaporation of larger droplets ahead of the flame front is increasingly low, because of their small surface area to volume ratio, and the flame speed is significantly reduced because of a lack of vapor.

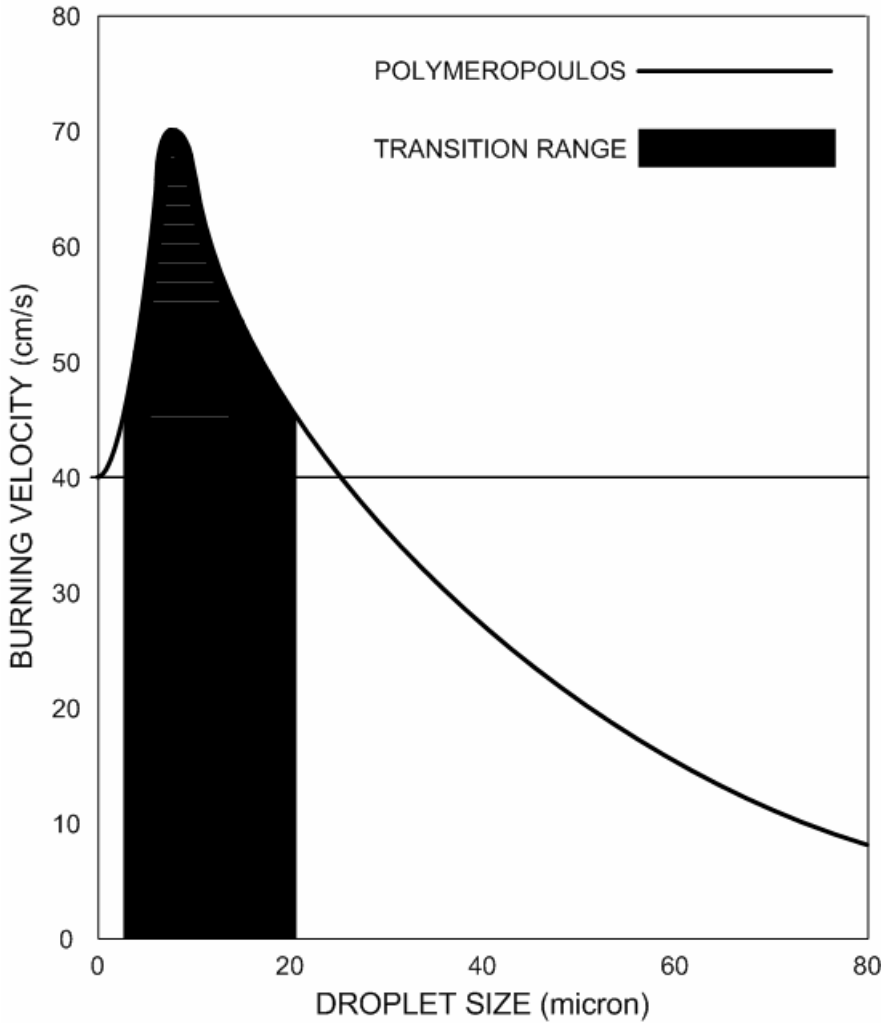

Figure II-3. Burning velocity predictions vs. aerosol droplet size

In the transition range between the smaller and larger droplets, we have droplets that are small enough to generate sufficient vapor by the radiation from the flame front, but are large enough to remain as droplet mist after the evaporation. It is also known that flames have a tendency to accelerate when constricted by obstacles (droplet mist in

this case). And hence it is postulated and analytically derived that the flame speed in this transition range could be enhanced. In addition to this flame acceleration by obstacles, the droplets may also vaporize extremely rapidly, if they are small enough, thereby appearing to ignite directly, and because of their higher enthalpy concentration in the liquid state, will provide additional thrust to the flame front. (Chan and Jou, 1988, 1989, Laster and Annamalai, 1989)

The flame propagation speed also depends upon the upstream fuel to air ratio and the vapor fuel to liquid fuel ratio (omega). For highly volatile fuels such as hydrocarbons, omega approaches unity and flame propagation occurs largely in the vapor phase. This results in a negligible enhancement of the flame propagation velocity in the transition range. As omega approaches zero for low volatility industrial fluids such as HTFs, the theory predicts that this enhancement becomes more pronounced (Figure II-4). Polymeropoulos concluded that, in order to clearly demonstrate this effect, a fuel with low volatility has to be studied (Burgoyne and Cohen, 1954, Polymeropoulos, 1984). HTFs generally have low volatilility with high boiling points (omega$\rightarrow$ 0) and would offer us a more observable flame speed enhancement.

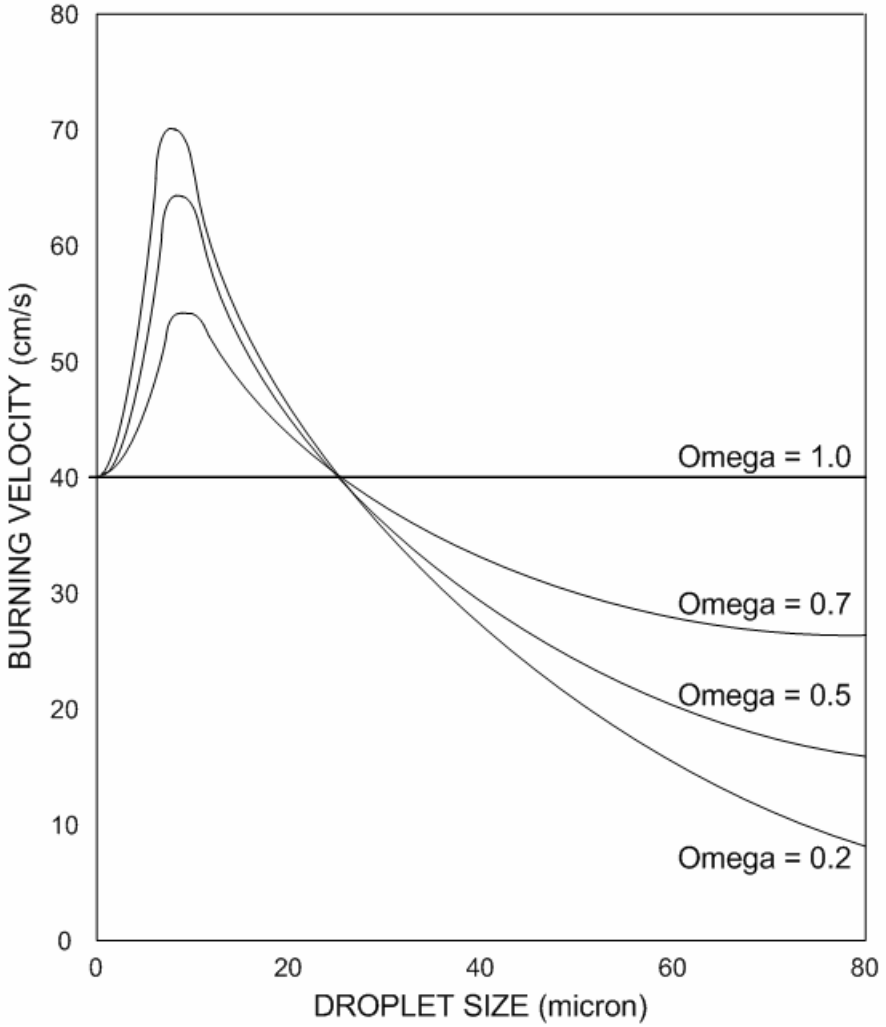

Figure II-4. Burning velocity predictions vs. aerosol droplet size at different values of Omega (Ω)
(adapted from Polymeropoulos, 1984)

The experimental study by Chen et al. (1996) on the mechanisms of flame propagation through aerosol clouds of pure 1-octadecanol showed that smaller particles of the order of 10 to 20 microns rapidly gasified ahead of the flames, while particles with diameters larger than 80 microns have an ignition delay and also continue to burn

after the propagating flame has passed through them. The flame propagation was mainly supported by the smaller particles gasifying across the flame front. The interesting conclusion here is the velocity of the flame front is seen to increase with the number density of the smaller particles. This observation confirms Polymeropoulos' theory discussed earlier. As the number density of particles increase, more obstacles increase the confined space, thereby accelerating the flame through the aerosol cloud. However, more direct evidence of this cannot be extracted from the paper though Ballal and Lefebvre (1981) have published data of flame propagation in aerosols of higher droplet sizes.

Vincent and Howard (1976) studied the effect of explosion suppression systems (Halon 1301) on mist explosions. In their large scale tests these suppression systems were found to effectively suppress the explosion, however the large quantities of the Halon required to provide effective suppression made the cost of such a system highly prohibitive.

Subsequently Vincent et al. (1976), conducted similar tests using a water fog suppression system and found that the resulting explosion was less damaging than without the system. Full protection was deemed possible with higher amounts of fog. Shorter response times were also found to reduce the explosive damage. However, prevention of ignition by the water fog was not achieved, especially if the ignition source was close to the leak. The advantages of the water fog system over the traditional Halon systems were lower cost, easy maintenance, and easy access to existing fire water systems.

The combustion of droplets is directly related to the dispersion and ignition of the aerosol and hence we see that droplet size is a very important factor in the combustion process.

Ignition

In any process plant, there are number of possible ignition sources. In many cases, it would be impossible for all possible ignition sources to be identified. However, whenever possible, the identified ignition sources must be eliminated. Ignition sources for over 25000 fires were studied and tabulated by Factory Mutual Engineering Research Corporation (1974), as shown in Table II-1.

Table II-1. Ignition sources for major fires

(Adapted from Factory Mutual Engineering Research Corporation, 1974)

Ignition source	Percentage occurrence
Electrical (wiring of motors)	23
Friction (bearings or broken parts)	10
Overheated materials (abnormally high temperatures)	8
Hot surfaces (heat from boilers, lamps, etc.)	7
Burner flames (improper use of torches)	7
Combustion sparks (sparks and embers)	5
Cutting and welding (sparks, arc, heat, etc.)	4
Mechanical sparks (grinders, crushers)	2
Static sparks (release of accumulated energy)	1

The main consideration in the problem of mist flammability would be the minimum ignition energy (MIE), which is the energy in joules stored in a capacitor which upon discharge is just sufficient to effect ignition of a given fuel mixture under specified test conditions (Britton, 1999).

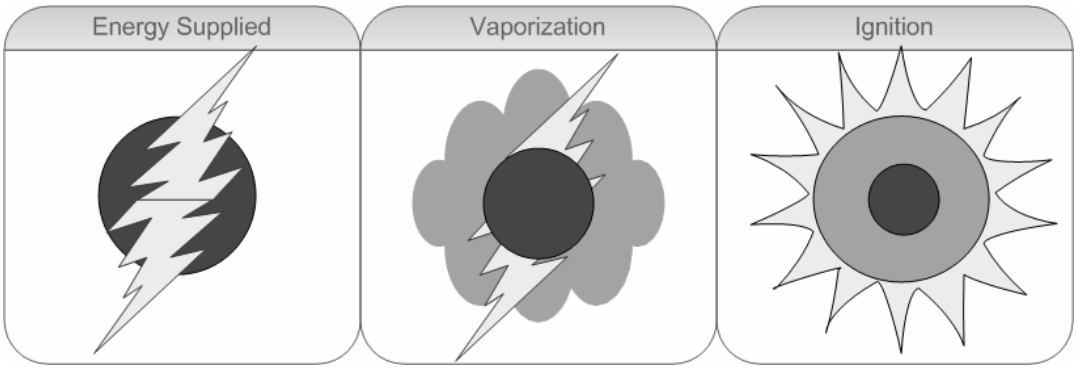

Figure II-5. Droplet ignition

The process of droplet ignition starts with the droplet receiving a certain amount of energy. This energy raises the temperature of the droplet and vaporizes some of the liquid from the droplet surface area. If a flammable vapor air mixture is then formed in the vicinity of the droplet, the remaining energy ignites this mixture, triggering the droplet combustion (Figure II-5). The energy supplied has to be sufficient to support this entire process, and Minimum Ignition Energy (MIE) defines the lower limit of the energy requirement for ignition to occur.

The increased surface area of the dispersed liquid phase that comprises a mist/aerosol is responsible for enhanced rates of heat and mass transfer, and this is the distinction that makes mists more hazardous than liquid spills. The ease of ignition is increased as the mean drop diameter of the mist decreases (Lewis and von Elbe, 1987). This is because the liquid must partially vaporize before it ignites. At smaller diameters, the increased surface area to volume ratio accelerates the evaporation process, which is

essentially a combination of heat and mass transfer (Britton, 1999). Also it is found that in a distribution of drop sizes, the smaller droplets ignite faster, and burn ahead of the resultant propagating flame front. Annamalai et al. (1993) modeled evaporation in multi-component drop arrays and found that there are a number of other complexities that govern the vaporization process when one considers droplet interactions.

Wong et al. (1997) studied the ignition behavior of n-hexadecane and confirmed the inverse relationship between ignition time and droplet size. However the experimental results were obtained for large droplets above 1000 microns. In aerosol dispersions, the droplets of less than 100 microns are more likely, as the larger droplets will rainout. Additionally, the ignition mechanism of aerosol dispersion is more complex than single droplet ignition modeled here. Wong et al. concede that ignition may occur in the vapor phase, causing flame propagation through the droplets.

Bowen and Shirvill (1994) point out that the hazard potential of aerosols is dominated by the size of the droplets generated by the leak. Their proposed correlation indicates a cubic dependence of the minimum spark ignition energy on droplet size for a given air-fuel ratio.

Pidoll (2001) was able to demonstrate, experimentally, that ignition of fuel clouds by electric sparks was possible and also showed that spray clouds may be flammable inspite of a water content of more than 50% by weight. Additionally, flammability of high flash point sprays was also demonstrated.

The MIE model (Ballal and Lefebvre, 1979) uses a dimensionless mass transfer driving force B, which is a ratio of the excess enthalpy in the bulk gas adjacent to the droplet surface to the enthalpy increase of the vaporizing liquid (Spalding, 1979). In simpler terms it represents the ratio of the energy available for vaporization to the energy required for vaporization. This experimental analysis resulted in empirical models that relate the MIE to a combination of liquid physical properties, temperature, and the mass transfer driving force. The mass transfer ratio was found to increase with volatility with a range of values between 1.2 for very heavy fuel oils to about 8 for highly volatile liquids.

The approximations of the air density and the air temperature used in the calculations as well as the errors in calculating the mass transfer ratio limit the applicability of the resulting model. The drawback of the model is its assumption that evaporation is the rate-controlling step (Peters & Mellor, 1980). For larger mean drop sizes, the smaller surface to volume ratio limits the evaporation and thus is in agreement with this assumption. But smaller mean drop sizes, having rapid evaporation rates, do not conform to this approach. Also it is found that in a distribution of drop sizes, the smaller droplets ignite faster, and burn ahead of the resultant propagating flame front.

When considering mists formed by the spraying of liquids, it is important to understand that the drops will inherently have an associated electrostatic charge about them. The question about whether this charge is sufficient to cause a depression in the MIE has not been addressed in detail. However, the relation between evaporation and

droplet charge has been studied in detail (Abbas and Latham, 1967). As the charged droplet evaporates, it loses mass but retains its charge, thereby increasing its charge-to-mass ratio. As evaporation proceeds, the charge-to-mass ratio increases until it reaches the Rayleigh limit (Bailey, 1988). At this point the droplet is unstable and ejects a couple of highly charged micro-droplets, while itself retaining about 75% of its mass. This continues infinitely until the entire droplet is evaporated and is described by Figure II-6.

When extending a theory to droplet arrays in a mist, the complicated behavior of the charged cloud is yet to be examined. It is the effect of this charged cloud on the MIE that is of importance. Studies on these phenomena will clarify the importance of electrostatics in mist flammability.

The main methods of removing the ignition arm from the fire triangle would involve prevention of electrostatic discharge. Methods of controlling electrostatic hazards have been extensively studied (Britton, 1999).

Hence aerosol/mist droplet size is a critical parameter for both ignition as well as combustion processes. Smaller droplet sizes seem to possess a greater hazard as they ignite easily and undergo vigorous combustion. Therefore any preventative measure should ensure that smaller droplet sizes are not generated during a leak of a heat transfer fluid.

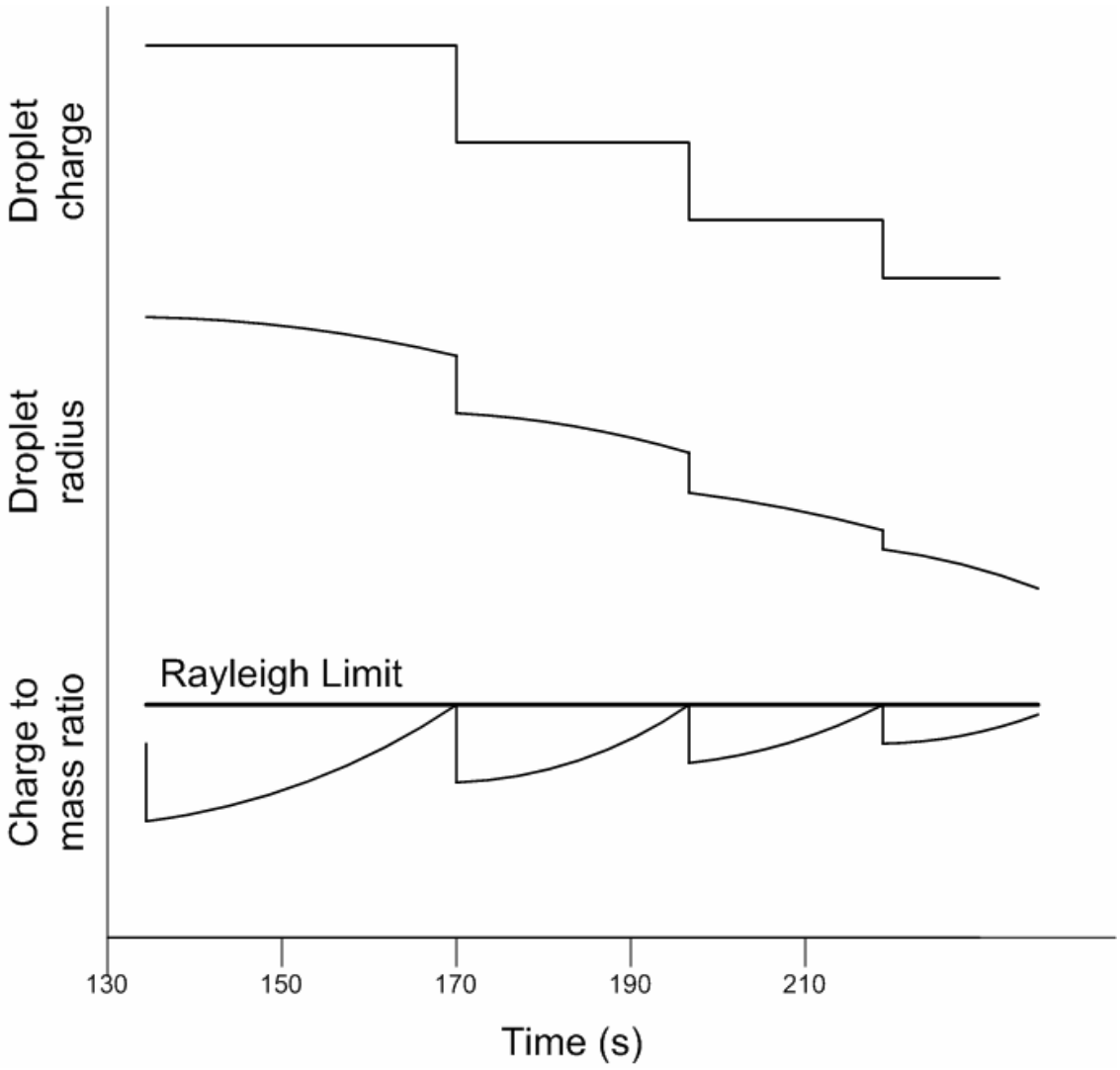

Figure II-6. Changes in drop charge and mass during evaporation

Dispersion

The process that precedes the ignition and combustion phases is the dispersion phase. Following the formation of the aerosol from the leak, the droplets are dispersed to the surroundings. During the dispersion process the droplets are subjected to mass, momentum, and heat transport processes, all of which are dependent on the surface-to-volume ratio. Smaller droplets present a larger surface-to-volume ratio and hence are more susceptible to change. Two important phenomena that alter the droplet size distribution of the aerosol are evaporation and coalescence. Evaporation results in a decrease in droplet diameter and coalescence results in the increase in the droplet diameter.

Droplets that are too large, or those that become too large because of coalescence rain out of the dispersed aerosol resulting in the reduction of the concentration of the dispersed aerosol (Figure II-7). Other factors that influence the dispersed aerosol are air currents, obstacles, the presence of suspended particulates, temperature profiles, etc.

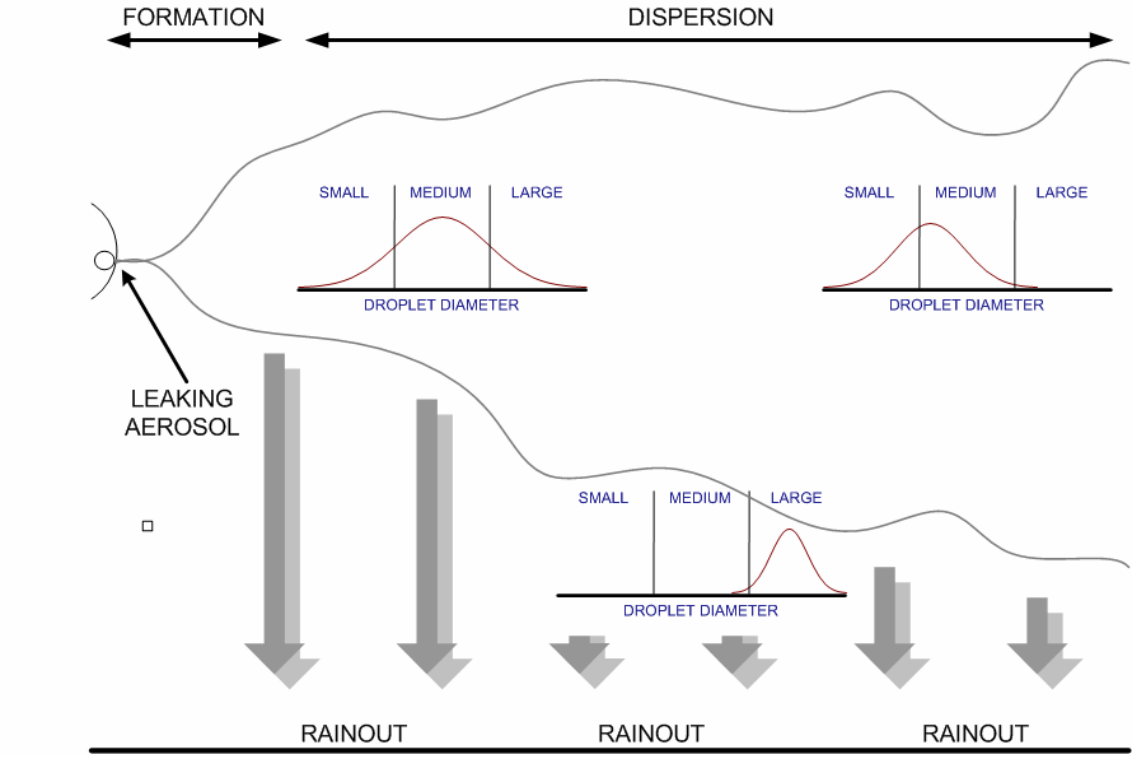

Figure II-7. Aerosol dispersion and rainout

The behavior of the aerosol cloud has been studied on both the micro and macro-scale, however scale-up of micro-scale observations to the macro-scale cloud behavior has not been achieved. Orme (1997) presents some interesting work on micro-scale droplet phenomena: bounce, coalescence, disruption, and fragmentation. Orme however, concludes that factors such a droplet charging, humidity, and local gas pressure are vital to the understanding of the whole picture. Sommerfeld and Qiu (1998) deem the spray to have three "personalities": dense spray, where interactions

between the droplets are dominant; dilute spray, where aerodynamic transport of the droplets becomes important, and lastly, interaction of the spray droplets with obstacles.

Woodward and coworkers (1995) have assessed the importance of rainout in the assessment, modeling, and validation of large aerosol releases. While rainout does reduce the total mass of the aerosol cloud, once the rainout collects in pools, it can evaporate and re-enter the cloud, though the time scales for this re-entry are much greater. Droplet size of the aerosol is indicated as an important parameter in modeling the vapor content, rainout, dispersion distances, and eventually flammable mass. However, Nikmo et al. (1994) suggest that initial droplet size is not critically important to the heat and mass transfer process within an aerosol cloud because the evaporation-condensation process within a cloud is self controlling.

It is therefore essential that we study the source term, which, in the case of fluids leaking below their flash points, requires aerosol drop size distributions and formation distances.

Formation

The process by which a liquid stream disintegrates into an aerosol is known as atomization, which is the subject of extensive research and publications. Bayvel and Orzechowski (1993), for example, provide a summary of the existing theory on the stability and disintegration of liquid streams. However, since atomization is a random process, no fundamentally theoretical approach is able to answer all the questions

regarding atomization (Schweitzer, 1937, Faeth, 1983, 1990). Faeth (1990) examined the properties of sprays near the exit nozzle/orifice and formalized a classification of the different regimes of spray breakup.

The classification by Faeth (1990) is based on an increasing flow rate out of the orifice (Figure II-8), with the regimes occurring in the following order: Rayleigh, first wind induced, second wind induced, and atomization breakup. Rayleigh breakup results in droplet diameters slightly larger than the orifice diameter due to interactions between the surface tension and inertial forces. In this regime the break up length increases with an increase in liquid flow rate, as the surrounding gas phase does not contribute to the break up mechanism. The remaining regimes all involve gas phase aerodynamics and hence break up lengths decrease with increasing flow rates. The first-wind induced regime is characterized by twisting of helical instability in the liquid column as a whole and droplets of size similar to that of the orifice diameter. The second-wind induced regime is characterized by both column and surface instabilities. The relative velocity between the gas and liquid phases begins to create surface shear that rips off droplets from the surface of the liquid column. Droplets in this regime will vary in size with an upper limit at the orifice diameter. Atomization breakup is characterized by surface shear instabilities occurring right at the orifice and results in droplets that are generally smaller in size than the orifice diameter. Sprays produced in this regime are dense, produce very small droplets, and hence are critical from the point of view of this dissertation.

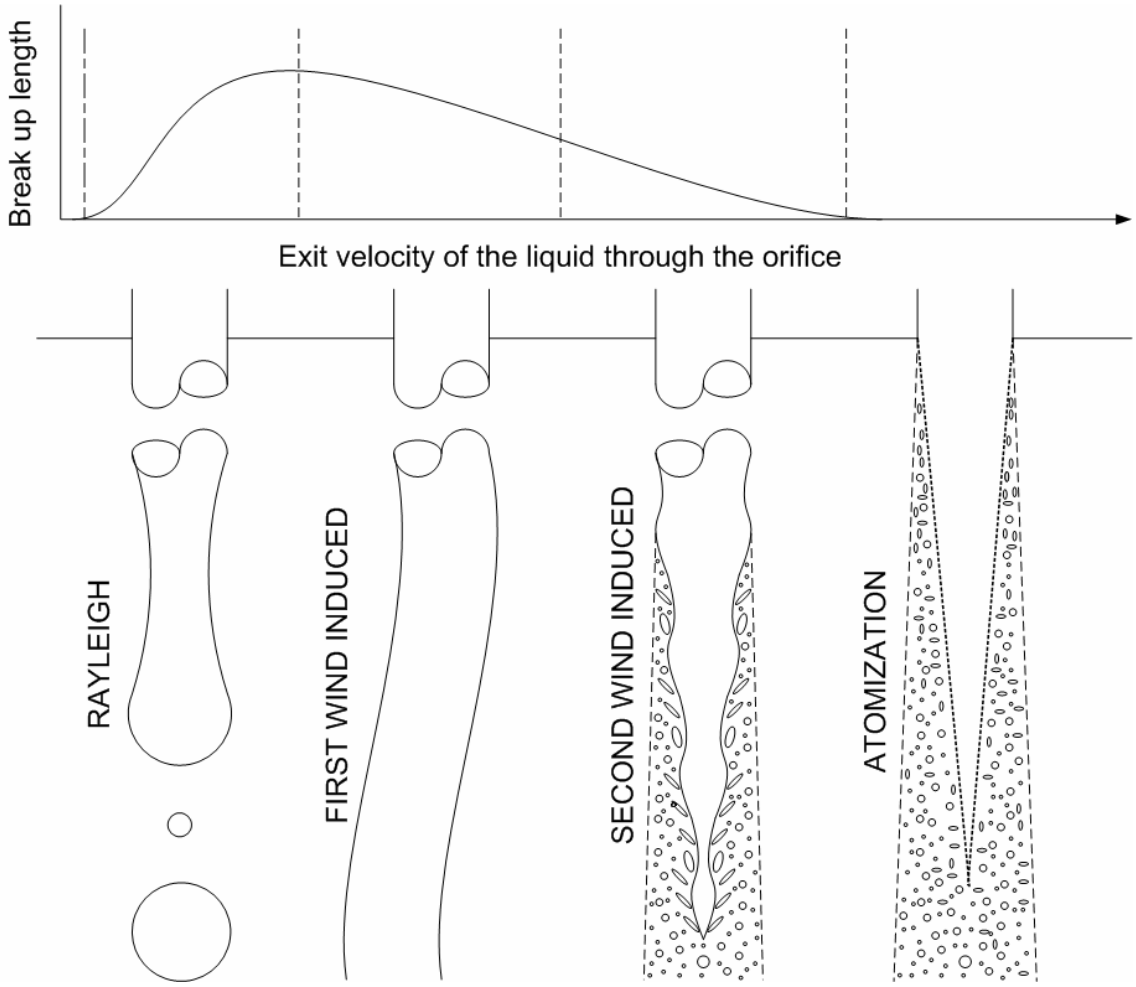

Figure II-8. Spray break up regimes for round jets in still air

In systems where the industrial fluids are operated at high pressures, for example in heat exchangers with heat transfer fluids, second wind induced and

atomization regimes are more likely to occur. The structure of the breakup process in these two regimes is generalized into three zones, as shown in Figure II-9.

The relative velocity between the ejected liquid column and the surrounding still air results in shear forces that rip the surface of the liquid column, generating non-spherical droplets known as ligaments as seen in the disintegration zone. These ligaments undergo further break up into smaller droplets in the fully atomized zone. The distance from the orifice to the fully atomized zone is known as the aerosol formation distance. The distance from the orifice to the disintegration zone is the breakup length. The breakup length represents the point at which droplets begin to detach themselves from the liquid column. The aerosol formation distance represents the distance at which the break up process is complete.

Richer et al. (1994) attempted to arrive at a source term and studied the atomization process with regard to water and kerosene. They demonstrated the effects of nozzle size and geometry, spray duration, and liquid properties on the transient behavior of aerosols in a confined space. They, however, did not try to describe the atomization process.

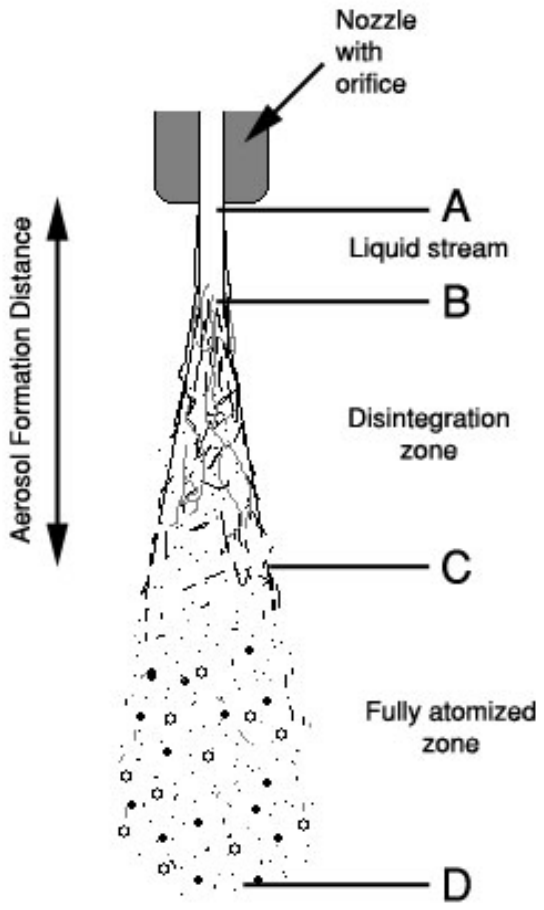

Figure II-9. Atomization of a liquid column

To resolve this problem, lessons can be applied from the field of fuel combustion, where the atomization process is well established for fuels. Elkotb (1982) provided an extensive study of aerosol spray modeling for fuels. He used dimensional analysis, to obtain an empirical correlation of the aerosol drop diameter with the operating conditions and the fluid properties. Hiroyasu (1991) studied the drop size

distribution in diesel combustion chambers and also used dimensional analysis to generate an empirical model. Semião et al. (1996) derived correlations for pressure jet and airblast atomizers and their study provides vital information about the factors important to aerosol formation through leaks in process equipment.

To study the process of atomization effectively, the adopted analysis must be non-intrusive, because of the nature of a developing spray. The use of optical techniques has been well established in this regard. Bayvel and Orzechowski (1993) have listed the various optical techniques used in spray characterization.

SUMMARY OF CHAPTER II

In examining the problem of aerosol explosions through its various domains, in the chapter, the importance of the aerosol formation process is seen to be critical. The initial drop size distribution of the aerosol is critical to the dispersion process, which in turn feeds the ignition and explosion phases. In terms of consequence analysis, we first perform source term calculations, followed by dispersion modeling and finally explosion analysis (Figure II-10). Inaccurate source term modeling will propagate through the analysis and result in an incorrect perception of the consequence and risk.

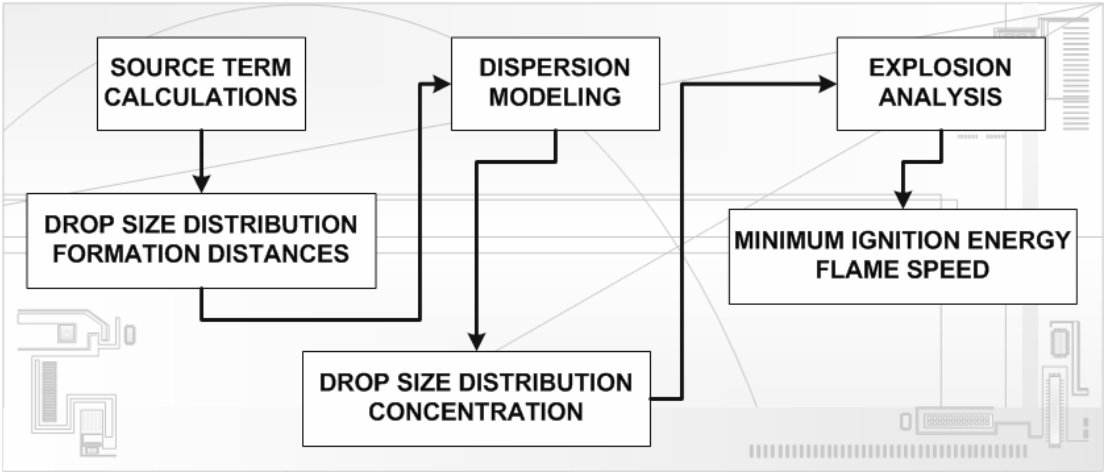

Figure II-10. Basic steps in consequence analysis

In order to get a good understanding of aerosol hazards related to explosions, any study must first deal with the issue of aerosol formation. The best method of preventing an aerosol explosion would seem to be the suppression. Hence the initial drop size distribution of the aerosol is critical to the dispersion process. Studying the mechanism of formation of aerosols through leaks will, therefore, also help in developing such suppression methods.

CHAPTER III

EXPERIMENTAL MEASUREMENTS

This chapter deals with the experimental aspects of the dissertation: the tools and techniques utilized in the research, the experimental apparatus, fluid characterization, data collection and methodology, and initial data assessment.

The previous chapter details the significance of studying the atomization process, with particular emphasis on the droplet size measurements. There are a variety of techniques that are helpful in the measurement of particle sizes, starting with primitive sieving techniques. The techniques utilized depend on the type of particle: solid, liquid or composite; and the particle life: transient or intransient.

For liquid droplets formed during a leak, the process of droplet size measurement requires a non-intrusive technique, which does not interfere with the formation process or with the individual droplets formed. The atomization process is very rapid and requires an equally rapid measurement technique. Optical techniques have such advantages and are hence very useful in studying the atomization process. Chabay and Bright (1979) have provided a list of 32 instruments based on 15 different

---

Part of this chapter is reprinted from "Predictive correlations for leaking heat transfer fluid aerosols in air" by Krishna, K., Kim, T.K., Kihm, K.D., Rogers, W.J., and Mannan, M.S., (2003). *Journal of Loss Prevention in the Process Industries, 16* (1), 1-8, Copyright 2003, with permission from Elsevier.

optical principles, for sizing aerosol particles. An updated version of the list would be much larger, but this list provides a good starting point for any search.

The principle of Fraunhofer Diffraction is a well-known rigorous optical principle that needs limited calibration. With proper configuration, it can be used to measure both solid and liquid aerosol particles, even in transient systems, like the aerosol formation process. This technique is elaborated in further detail in this chapter.

BASIC OPTICS

When a beam of light is incident upon a particle, it can be absorbed, scattered, or transmitted. By applying the law of conservation of energy, the sum of these three interactions must be equal to the incident light.

$$I = S + A + T \tag{III-1}$$

where I is the incident light energy, S is the energy scattered, A is the energy absorbed by the obstacle, and T is transmitted through the obstacle.

Scattering of the light energy can take place in three ways: reflection, refraction and diffraction. While reflection and refraction are not of particular interest to this research, diffraction, or the “bending” of light rays around obstacles, can be advantageously exploited in particle sizing.

FRAUNHOFER DIFFRACTION THEORY

Fraunhofer diffraction theory was originally utilized to account for the "bending" of light caused by the edges of an aperture. Fraunhofer diffraction is a limiting case for Fresnel-Kirchhoff theory where the area of the aperture or obstacle must firstly be smaller than the product of the wavelength and the distance between the point light source and the diffracting plane; and secondly be smaller than the product of the wavelength of light and the distance between the observation plane and the diffraction plane. Therefore Fraunhofer Diffraction is also known as far-field diffraction.

For plane waves incident on the apertures or obstacle, the source is at infinity, thereby satisfying the first criterion (Figure III-1). To satisfy the second criterion, the observation plane has to be placed far away, or a lens is used to focus the image onto the observation plane placed in the focal plane of the lens.

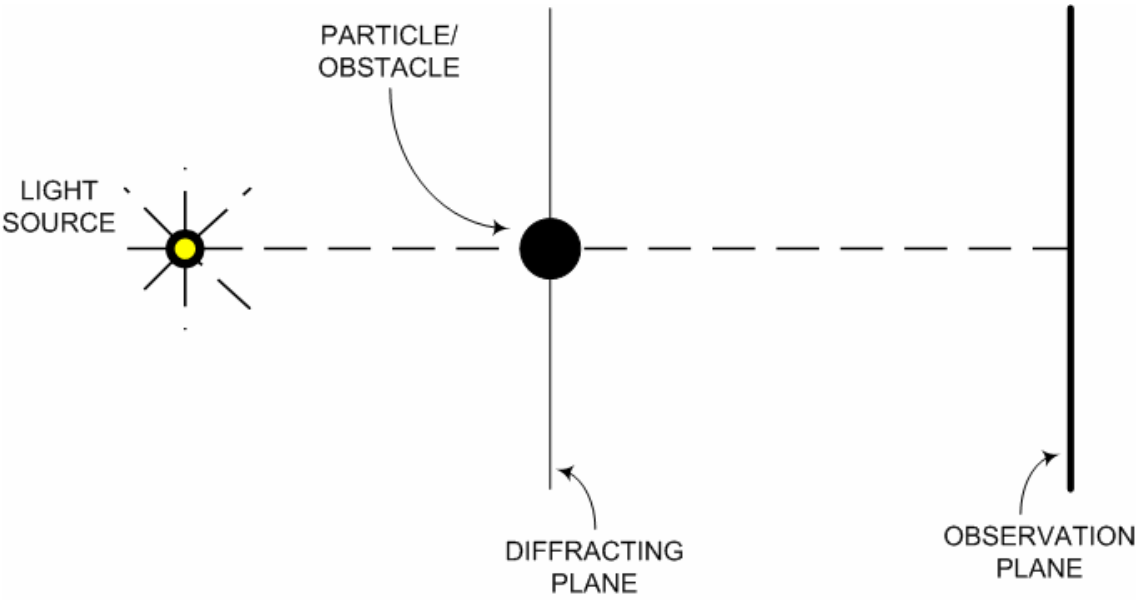

Figure III-1. Schematic of the light source, obstacle, and observation plane in the diffraction setup

The light intensity of a diffraction pattern for a spherical droplet of radius r is described by the well-known Airy function, which is shown in Figure III-2:

$$I = I_0\left[\frac{2J_1(x)}{x}\right]^2 \tag{III-2}$$

where I_0 is the intensity at the center diode, J_1 is the first-order spherical Bessel function, and x is given by

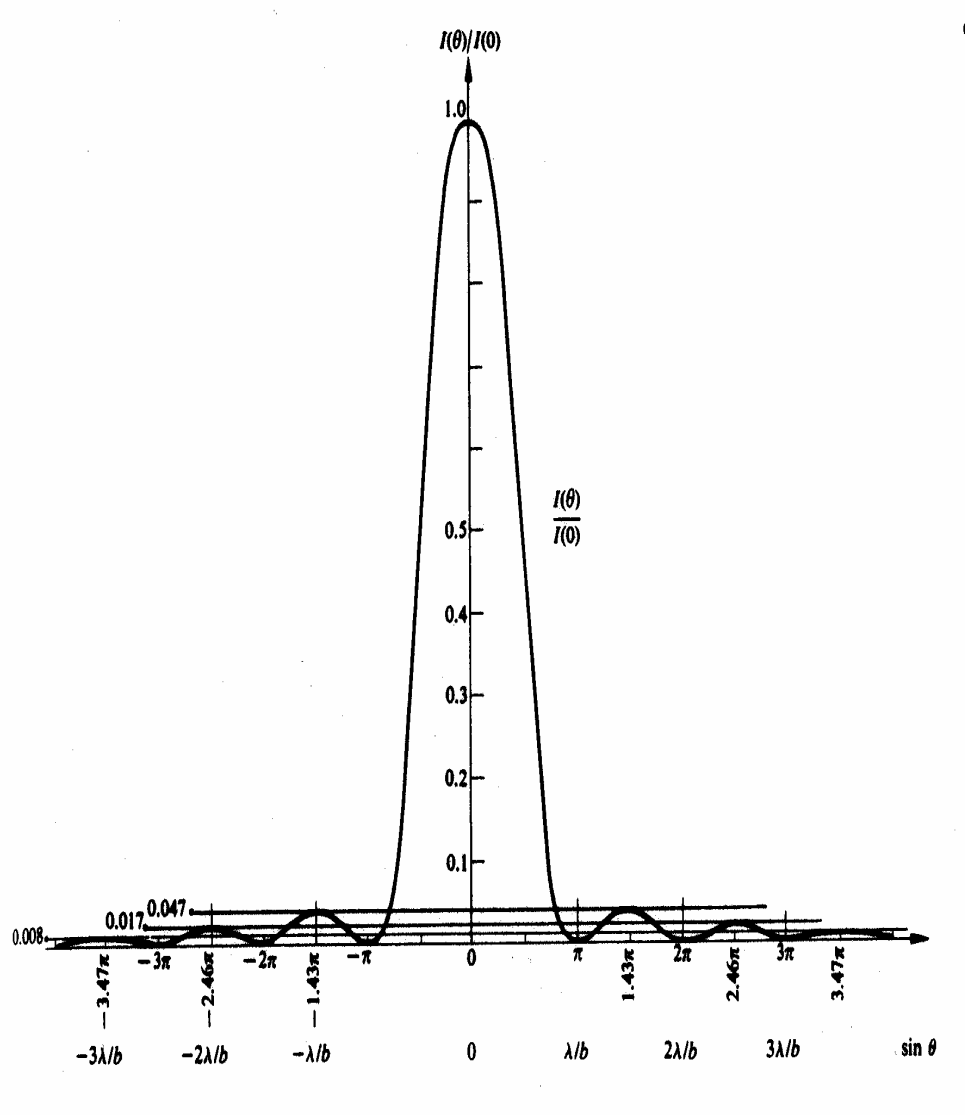

Figure III-2. The Fraunhofer diffraction pattern of a single slit (Airy function) (Hecht, 1998)

$$x = \frac{2\pi rs}{\lambda F} \tag{III-3}$$

where s is the radial distance in the detection plane measured from the optical axis and F is the focal length of the lens.

By integrating equation (III-2) we obtain the fraction of light energy, L, contained within a circle of radius s on the detector plane.

$$L = 1 - J_0^2(x) - J_1^2(x) \tag{III-4}$$

where J_0 is the zero-order spherical Bessel function.

For the series of detector rings in the Malvern system, the light energy incident between the radii s_1 and s_2, due to a single droplet of radius r is

$$L_{s1,s2} = C\pi r^2 \left[J_0^2(x) + J_1^2(x)\right]_{s1} - \left[J_0^2(x) + J_1^2(x)\right]_{s2} \tag{III-5}$$

where C is an optical constant based on the power of the light source and the detector sensitivity.

Therefore for N droplets of radius r, neglecting multiple diffractions, we have

$$L_{s1,s2} = C\pi \sum_{i=1}^{M} N_i r_i^2 \{\left[J_0^2(x_i) + J_1^2(x_i)\right]_{s1} - \left[J_0^2(x_i) + J_1^2(x_i)\right]_{s2}\} \tag{III-6}$$

where the size distribution consists of M size classes.

Writing equation (III-6) in terms of the mass of the droplet, W, assuming droplet density is independent of size, we get

$$L_{s1,s2} = K\sum_{i=1}^{M}\frac{W_i}{r_i}\{\left[J_0^2(x_i)+J_1^2(x_i)\right]_{s1}-\left[J_0^2(x_i)+J_1^2(x_i)\right]_{s2}\} \qquad \text{(III-7)}$$

where K contains the optical constant and the density and

$$N_i = \frac{3W_i}{4\pi r^3\rho} \qquad \text{(III-8)}$$

The procedure for obtaining weight distribution uses the iterative least-square method. The initial values of W were estimated using a Rosin-Rammler distribution. These initial estimates are then used to calculate expected W values of the light intensity L, which are then compared with the measured L values, and the least-square error is calculated. A number of iterations are performed until the least-square error has been minimized.

The Rosen-Rammler distribution (1933), and other details of the droplet statistics are further elaborated in Chapter IV.

THE MALVERN LASER DIFFRACTION PARTICLE ANALYSER

The Malvern laser system consists of a 2 mW Helium-Neon laser tube and a detector with an array of concentric photosensitive ring diodes. The laser beam is a collimated monochromatic beam of wavelength 780-662 mm and 1.8 mm in diameter. When the aerosol droplets pass through the beam, they diffract the light by amounts inversely proportional to their diameter. The diffracted light falls on 30 concentric ring diodes in the detector with each ring detecting a certain size range of droplets. The light

intensities on each of these diodes are converted into drop size data by the computer. A schematic of the diffracted light is shown in Figure III-3.

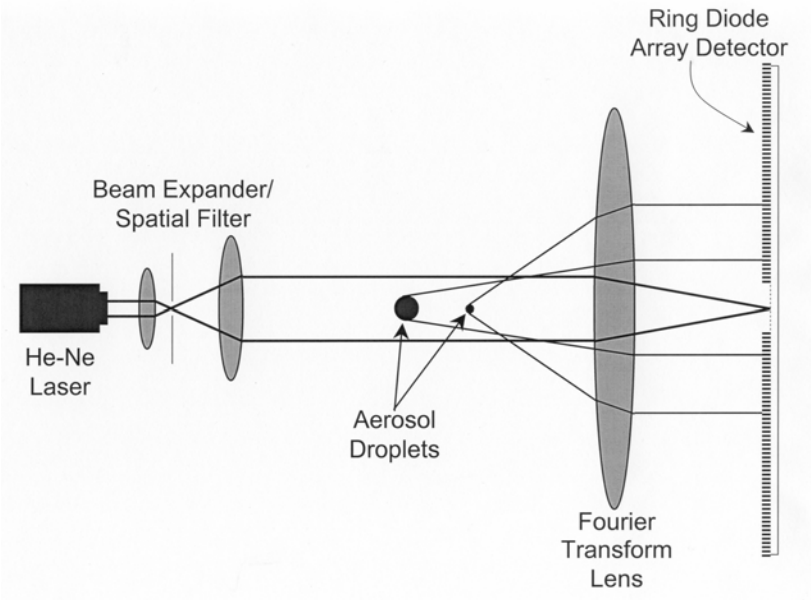

Figure III-3. Diffraction particle analyzer to measure drop sizes and concentrations

Three focal length lenses are commonly available: 63, 100, and 300 mm. The lens focuses the light onto the ring diode detector. At the center is a circular photo detector used for measuring the transmittance. The selection of the focal lens is done to suit the system being studied. For this research the 300 mm focal length lens was used.

The size range covered by any one lens is divided into 15 logarithmically increasing size classes. Table III-1 shows the size classes for each focal length

Table III-1. Size classes (μm) for Malvern Fraunhofer diffraction instruments (Barth, 1984)

#	63 mm focal length		100 mm focal length		**300 mm focal length**	
	Upper	Lower	Upper	Lower	**Upper**	**Lower**
1	118.4	54.9	188.0	87.2	**564.0**	**261.6**
2	54.9	33.7	87.2	53.5	**261.6**	**160.4**
3	33.7	23.7	53.5	37.6	**160.4**	**112.8**
4	23.7	17.7	37.6	28.1	**112.8**	**84.3**
5	17.7	13.6	28.1	21.5	**84.3**	**64.6**
6	13.6	10.5	21.5	16.7	**64.6**	**50.2**
7	10.5	8.2	16.7	13.0	**50.2**	**39.0**
8	8.2	6.4	13.0	10.1	**39.0**	**30.3**
9	6.4	5.0	10.1	7.9	**30.3**	**23.7**
10	5.0	3.9	7.9	6.2	**23.7**	**18.5**
11	3.9	3.0	6.2	4.8	**18.5**	**14.5**
12	3.0	2.4	4.8	3.8	**14.5**	**11.4**
13	2.4	1.9	3.8	3.0	**11.4**	**9.1**
14	1.9	1.5	3.0	2.4	**9.1**	**7.2**
15	1.5	1.2	2.4	1.9	**7.2**	**5.8**

An experiment begins with collecting data for the background and then for the spray system plus background. A single sweep consists of gathering data from all the ring diodes and storing them for averaging with the next sweep. A minimum of 10 sweeps is essential for limiting statistical fluctuations. In general a higher number of sweeps improves the data analysis and averaging. However in transient systems, more sweeps implies a greater time needed for data collection, which could affect the analysis adversely. During this research 500 sweeps were averaged for each measurement.

At the end of a particular experiment, the background is subtracted from the averaged signal plus background, following which each successive ring pair is averaged. The resulting 15 data points are then normalized against the incident light. They now represent the 15 L values used in the calculations according to the Fraunhofer Diffraction theory as shown in the previous section of this chapter.

The accuracy of the Malvern data with the Rosin-Rammler model is provided by the function Log. Diff. that is interpreted in Table III-2.

Table III-2. Interpretation of *Log. Diff* number (Malvern Laser Manual, 1993)

Log. Diff	**Interpretation**
Log. Diff > 6	Model not appropriate or experiment incorrectly performed.
5.5 < *Log. Diff* > 6	Poor fit. May be adequate for trend analysis only.
5 < *Log. Diff* > 5.5	Adequate fit but look for evidence of systematic misfitting.
5 < *Log. Diff* > 4	Good fit. Well-presented sample.
Log. Diff < 4	Very unlikely with measured data but normal with analytic data.

Though Fraunhofer diffraction and the Malvern system provide a useful, versatile, and non-intrusive method of droplet sizing, it is important to know the limitations of this technique. Barth (1984) has listed the limitations and recommends that the user know the level of compromise acceptable to his or her application. Hirleman and Dodge (1985) studied the performance of the Malvern and provide an evaluation of the instrument. The use of laser diffraction, as a method of particle size measurement, has also been studied by Felton and his coworkers (1981, 1985), Watson & Tech (1985), and Miles et al. (1989)

LIMITATIONS OF THE MALVERN SYSTEM

The Malvern Laser Diffraction Particle Analyzer (Malvern laser) has certain limitations, which are important in the preliminary set up of the experiment and the data

analysis. Knowledge of these limitations helps in excavating a complete story about the system being studied.

Theoretical Errors

The division of the size classes during analysis of the ring diode data shows a distinct lack of sensitivity below 10 μm. This implies that a larger error, generally higher than 20%, is associated with particle sizes smaller than 10 μm. These limitations are not restricted to the Malvern system but are common to all Fraunhofer diffraction type instruments.

Concentration Errors

Fraunhofer diffraction theory can account for a beam of light being diffracted only once before being detected by the ring diode. Multiple diffractions before being detected would cause the outer rings to detect a greater amount of light thereby biasing the measurements to indicate lower particle sizes. This is very evident at transmission ratios lower than 30% (obscurations above 70%). Additionally low concentrations result in insufficient data to provide statistically robust analysis and result in non-physical measurements. Obscuration ratios below 10% would clearly demonstrate this trend. Ideally obscuration ratios between 20% and 30% provide the best results.

Vignetting

If the particles to be measured are too far away from the receiving lens, the diffracted light may be cut off from the lens' finite aperture. As the smallest particles cause the largest diffraction angles, the data due to such particles is lost, thereby biasing the measurement towards the larger particle sizes. The effect of vignetting on the measurements has been studied by Wild & Swithenbank (1986) and Hamidi & Swithenbank (1986b)

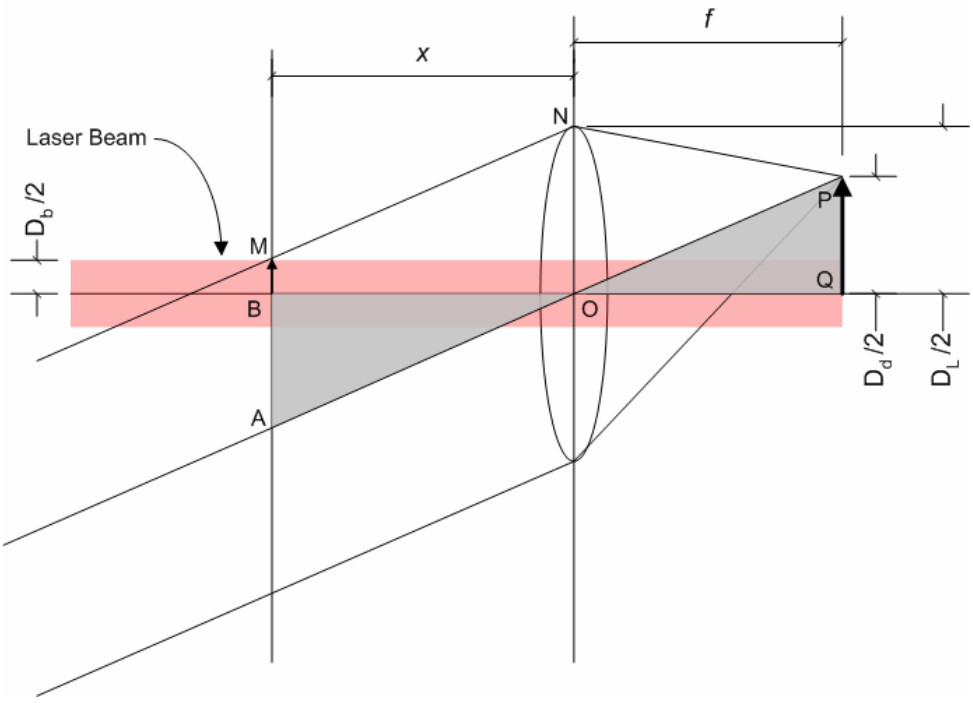

Figure III-4. Optical ray diagram for calculating the effect of vignetting

The maximum distance of the particles from the receiving lens can be calculated, with reference to Figure III-4, as follows:

Light rays MN and OA, being parallel, imply that NO is equal in length to MA. NO is the lens radius, and MB is the laser beam radius. Therefore,

$$MA = NO \tag{III-9}$$

$$MB + AB = NO \tag{III-10}$$

$$AB = NO - MB \tag{III-11}$$

$$AB = \frac{D_L}{2} - \frac{D_b}{2} = \left(D_L - D_b\right)\Big/2 \tag{III-12}$$

Triangles OAB and OPQ being similar, we have

$$\frac{AB}{BO} = \frac{PQ}{OQ} \tag{III-13}$$

$$\frac{\left(D_L - D_b\right)\Big/2}{x} = \frac{D_d\Big/2}{f} \tag{III-14}$$

Therefore, the maximum distance between the particles and the receiving lens, *x*, is given by,

$$x = f\,\frac{\left(D_L - D_b\right)}{D_d} \tag{III-15}$$

For example, with a laser beam diameter of 1.8 mm, a usable lens diameter of 48 mm, a lens focal length of 300mm, and an outer ring diameter of 28.6 mm, we have a

maximum distance to prevent vignetting as 484.6 mm. Hence to prevent vignetting the particles must be within 48.46 cm of the observing lens.

Beam Steering

The Malvern system is based on scattering due to diffraction only. Any light impinging on the ring diodes that is generated by any other form of scattering corrupts the measurements obtained. In the case of vapors present in the path of the laser beam, the difference in refractive index between the air and the vapor causes the beam to refract. This steering of the beam away from its normal path causes an increase in the amount of light impinging on the inner ring diodes, incorrectly implying that there are more large particles, thereby biasing the measurement to larger particle sizes. This can be clearly seen in the case of heated fluid aerosols. Hence care must be taken to ensure that vapors do not enter into the path of the laser beam.

APPARATUS CALIBRATION AND ESTIMATED EXPERIMENTAL ERRORS

Calibration of the equipment is necessary to ensure accuracy and knowledge of errors incurred during measurement. For this purpose, the thermocouples, pressure transducer, and the Malvern were calibrated.

Malvern Laser

The alignment of the Malvern laser is critical to the operating accuracy of the droplet measurement system. The laser must be aligned to ensure that the maximum intensity of light is incident upon the central diode. The receiver's pinhole is adjusted to ensure this. In the absence of droplets the light incident on the ring diodes nearest to the central diode must be as low as possible: ideally zero. The remaining step of the calibration is performed using a standardized reticle, which consists of a prepared particle distribution on an optical plate, where the size of each particle is determined using electron microscopy and the mean diameter then calculated. The reticle used in this research has a reported distribution of 46.5 ± 4.7 micron and during calibration, only values in this range were accepted. The calibration of the Malvern was repeated every day.

Pressure Transducer

The pressure transducer readings are obtained as a ratio of the transducer output to the input voltages, which are measured with a DC voltmeter. The pressure transducer was calibrated against the atmospheric pressure using a dead weight pressure gauge. The transducer was connected in parallel with the dead weight gauge and a regulated compressed nitrogen cylinder was used as a pressure source. A variable volume also was connected in parallel to adjust for any pressure fluctuations. The value for local atmospheric pressure on that day was obtained from the Department of Meteorology at

Texas A&M University. The ratios of the output to input voltages were then plotted against the absolute pressure, for both increasing and decreasing pressure tracking to account for hysterisis. Appendix D contains the pressure calibration data for the Sensotek pressure transducer. The total uncertainty of the pressure transducer data is a sum of the following

1. The uncertainty of the dead-weight gauge: < 0.0100 psia
2. The Sensotek pressure transducer error: ± 0.25 psia
3. The error of fit: < 0.01 psia
4. The error in the reported local atmospheric pressure: ± 0.1 psia

Therefore the maximum error in the pressure data is ± 0.37 psia

Thermocouples

The thermocouples measuring the nozzle, fluid cell, and air temperatures were all factory calibrated and reported maximum departures of + 1.5 °C and –1.11 °C over a temperature range of 0 °C to 419 °C. The calibration data is provided in Appendix E.

Hence the total uncertainty associated with the temperature data is + 1.5 °C and –1.11 °C.

Orifice

For the orifices, the total uncertainty is the sum of the following

1. Drill tolerance: ± 0.0051
2. Drill measurement: ± 0.0051
3. Hole drilling error: + 0.0051

Hence the total uncertainty of the orifice diameter is +0.015 mm, -0.010 mm. Therefore, the use of two decimal places in reporting orifice sizes is acceptable.

EXPERIMENTAL METHODOLOGY

The objective of this research is to study the atomization characteristics of heat transfer fluids. The emphasis is on formation distances and drop size distributions of aerosols created by plain orifice atomization to emulate a leak in a process system. An experimental approach employs the Malvern Laser Diffraction Particle Analyzer (Malvern laser) for a non-intrusive analysis technique.

Figure III-5 shows a schematic of the experimental equipment, which consists of a pressurized fluid cell and delivery system, a spray collection and exhaust system, and the Malvern laser. The fluid cell is a 5.9 liter aluminum cylinder with an internal diameter of 17 cm and a height of 36 cm. To simulate leaks, orifices are drilled into brass plugs. The positioning system consists of two precision rails for the X direction along the centerline of the spray from the orifice and the Y or radial direction

perpendicular to the X direction. The exhaust system includes a collection chamber for the spray, a mist separator that removes aerosol larger than 5 micron in diameter, and an explosion proof blower to remove the vapor and aerosol phases.

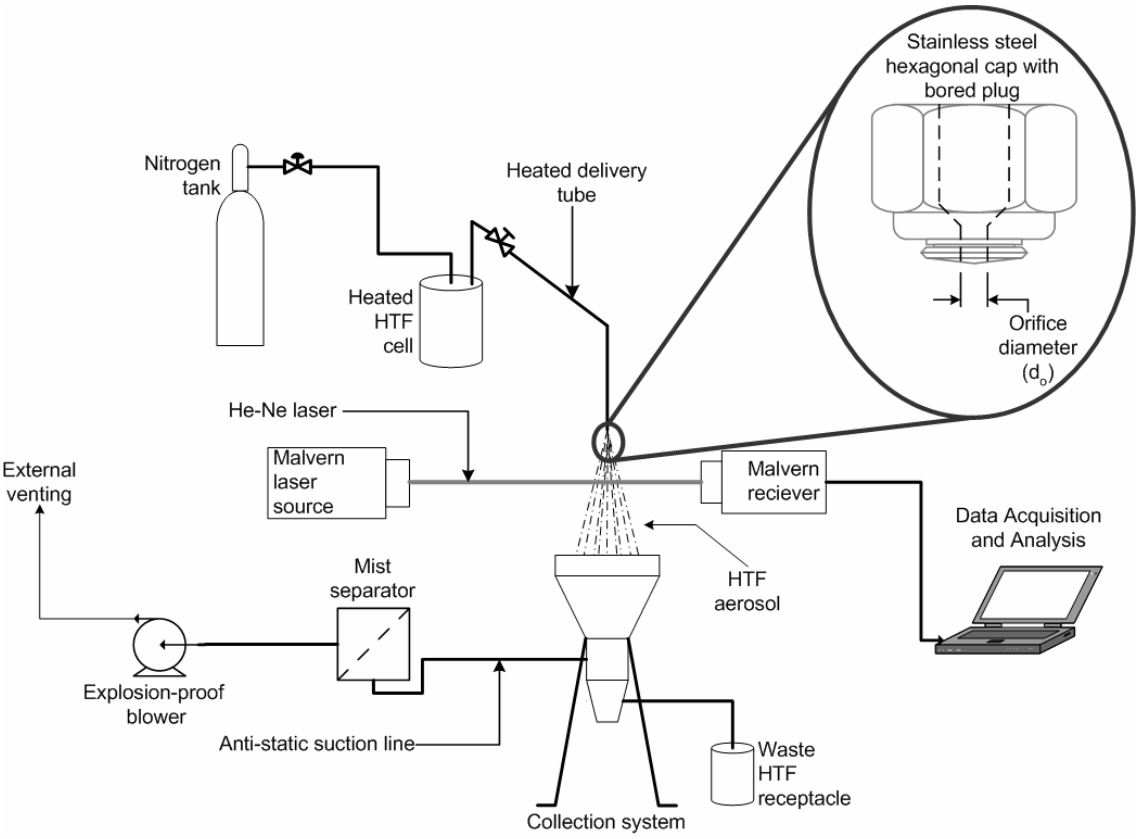

Figure III-5. Aerosol measurement apparatus

The Malvern laser consists of a 2mW Helium-Neon laser tube and a ring diode detector. The laser light at a wavelength of 632.8 nm is a parallel beam with a diameter of 1.8 mm (Barth, 1984). When the aerosol droplets pass through this beam, they diffract the light by amounts inversely proportional to the droplet diameter (Hecht, 2002). This diffracted light falls on 30 concentric ring diodes in the detector with each ring detecting a certain diameter range of droplets. The light intensities on each of these diodes are converted into mean droplet diameter data by a computer. The Malvern laser measurement technique for aerosols has been widely studied in the area of automotive fuel spray combustion (Kihm et al., 1994). Sukmarg et al. (2002) have provided additional information.

The HTF is transferred to the aluminum fluid cell to a volume not exceeding 70% of its capacity. The HTF in the fluid cell is heated to the required temperature using heating tape and is pressurized with nitrogen gas to propel it through the orifice. Measurement of the HTF temperature and pressure are made as close to the orifice as possible. Upon pressurization the heated HTF is sprayed through the laser beam and into the collection chamber. Each drop size distribution measurement is an average of data from 500 diode sweeps. The step-by-step experimental procedure is listed in Appendix F. The uncertainty in the measurement of aerosol droplet diameters by the Malvern is estimated to be ± 5 microns, which combines the Malvern laser instrumentation contribution and the limitations of the diffraction technique. Additionally, the Malvern laser system was calibrated within ± 3% using a standard

reticle. Hence the total error for spherical droplets over a measurement range of 0 to 100 microns is within ± 8 microns.

Photographs of the sprays at various conditions help to interpret the non-spherical droplet size data in the transition regions (Sukmarg et al., 2002), where the stream atomizes into aerosol. In these regions the Malvern laser reports mean droplet diameters with a higher uncertainty because the Malvern laser assumes the droplets are spherical.

PRELIMINARY DATA ANALYSIS

The Malvern Laser Diffraction Particle Analyzer system detects the light intensity on the ring diodes, converts it into a histogram of the drop size distribution, and generates a large array of statistical data. From each of these stages, information about the atomization process is available.

As mentioned in Chapter II, the spray can be divided into three zones: the compact stream zone, the disintegration zone, and the fully atomized zone. The aerosol formation region extends from the nozzle to the onset of the fully atomized region. This undeveloped region, comprised of the compact stream zone and the disintegration zone, represents the region where spherical droplets are in a minority.

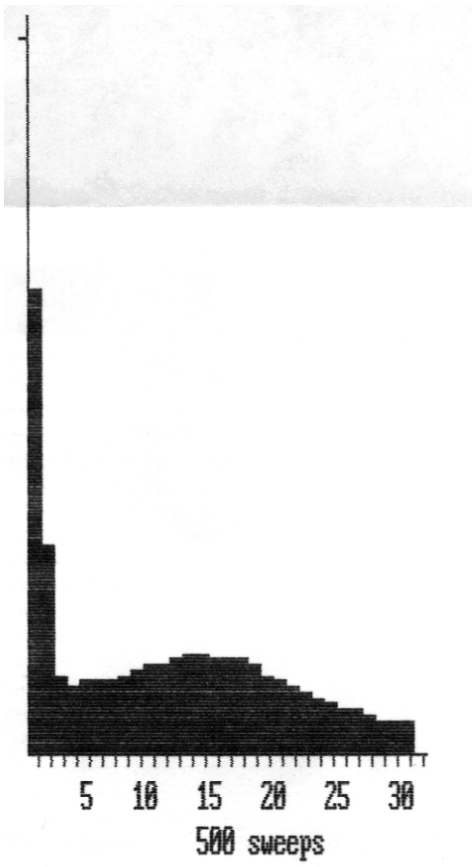

Figure III-6. Light intensity plot for the undeveloped region

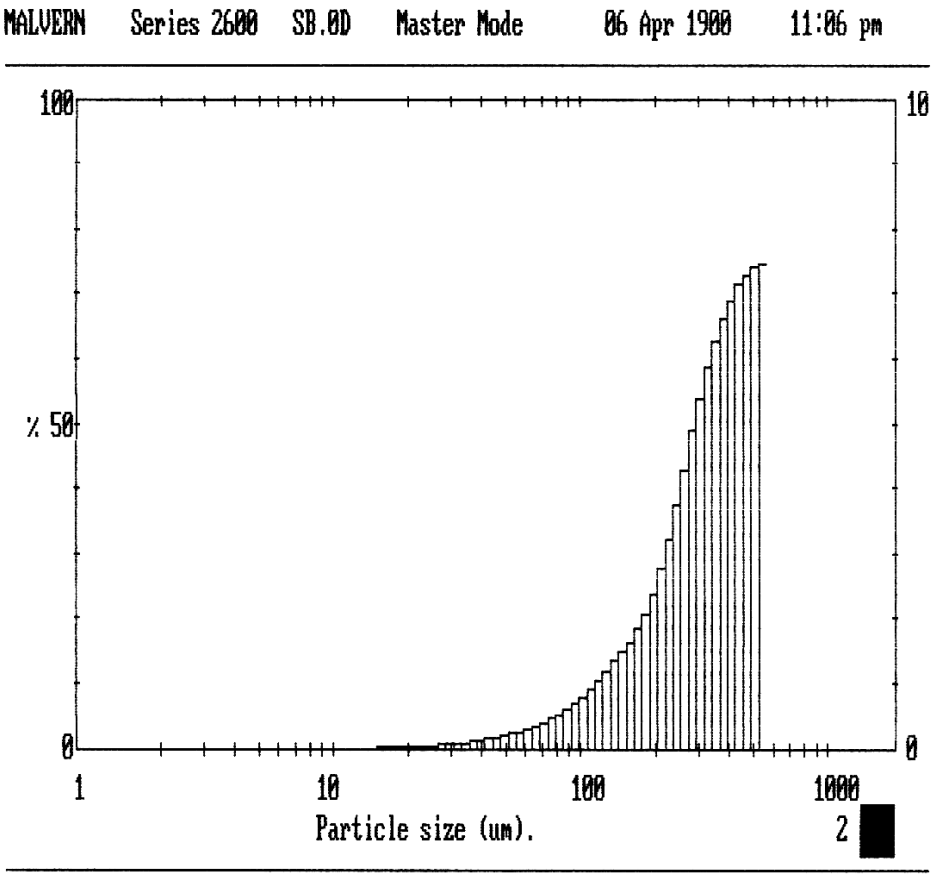

Figure III-7. Histogram for the undeveloped region of the spray

Since the Malvern analysis assumes that all diffraction is a result of spherical droplets, the output data in this region will not be an accurate representation of the true physical picture. The Malvern sees the liquid stream and ligaments as large spherical drops and hence gives a very high mean droplet diameter as its output. This result can be clearly seen on the light intensity curve, where a high intensity is observed from the

first two ring diodes, as shown in Figure III-6. This result is seen also in the drop size distribution histogram, where an incomplete bell-shaped curve is biased towards the higher drop sizes, as shown in Figure III-7.

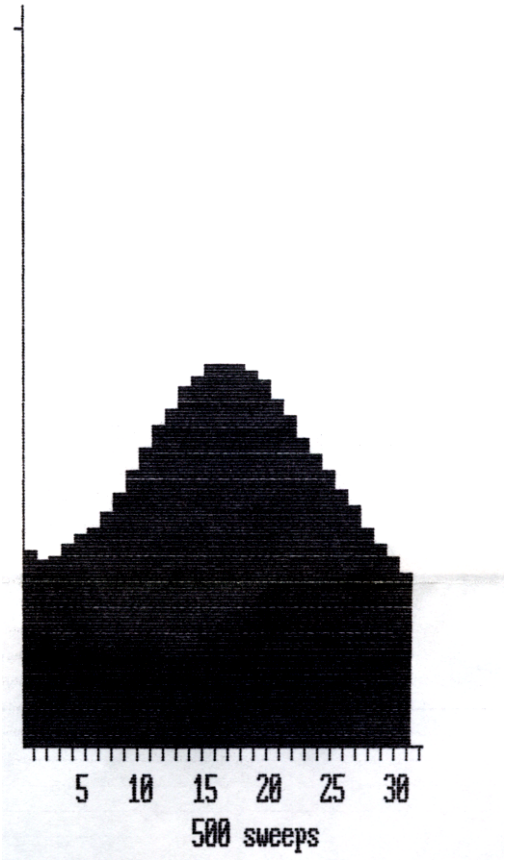

Figure III-8. Light intensity plot for the fully atomized region

The fully atomized zone is composed of a majority of spherical droplets and hence is detected as a mono-modal distribution on the light intensity curve and a complete bell shaped drop size distribution histogram. Figures III-8 and III-9 show the light intensity and drop size distribution histogram, for the fully atomized region, respectively.

The aerosol formation distance is determined by analyzing the light intensity plots and drop size distribution histograms at each measurement distance. The transition between the stream disintegration and the fully atomized zone is not distinct, but it can be approximated. In general, measurements were made at 5 cm intervals and the uncertainty about the aerosol formation distance is estimated to be $\pm$ 5 cm.

The characteristic parameter used to represent the mean drop size of the spray was the Sauter Mean Diameter (SMD). The definition of SMD and its advantages are discussed in Chapter IV. From the analysis of data at various conditions, it was found that the SMD tends to remain fairly constant in the fully atomized zone. This constancy can provide a quick estimate of the aerosol formation distance, but results must be confirmed from the histograms and the light intensity plots.

The other parameter that was used to determine the reliability of the data with respect to the Rosen Rammler distribution was Log. Diff. The criteria for interpreting the Log. Diff. values are provided in Table III-2 of this chapter. This differentiation between the regimes of atomization is very important in selecting data for modeling the atomization process.

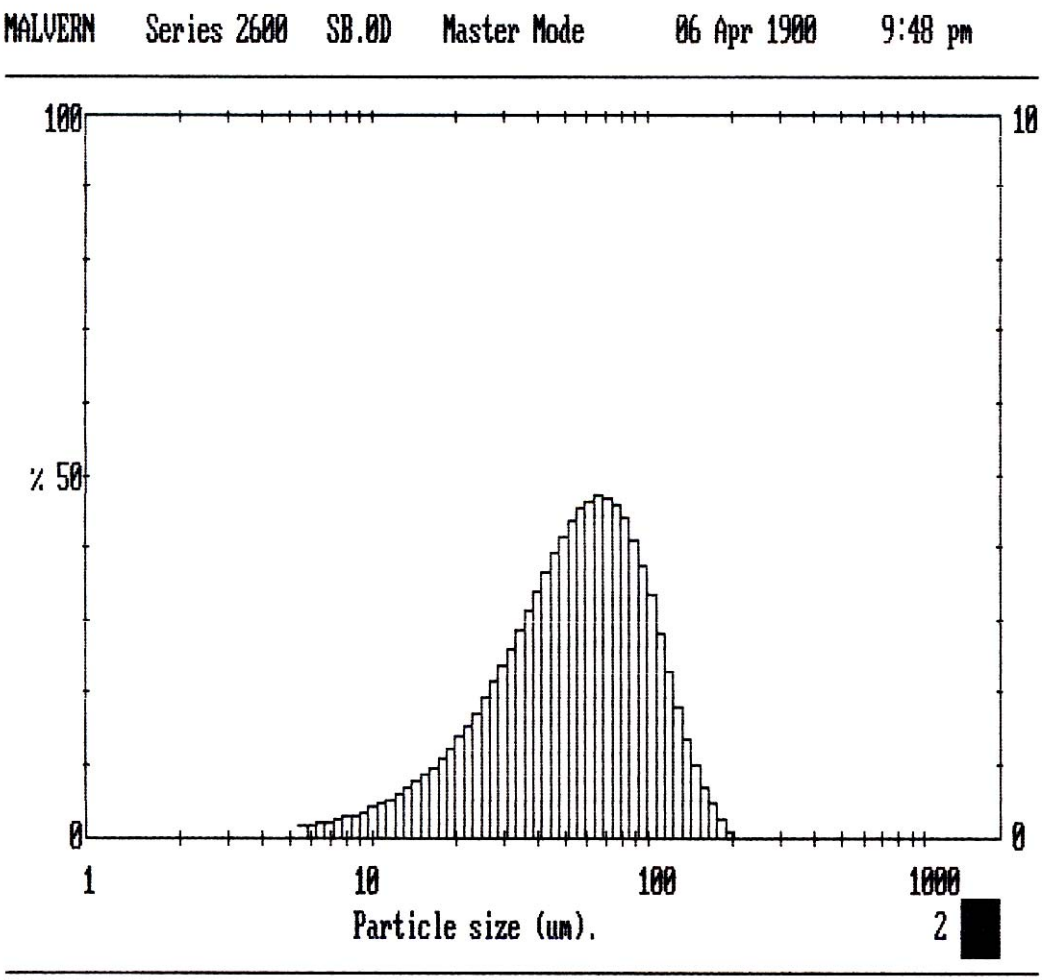

Figure III-9. Histogram for the fully atomized region

The validity of data is affected not only by the atomization regime but also by two other scenarios: high obscuration values and presence of significant amounts of HTF vapor.

Obscuration is defined as the ratio of light diffracted to the light emitted and is calculated as

$$Obscuration = 1 - \frac{Light \quad incident \quad on \quad the \quad central \quad diode}{Light \quad emitted \quad by \quad the \quad laser} \qquad \text{(III-16)}$$

When the obscuration is very high, there are a large number of droplets intersecting the laser. The highest accuracy of results is obtained for obscurations between 10% and 30%. The accuracy at about 50% is acceptable but beyond 50% the Malvern tends to yield results that are significantly biased towards the lower drop sizes. This tendency has been explained by Hamidi and Swithenbank (1986a) as resulting from multiple scattering. At the higher obscurations, because of an abundance of droplets, the probability of a light ray being diffracted by more than one droplet is high. This multiple diffraction leads to an increase in the diffraction angle and the light falling on the outer rings. The Malvern interprets this to represent a smaller drop, thereby biasing the results to indicate a smaller SMD. The Malvern system has utilized a method of correction for high obscurations developed by Hamidi and Swithenbank (1986a) to deal with this. This correction was applied to the analysis in this work by using the **correct on** function, which applies the correction to all cases where the obscuration exceeds 50%.

The other phenomenon that can compromise the reliability of the results is the presence of significant quantities of HTF vapor. HTF vapor is generally present at all injection temperatures and pressures. However as the temperature is raised closer to the flash point, the increased vapor causes significant laser beam refraction, which is known as *beam steering*. The refracted beam impinges on the rings close to the central diode. The Malvern interprets this light intensity as the contribution of large drops and biases the results towards higher drop sizes. Figures III-10 and III-11 display the effect of beam steering on the light intensity and drop size histogram.

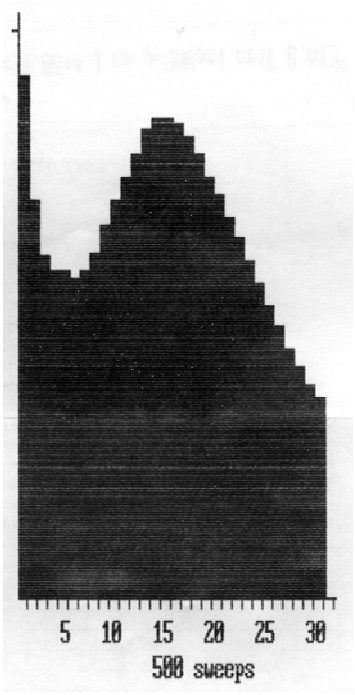

Figure III-10. Light intensity plot showing the effect of beam steering

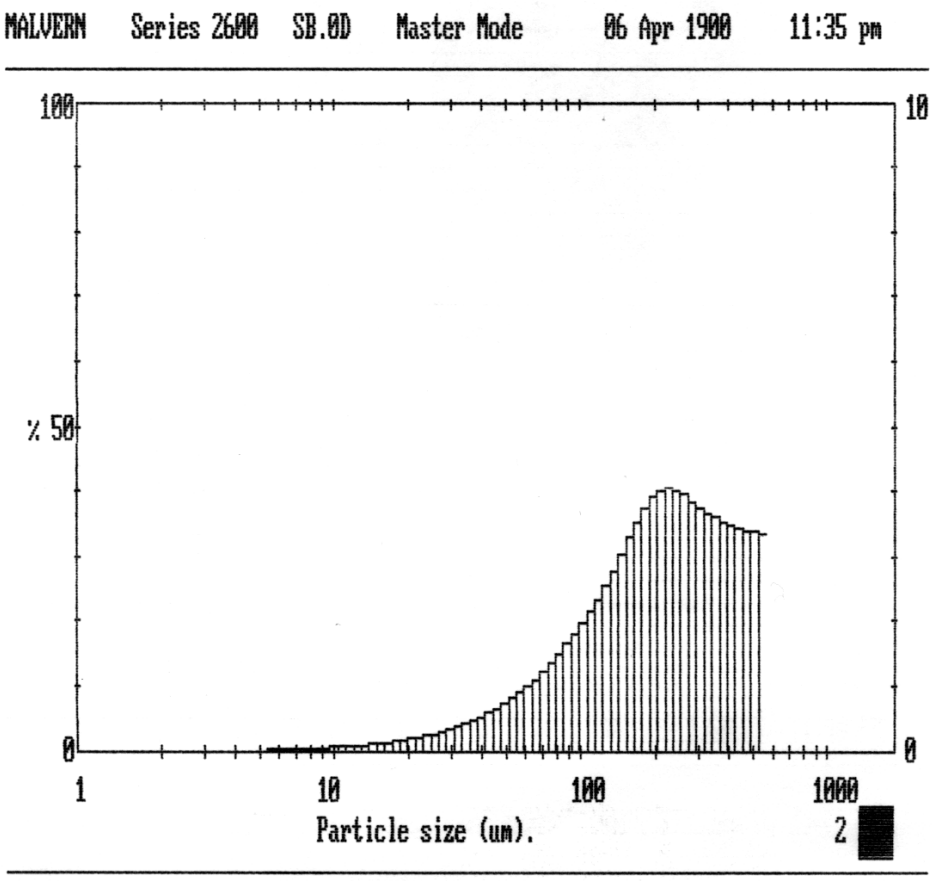

Figure III-11. Histogram showing the effect of beam steering

The results, in this case, can be recalculated by omitting the first ring diode from the calculations using the **kill data** function. This method is only an approximate solution to the effect of beam steering, because the contribution of the first ring to the true SMD is not known. Hence, SMD obtained by this method may be underestimated and should not be considered truly representative.

The volume concentrations too, must be treated in a similar manner. Only volume concentrations in the fully atomized zone, with no significant beam steering, are truly representative of reality.

These were the salient features of the analysis used for the reported data. High-speed digital photography was used also to confirm the data analysis. The effects of pressure, temperature, and orifice size on the atomization process with respect to each of the HTFs tested are discussed below.

PRELIMINARY EXPERIMENTAL OBSERVATIONS

The focus of this research was to emulate the formation of an aerosol from a HTF leak in an industrial process and to study the effects of process operating conditions, temperature and pressure, and leak sizes. A summary of the tested conditions for each fluid is presented in Figure III-12.

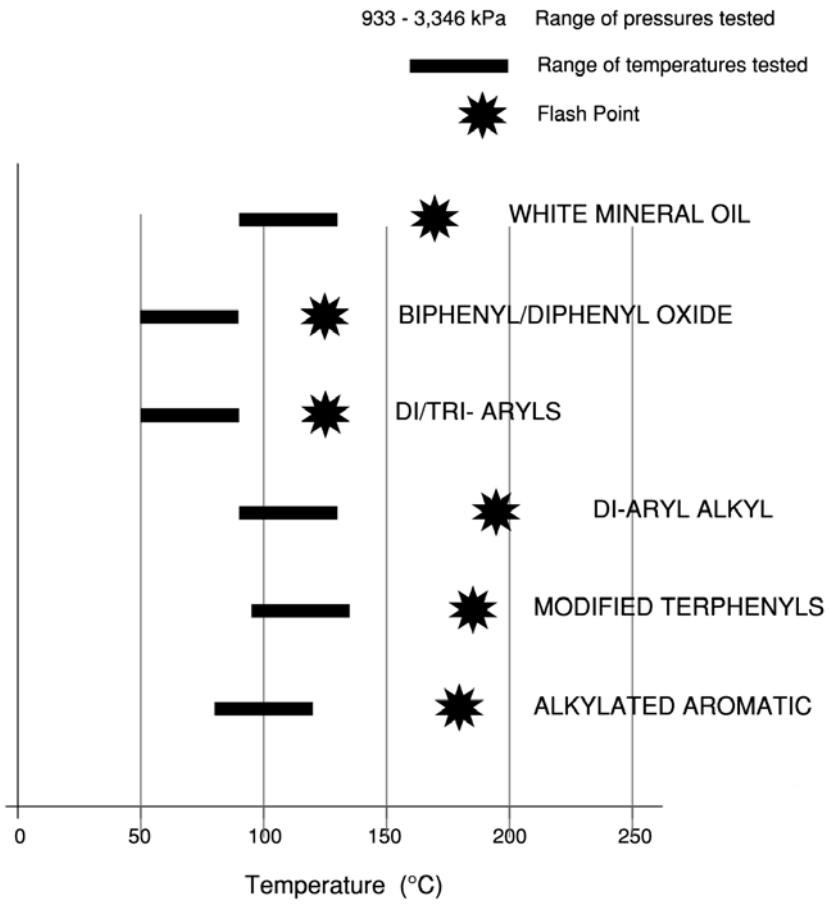

Figure III-12. Summary of the experimental conditions and flash points of the fluids tested

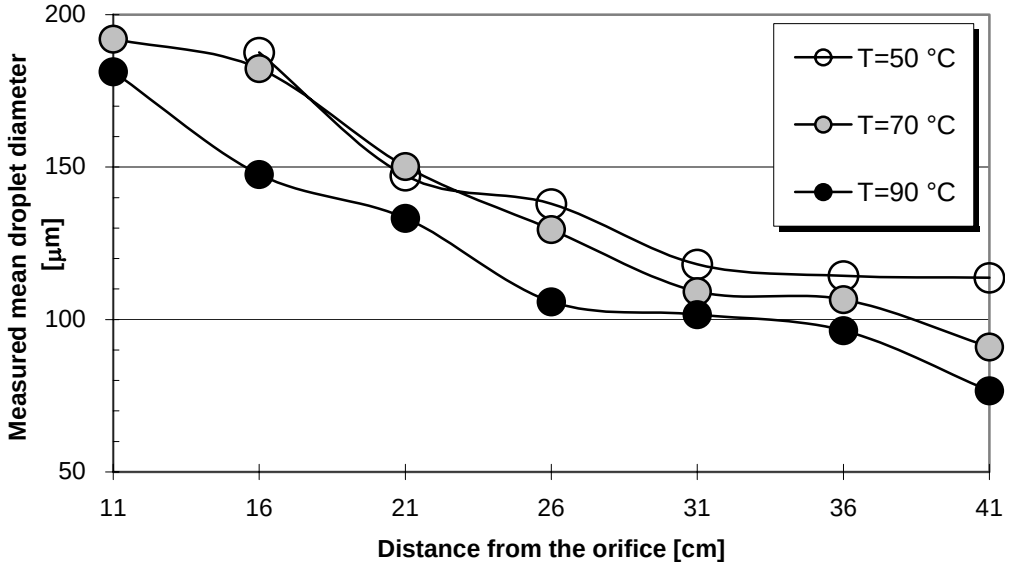

Figure III-13. The effect of temperature on the atomization of BDO, under a pressure of 1,967 kPa and through an orifice of diameter 0.38 mm

At higher temperatures, liquids have lower densities, lower viscosities, and lower surface tensions and therefore form aerosols with smaller mean droplet diameters, as shown in Figure III-13. Pressure has a more direct influence on the atomization. Higher injection pressures increase the liquid velocity, which shortens the aerosol formation distances and also produces smaller mean droplet diameters, as shown in Figure III-14. All fluids tested followed similar trends with respect to temperature and pressure.

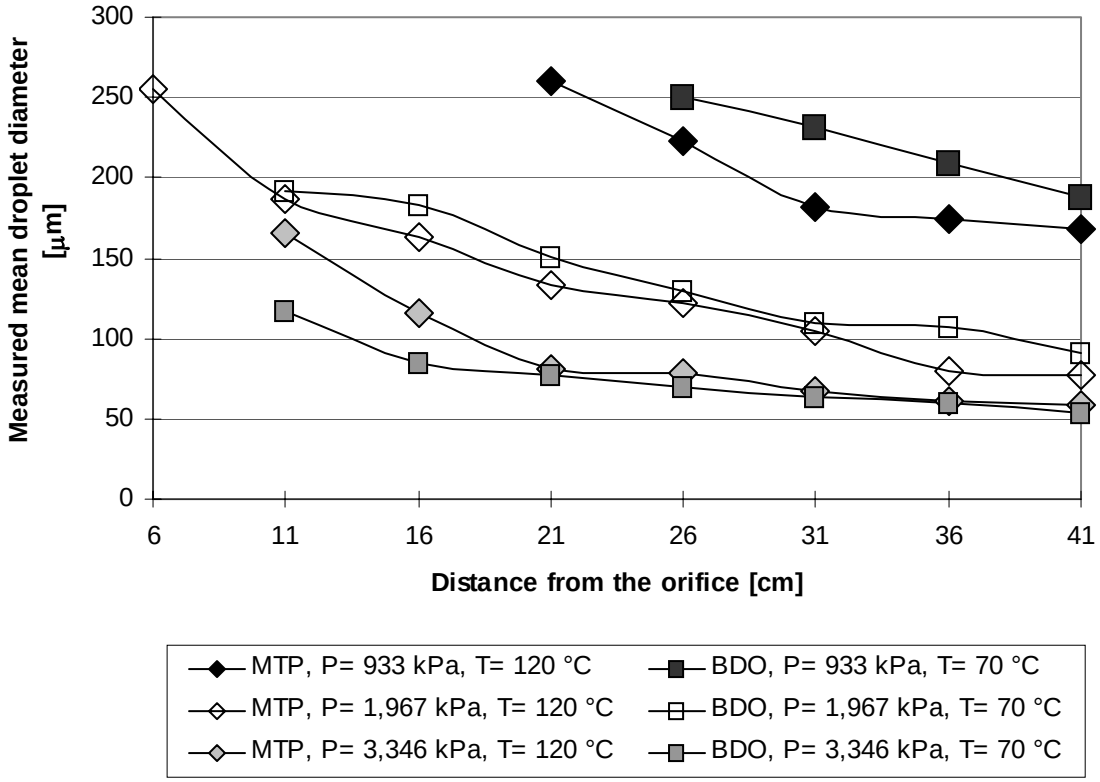

Figure III-14. The effect of injection pressure on the atomization of two heat transfer fluids through an orifice of diameter 0.38 mm
MTP (T= 120 °C); BDO (T= 70 °C)

SUMMARY OF CHAPTER III

Thus far the dependence of aerosol drop size distributions on the operating conditions has been demonstrated. The most important conclusion for process safety is that significant quantities of aerosol are formed from HTFs at conditions well below their flash points. However, there are threshold conditions below which significant amounts of aerosols were not formed in the tested ranges. Further statistical analysis, in the subsequent chapter, will reveal details about the effect of fluid properties on the aerosol formation process.

CHAPTER IV

THEORETICAL CHARACTERIZATION

The study thus far has inferred that aerosol formation behavior is dependent on the operating conditions, fluid properties, as well as the leak sizes. The experiments were carried out in a system designed to study the formation of aerosols from leaking heat transfer fluids. While these observations are critical in that they prove the existence of hazardous scenarios, the real utility of the research will be the development of empirical correlations to relate the operating conditions and liquid properties and to characterize the atomization process of HTFs. With these correlations the prediction of aerosol formation behavior *a priori* will help institute design level changes for equipment and processes that will help in managing the hazard.

This chapter describes how the data is analyzed to develop correlations to model the atomization process. Theoretical aspects of droplet statistics and regression analysis are detailed. Model development, model validation, and model testing are also included to fulfill the research objectives.

Part of this chapter is reprinted from "Predictive correlations for leaking heat transfer fluid aerosols in air" by Krishna, K., Kim, T.K., Kihm, K.D., Rogers, W.J., and Mannan, M.S., (2003). *Journal of Loss Prevention in the Process Industries, 16* (1), 1-8, Copyright 2003, with permission from Elsevier.

DROPLET STATISTICS

As the liquid is being “tortured” through the orifice, the break up of the liquid stream into the droplets is governed by both controllable and uncontrollable parameters. Process conditions such as temperature and pressure are designed into the system, choice of fluid decides the fluid properties, and for a given leak, the leak geometry is fixed. Near orifice liquid turbulence and liquid stream vibrations are some of the uncontrollable parameters that make the drop size characterization on the basis of a disintegration mechanism, itself, unfeasible. The resulting effect is that we end up with a distribution of droplet sizes, giving the atomization process a statistical character. It is therefore important to study the statistics of droplet characterization with the idea of characterizing the randomness of the atomization process.

In any statistical set of droplets, with the variable D as the droplet diameter, the distribution of droplet diameters results in a spectrum of drop sizes. The number of droplets Δn_i, corresponds to the diameter range $\left\langle D_i - \frac{\Delta D}{2}, D_i + \frac{\Delta D}{2} \right\rangle$, and the diameter D_i, corresponds to the center of the ith range, with ΔD as the constant width of the range. Aerosol measurement is done on a discrete basis and the size of the range depends on the method of measurement and the required accuracy.

The total number of droplets is given by

$$N = \sum_{i=1}^{m} \Delta n_i \qquad \text{(IV-1)}$$

where *m* is the total number of diameter ranges. We can also define the number fraction of the droplets in a given range.

$$\Delta\bar{n}_i = \frac{\Delta n_i}{N} \tag{IV-2}$$

A histogram depicts the number fraction of droplets $\Delta\bar{n}_i$ that corresponds to each diameter range. The cumulative total of the heights of all the fractions is equal to 100%. The histogram can be replaced by a continuous curve representing the frequency or the probability density of the number fraction of a certain droplet diameter, and is referred to as the number distribution curve (Figure IV-1).

We can also treat the diameter D as a continuous function with a range from zero to infinity, and thereby define the function of the number density.

$$f_n(D) = \frac{d\bar{n}}{dD} = \frac{dn/dD}{\int_0^\infty (dn/dD)dD} \tag{IV-3}$$

The cumulative distribution function of *D* is given by

$$F_n(D) = \int_0^D f_n(D)dD = \frac{\int_0^D (dn/dD)dD}{\int_0^\infty (dn/dD)dD} \tag{IV-4}$$

and represents the total number of droplets below the droplet diameter *D*. This function is depicted in Figure IV-2, and shows that the function has a maximum value of 100%.

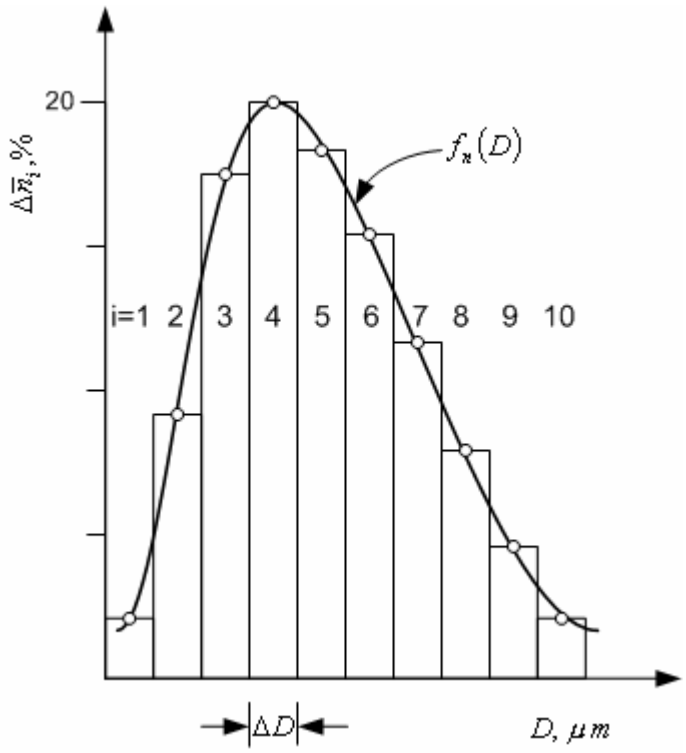

Figure IV-1. Droplet size distribution curve

Experimental size distributions of droplets formed by the atomization process can be approximated by various equations used to describe the functions $f_n(D)$ and $F_n(D)$. The most commonly used distributions are the Rosin-Rammler, the Nukiyama-Tanasawa, and the lognormal distribution equations. These equations are two-parameter equations and are used to calculate droplet statistics like mean droplet diameters.

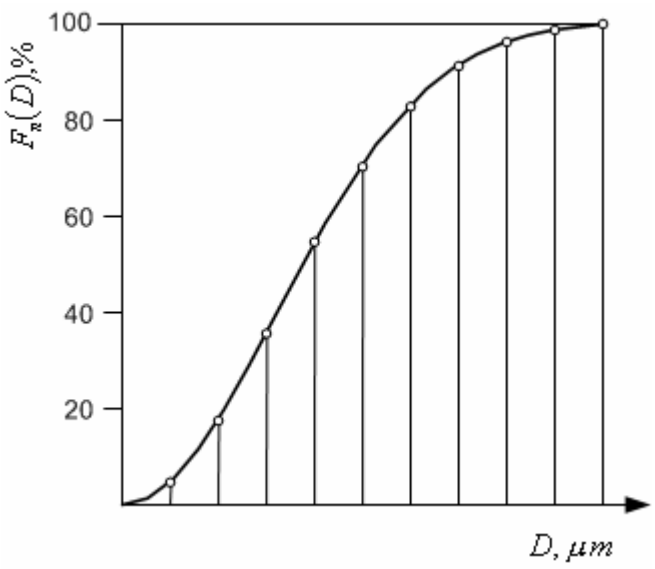

Figure IV-2. Cumulative droplet size distribution curve

The Rosen-Rammler distribution is a cumulative mass or volume distribution function

$$F_3(D) = 1 - \exp\left[-\left(\frac{D}{X}\right)^{\delta}\right] \qquad \text{(IV-5)}$$

where F_3 is the cumulative droplet volume present in the droplets of diameter less than *D*, and the two descriptive parameters of the Rosin-Rammler distribution *X* and δ are the size parameter and the spray uniformity (distribution) parameter.

The significance of the Rosin-Rammler distribution parameters is depicted in Figure IV-3. In Figure IV-3a, the variation of *X* for a given δ is shown. The value of *X*

can be determined from equation IV-5 by taking $D = X$. This implies that $D/X = 1$, and therefore $F_3(D) = 1 - e^{-1} = 0.632$. Hence X corresponds to the value of D for a cumulative frequency of 63.2% or 63.2% of the volume of the atomized liquid is present in droplets with diameters smaller than X.

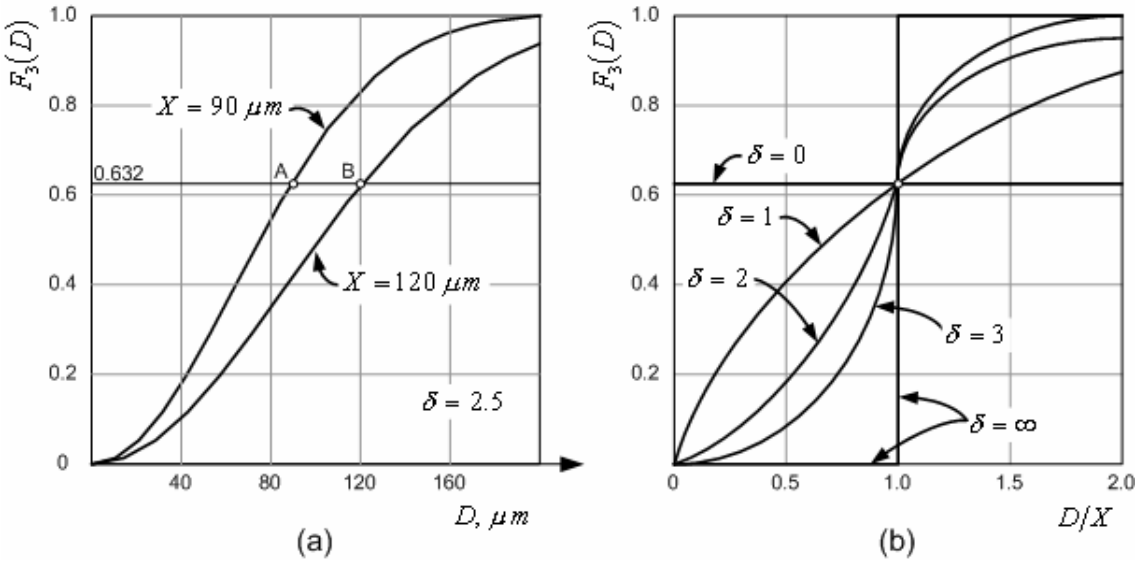

Figure IV-3. Interpretation of Rosin-Rammler distribution parameters

For the same value of X, the variation of the distribution with respect to δ is shown in Figure IV-3(b). A higher value of δ represents greater uniformity of the droplet size distribution. Atomization generally produces aerosols with δ values in the range of 2 to 4.

Differentiating equation IV-5 yields the volume distribution function $f_3(D)$:

$$f_3(D) = \frac{d\,F_3(D)}{dD} = \frac{\delta}{X^{\delta}} D^{\delta-1} \exp\left[-\left(\frac{D}{X}\right)^{\delta}\right] \tag{IV-6}$$

Additionally, all other statistical parameters can be derived from equation IV-5.

The Nukiyama-Tanasawa distribution represents a droplet number distribution:

$$f_0(D) = \frac{d\overline{n}}{dD} = BD^2 \exp(-bD^{\delta}) \tag{IV-7}$$

where *B* is a constant, *b* is the distribution size parameter, and δ is the distribution parameter. This distribution is cumbersome to use since it requires the estimation of constant B in addition to the two distribution parameters.

The lognormal distribution equation represents a volume distribution of droplets.

$$f(y) = \frac{d\overline{V}}{dy} = \frac{h}{\sqrt{\pi}} \exp\left(-h^2 y^2\right) \tag{IV-8}$$

where $d\overline{V}$ is the volume fraction of droplets in a given range, $y = \ln\left(D/\overline{D}\right)$, given by $D = \overline{D}e^{y}$, *h* is the mean standard deviation of *y*, and $\overline{D}$ is the mean droplet diameter.

Of the three distributions described here, the Rosin-Rammler distribution is found to describe droplet distribution best for the atomization process. The simple form of the distribution with its two parameters that can be easily determined graphically, make this a popular choice for utilization in the area of spray characterization. This

work uses the Rosin-Rammler distribution to characterize the droplet size distributions of the aerosols generated.

MEAN DROPLET DIAMETERS

The most informative quantity used to describe a distribution of droplets in an aerosol is the mean droplet diameter. Depending on the way it is calculated, it can provide information about the various characteristics of the aerosol: number, diameter, surface, and volume of droplets. The mean droplet diameter does not provide information about the distribution itself. It is very useful in engineering calculations of droplet motion, as well as transport processes like heat and mass transfer.

The generalized definition of the mean droplet diameter is given by:

$$D_{pq} = \sqrt[p-q]{\frac{\sum_{i=1}^{m} D_i^p \, \Delta n_i}{\sum_{i=1}^{m} D_i^q \, \Delta n_i}} \qquad \text{(IV-9)}$$

where p and q are the parameters used depending on the type of mean diameter required as shown in Table IV-1.

The simplest form, the arithmetic mean diameter D_{10}, is the diameter of a uniform equivalent set of droplets whose sum of diameters is equal to the sum of droplet diameters of the real set of droplets. This can be visualized in Figure IV-4, where the 10 droplets with varying diameters have been replaced by 10 equi-diameter droplets.

Table IV-1. Mean droplet diameters

(Adapted from Bayvel and Orzechowski, 1993)

		Mean diameter		
p	*q*	Symbol	Name	Application
1	0	D_{10}	Arithmetic	Comparison of disperse systems
2	0	D_{20}	Surface	Surface area control, surface phenomena, e.g., absorption, vaporization
3	0	D_{30}	Volume	Volume control, volumetric phenomenon
2	1	D_{21}	Relative surface	Drop disintegration, absorption
3	1	D_{31}	Relative volume, Probert's	Evaporation, molecular diffusion, combustion
3	2	D_{32}	Volume-surface, Sauter's	Drop range, mass transfer, heat transfer, combustion, dispersion
4	3	D_{43}	Mass, de Brouckere's or Herdan's	Drop fractionation, combustion

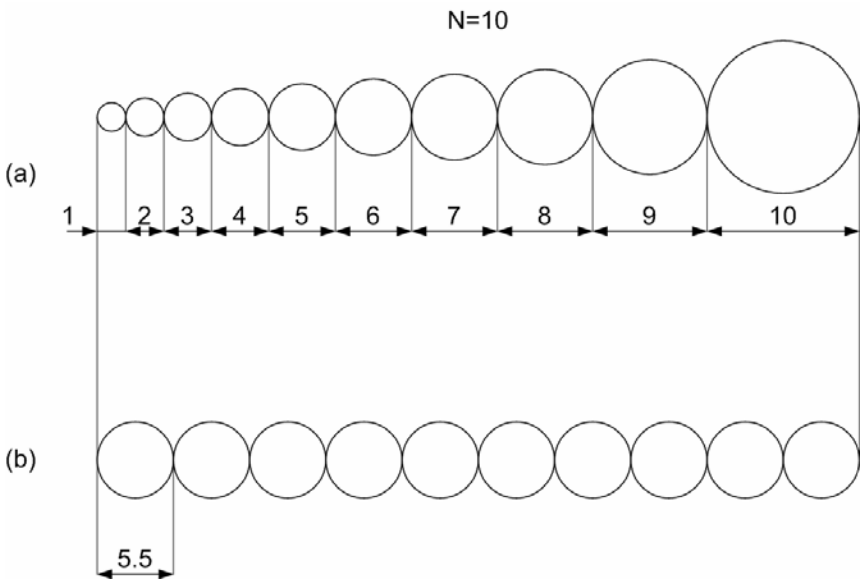

Figure IV-4. Representation of the arithmetic mean droplet diameter of a non-uniform set of droplets

The set (a) consists of 10 droplets with diameters from 1 to 10, having a sum of diameters of 55. Therefore the arithmetic mean droplet diameter is 5.5. From equation 2-9, using p=1 and q=0, we have the expression for the arithmetic mean droplet diameter.

$$D_{10} = \frac{\sum D\,\Delta n}{\sum \Delta n} \qquad \text{(IV-10)}$$

The surface area mean diameter, D_{20}, is the diameter of a uniform equivalent set of droplets whose sum of surface areas is equal to the sum of droplet surface areas of the real set of droplets.

$$D_{20} = \frac{\sum D^2 \Delta n}{\sum \Delta n} \tag{IV-11}$$

The volume mean diameter, D_{30}, is the diameter of a uniform equivalent set of droplets whose sum of volumes is equal to the sum of droplet volumes of the real set of droplets.

$$D_{30} = \frac{\sum D^3 \Delta n}{\sum \Delta n} \tag{IV-12}$$

The relative surface diameter, D_{21}, is the droplet diameter of a uniform equivalent set with the same sum of diameters and the same total surface area of droplets as the real set.

$$D_{21} = \frac{\sum D^2 \Delta n}{\sum D \Delta n} \tag{IV-13}$$

The ultimate aim, in this research, is for drop size data to be utilized in determining the flammability limits of aerosols. Hence the most applicable diameter is the Sauter Mean Diameter (SMD).

The Sauter Mean Diameter or the volume-to-surface-area mean diameter is the diameter of a uniform set of equivalent droplets with the same total volume and the surface of all droplets as in the real set.

$$D_{32} = SMD = \frac{\sum D^3 \Delta n}{\sum D^2 \Delta n} \tag{IV-14}$$

The SMD is generally the most commonly used mean diameter statistic, because it can be used to characterize important processes such as droplet penetration or heat and mass transfer.

The penetration of droplets is a measure of the ratio of the forces of inertia to the forces of aerodynamic drag.

$$D_{32} \approx \frac{\sum \rho_L \left(\pi D^3/6\right) a \, \Delta n}{\sum C_D \left(\pi D^2/4\right)\left(\rho_G V^2/2\right)\Delta n} \tag{IV-15}$$

where ρ_L and ρ_G are the densities of the liquid and ambient air, respectively, and a is the droplet acceleration.

The heat transfer between droplets and the ambient air can be measured as the ratio of the heat necessary to raise the temperature of the droplet by ΔT_{RISE} to the heat transferred from the surrounding air at a temperature gradient of ΔT_{GRAD}.

$$D_{32} \approx \frac{\sum c_L \, \rho_L \left(\pi D^3/6\right) \Delta T_{RISE} \, \Delta n}{\sum \alpha \, \pi \, D^2 \, \Delta T_{GRAD} \, \Delta n} \tag{IV-16}$$

where c_L is the specific heat capacity of the liquid, and α is the thermal conductivity.

The mass transfer between the droplets and the air can be represented as the ratio of the mass of the droplets to the evaporation rate per unit time.

$$D_{32} \approx \frac{\sum \rho_L \left(\pi D^3/6\right) \Delta n}{\sum \pi D^2 \beta \left(C_0 - C\right) \Delta n} \tag{IV-17}$$

where β is the mass exchange coefficient and C *and* C_0 represent the ambient gas concentration far away and at the droplet surface respectively.

Table IV-2 lists the mean droplet diameters for the case shown in Figure IV-4. While applying any particular mean droplet diameter, it is important to understand the meaning of that particular mean diameter and its implications on the application. As seen in Table IV-2, the choice of mean diameter can considerably vary the numerical value.

Table IV-2. Mean droplet diameters based on Figure IV-4

Mean diameter symbol	D_{10}	D_{20}	D_{30}	D_{21}	D_{31}	D_{32}	D_{43}
Diameter value	5.50	6.20	6.71	7.00	7.42	7.86	8.37

Because of the numerous droplet sizes, it is more convenient to use statistical distributions that approximate the drop size distribution of the spray. As mentioned earlier the distribution used in this research is the Rosin-Rammler distribution. The general equation for mean diameters can be written as:

$$D_{pq} = \sqrt[p-q]{\frac{\int_0^\infty D^p \left(d\bar{n}/dD\right)dD}{\int_0^\infty D^q \left(d\bar{n}/dD\right)dD}} \qquad \text{(IV-18)}$$

Converting this to a volume distribution

$$D_{pq} = \sqrt[p-q]{\frac{\int_0^\infty D^{p-3}\left(d\overline{V}/dD\right)dD}{\int_0^\infty D^{q-3}\left(d\overline{V}/dD\right)dD}} \qquad \text{(IV-19)}$$

Integrating equation (IV-19) we get the relation for the SMD in terms of the two-parameter Rosin-Rammler model

$$D_{pq} = X\sqrt[p-q]{\frac{\Gamma\left[\left(p-3\right)/\delta+1\right]}{\Gamma\left[\left(q-3\right)/\delta+1\right]}} \qquad \text{(IV-20)}$$

For the Sauter Mean Diameter, where *p=3* and *q=2*, we have

$$D_{32} = \frac{X}{\Gamma\left(1-1/\delta\right)} \qquad \text{(IV-21)}$$

where X and δ are the two parameters of the Rosin-Rammler model.

LIQUID DISCHARGE THROUGH AN ORIFICE

The process of atomization begins with the discharge of the fluid through the orifice, due to an adequate pressure drop ΔP, where $\Delta P = P_1 - P_2$ is the pressure drop across the orifice (Figure IV-5).

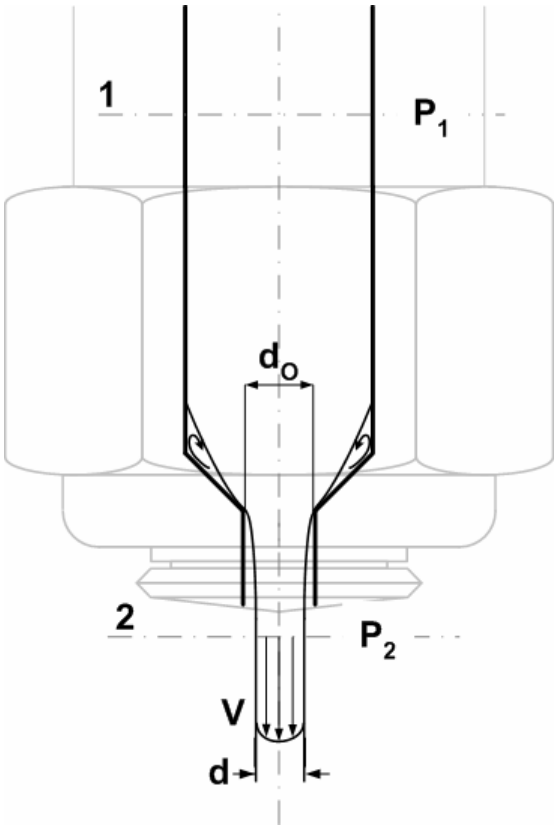

Figure IV-5. Discharge through an orifice

Applying Bernoulli's equation for the cross section 1 before the orifice and cross section 2 after the orifice, we have

$$\frac{\rho V_1^2}{2} + P_1 = \frac{\rho V_2^2}{2} + P_2 \qquad \text{(IV-22)}$$

Therefore,

$$V = V_2 = \sqrt{\frac{2(P_1 - P_2)}{\rho} + V_1^2} \approx \sqrt{\frac{2\,\Delta P}{\rho}} \qquad \text{(IV-23)}$$

since velocity V_1 is usually very small when compared to velocity V_2. The velocity determined in equation (IV-23) is the theoretical liquid velocity. The volumetric flow rate is given by

$$Q = C_D\, A_O\, V = C_D\, A_O \sqrt{\frac{2\,\Delta P}{\rho}} \tag{IV-24}$$

and the mass flow rate is given by

$$G = \rho Q = C_D\, A_O \sqrt{2\,\rho\,\Delta P} \tag{IV-25}$$

where C_D is the ratio of the actual to the theoretical discharge rate, known as the coefficient of discharge, and $A_O = \pi\, d_O^2 / 4$ is the cross section area of the orifice of diameter d_O.

The coefficient of discharge is determined experimentally and it depends on the Reynolds number. For large Reynolds numbers the value of the coefficient of discharge remains constant.

COEFFICIENT OF DISCHARGE

The coefficient of discharge (CD) of the orifices used was very important in determining the true velocity of the liquid stream being ejected from the orifice. The CD had to be determined at a wide range of velocities ranging from the laminar to the turbulent region. Estimation of the CD was done using a combination of measurements and empirical correlations.

Asihmin et al. (1961) have a correlation for CD values over a wide range of Reynolds numbers: 100 to 1.5*105; and for l_0/d_0 (Figure IV-6) in the range 2 to 5 and claim an accuracy of 1.5%.

$$C_D = \left[1.23 + \frac{58(l_0 / d_0)}{\mathrm{Re}}\right]^{-1} \qquad \text{(IV-26)}$$

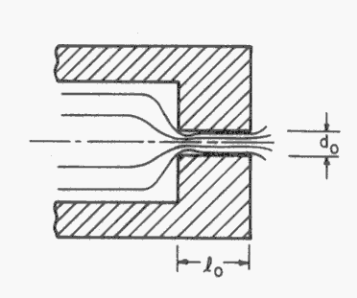

Figure IV-6. Characteristic dimensions of a plain orifice

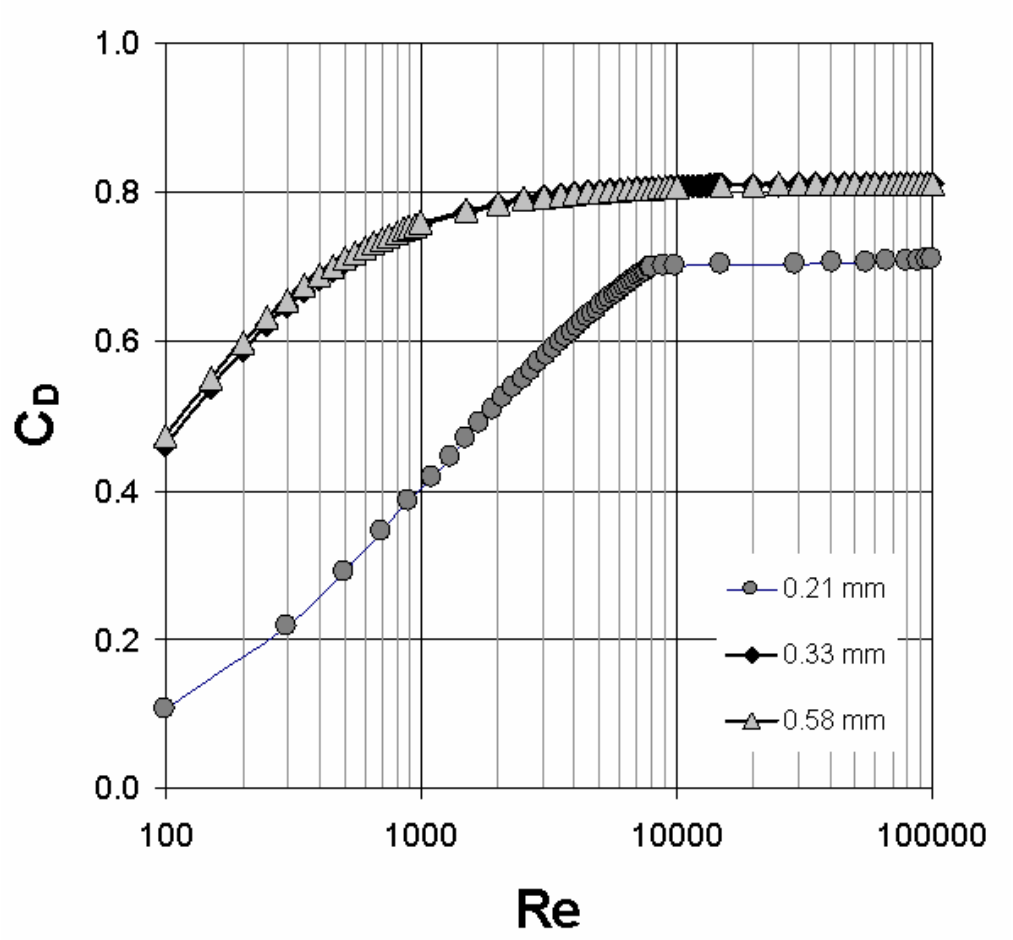

Figure IV-7. Variation of C_D with Reynolds Number (Re)

For the 0.38 mm and the 0.58 mm orifices, the C_D values are calculated using this formula. The results are plotted in Figure IV-7.

For l_0/d_0 (Figure IV-6) in the range 1.5 to 17 and Reynolds numbers in the range 550 to 7000, Nakayama (1961) provides the following correlation with accuracy within 2.8%:

$$C_D = \frac{\mathrm{Re}^{5/6}}{17.11 l_0 / d_0 + 1.65\,\mathrm{Re}^{0.8}} \qquad \text{(IV-27)}$$

This correlation was used to estimate the CD value for the 0.21 mm orifice, which is plotted in Figure IV-7.

DATA ANALYSIS

Atomization is the process by which aerosol is produced. Here, atomization is induced by forcing the liquid through a small orifice to emulate a leak in a process system. The liquid stream upon leaving the orifice is destabilized by the friction forces between the air and the liquid surface. These aerodynamic forces cause disturbances in the surface of the stream. If these disturbances are large enough to overcome the surface energy of the stream, the stream breaks up. This break-up results in the formation of non-spherical segments known as ligaments, which break-up further until they are small enough to form stable spherical droplets.

The atomization process is easily distinguishable into three zones as indicated in Figure IV-8: AB represents the compact stream, BC the disintegration zone, and CD the fully atomized zone.

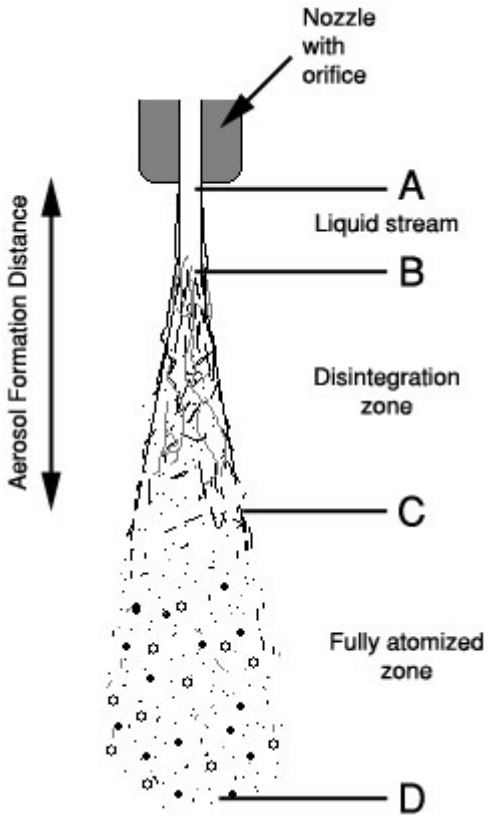

Figure IV-8. Atomization of a liquid stream

Stream atomization can be characterized by the dependence of droplet diameter on the droplet Weber number, We_D, which relates the shear forces that contribute to the stream breakup to the surface tension forces holding the stream together. $We_D = \frac{\rho_G V^2 D}{\sigma}$, where ρ_G is the air density, V is the initial velocity of the exiting liquid stream, D is the droplet diameter, and σ is the fluid surface tension (Ohnesorge, 1936). V was determined as a function of the pressure drop across the orifice (ΔP) and

the co-efficient of discharge (C_D) of the orifice, both of which were measured, as well as liquid density (ρ_L).

$$V = C_D \sqrt{\frac{2\Delta P}{\rho_L}} \tag{IV-28}$$

High Weber numbers indicate the dominance of shear forces over surface tension forces such that the stream is unstable and is breaking up. Low Weber numbers indicate that surface tension forces dominate, and the stream is stable because either the velocity is too low to induce breakup or much of the stream has already atomized into stable droplets (CD). The critical Weber number range between the stable steam or droplet region and the atomization region was estimated to be 12 to 22 by Johnson & Woodward (1998). This range is consistent with the data, as shown in Figure IV-9, where the critical Weber number determined from measurements is between 11 and 16. The maximum estimated uncertainty associated with the droplet Weber number is ± 10.5 %.

It is important to note that the HTF fluid properties have been listed in Appendices B and G, and air properties are obtained from Vasserman et al. (1966)

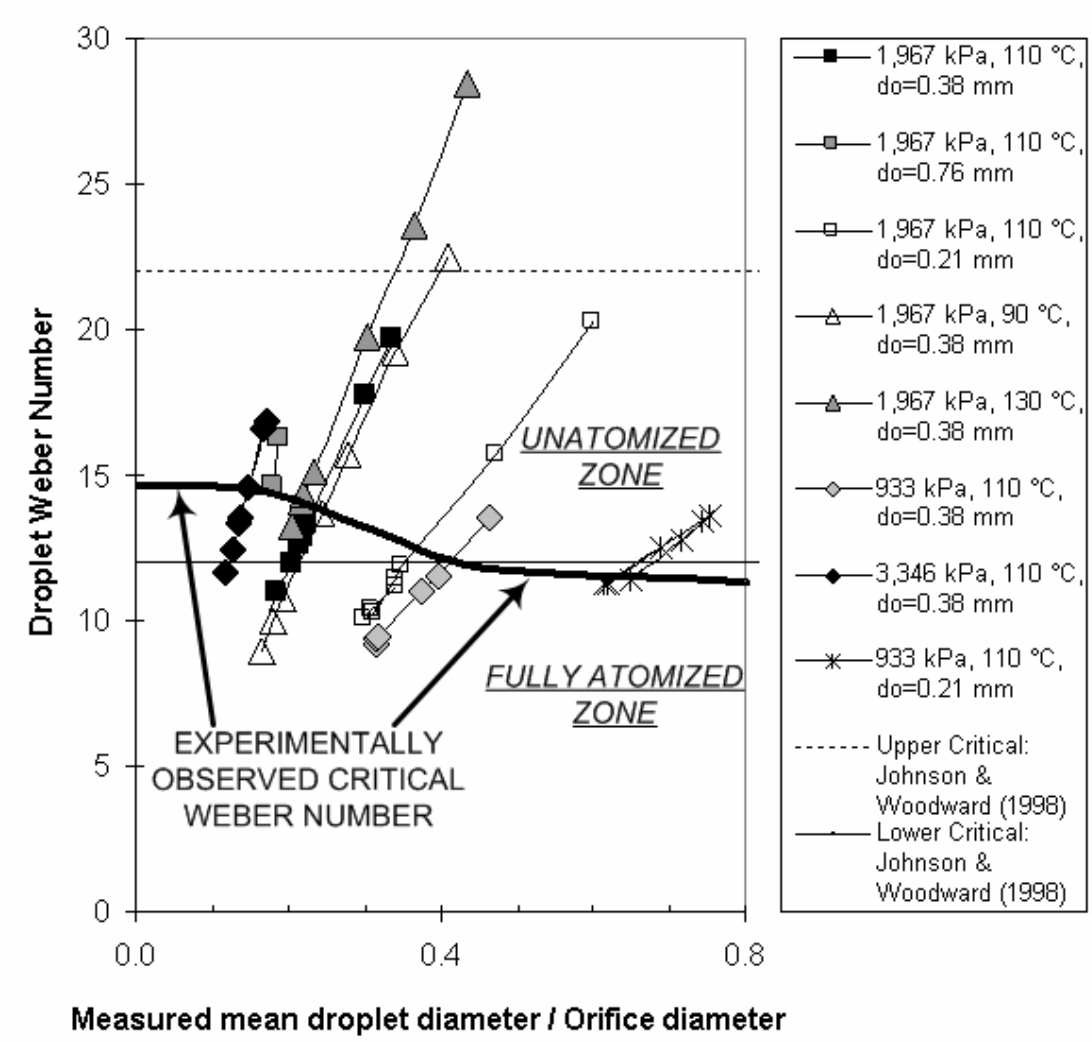

Figure IV-9. Analysis of droplet Weber number vs. measured mean droplet diameter / orifice diameter for WMO (white mineral oil) at various injection pressures, temperatures, and orifice diameters (d_0)

DIMENSIONAL ANALYSIS

With the data following established trends, the next step involves predictive correlations relating the mean aerosol droplet diameter to the injection conditions and

fluid properties. Modeling of the atomization process is very important in fuel combustion, where the fuel is generally sprayed before it is ignited to increase the combustion efficiency. A vast amount of research in this regard has confirmed that droplet diameter is the most important parameter of combustion efficiency. To circumvent the fact that no theory could completely and accurately describe the atomization process, various methods were adopted to describe quantitatively the atomization process. Dimensional analysis is the most popular quantitative method used, because the use of dimensionless groups decreases the number of experiments required to obtain an empirical expression. The resulting expression is based on experimental data and is therefore readily applicable to the system. Elkotb (1982), Park, et al. (1996), Bayvel and Orzechowski (1993), and Kihm and Chigier (1991) have provided analyses of the important parameters to characterize the atomization process.

The operating conditions, temperature and pressure, and the orifice diameter are the parameters that must be related to the mean aerosol droplet diameter. The temperature mainly affects the physical properties of the fluid, which in turn affect the atomization process. Pressure however has a direct influence on the atomization process. Higher pressures result in higher spray velocities and an increased shear at the liquid-air interface, which magnifies the instabilities on the liquid stream, causing a more rapid and effective atomization.

Parameters that are important to the atomization process are:

D Aerosol mean droplet diameter

d_0 Orifice diameter

X Axial distance from the orifice

V Initial velocity of the exiting liquid stream

σ Liquid surface tension

ρ_L Liquid density

ρ_G Gas (air) density

μ_L Dynamic liquid viscosity

μ_G Dynamic gas (air) viscosity

The mean droplet diameter used in this study is the Sauter Mean Diameter (SMD), which is the diameter of a uniform set of equivalent droplets with the same total volume and the surface of all droplets as in the real set.

$$D = SMD = \frac{\sum D_n^{\,3} \Delta n}{\sum D_n^{\,2} \Delta n} \tag{IV-29}$$

where Δn is the number of droplets of diameter D_n.

The basis of dimensional analysis is the selection of the dimensionless parameters by combining the above parameters (Bayvel and Orzechowsky, 1993).

$$D, d_0, X, V, \sigma, \rho_L, \rho_G, \mu_L, \mu_G \tag{IV-30}$$

All of these parameters can be described by a maximum of three units: M (mass), L (length), and T (time). From this list of eight parameters, we designate three

parameters, d_0, V, and ρ_G, as basic parameters, which contain all three units among them. The next step is to group each of the five remaining parameters with all three basic parameters raised to unknown powers. Each of these groups is a dimensionless parameter, which is determined from the powers on the basic parameters. A function, f, which includes all the dimensionless parameters, is then

$$f(\Pi_1, \Pi_2, \Pi_3, \Pi_4, \Pi_5, \Pi_6) = 0 \quad \text{(IV-31)}$$

where

$$\Pi_1 = D \quad d_0^{a1} V^{b1} \rho_G{}^{c1} \quad \text{(IV-32)}$$

$$\Pi_2 = \sigma \quad d_0^{a2} V^{b2} \rho_G{}^{c2} \quad \text{(IV-33)}$$

$$\Pi_3 = \mu_L \quad d_0^{a3} V^{b3} \rho_G{}^{c3} \quad \text{(IV-34)}$$

$$\Pi_4 = \mu_G \quad d_0^{a4} V^{b4} \rho_G{}^{c4} \quad \text{(IV-35)}$$

$$\Pi_5 = \rho_L \quad d_0^{a5} V^{b5} \rho_G{}^{c5} \quad \text{(IV-36)}$$

$$\Pi_6 = X \quad d_0^{a6} V^{b6} \rho_G{}^{c6} \quad \text{(IV-37)}$$

The condition that will make each Π dimensionless is for the right hand side of Equations IV-30 to IV-35 also to be dimensionless. From this criterion, the powers can be determined. Examining Equation IV-30 for unit L:

$$0 = 1 + a1 + b1 + c1$$

for unit M:

$$0 = c1$$

for unit T:

$$0 = -b1$$

Therefore,

$$a1 = -1$$

$$b1 = 0$$

$$c1 = 0$$

and hence

$$\Pi_1 = D\, d_0^{-1}$$

A similar analysis for the other dimensionless parameters yields the complete set of criteria.

$$\Pi_1 = \frac{D}{d_0} \tag{IV-38}$$

$$\Pi_2 = \frac{\sigma}{\rho_G V^2 d_0} \tag{IV-39}$$

$$\Pi_3 = \frac{\mu_L}{\rho_G V d_0} \tag{IV-40}$$

$$\Pi_4 = \frac{\mu_G}{\rho_G V d_0} \tag{IV-41}$$

$$\Pi_5 = \frac{\rho_L}{\rho_G} \tag{IV-42}$$

$$\Pi_6 = \frac{X}{d_0} \tag{IV-43}$$

We can replace Π_3 by Π_3':

$$\Pi_3' = \frac{\Pi_3^2}{\Pi_2 \Pi_5} = \frac{\mu_L^2}{\rho_L \sigma\, d_0} \tag{IV-44}$$

and Π_4 by Π_4':

$$\Pi_4' = \frac{\Pi_3}{\Pi_4} = \frac{\mu_L}{\mu_G} \tag{IV-45}$$

Substituting these values, equation IV-29 becomes

$$\frac{D}{d_0} = f\left(\frac{\rho_G V^2 d_0}{\sigma}, \frac{\rho_L \sigma\, d_0}{\mu_L^2}, \frac{\mu_L}{\mu_G}, \frac{\rho_L}{\rho_G}, \frac{X}{d_0}\right) \tag{IV-46}$$

or

$$\frac{D}{d_0} = f\left(We, Lp, \frac{\mu_L}{\mu_G}, \frac{\rho_L}{\rho_G}, \frac{X}{d_0}\right) \tag{IV-47}$$

Physical Significance

The Weber number (*We*) represents the effect of external forces on the droplet development and stream break up and is the ratio of the dynamic forces, contributed by the ambient air, to the surface tension. A higher Weber number indicates a dominance of the dynamic forces with break up of the stream.

$$We = \frac{\rho_G V^2 d_0}{\sigma} \tag{IV-48}$$

The Laplace number (*Lp*) represents the contribution of the liquid properties to the atomization process and is the ratio of the surface tension forces to the viscous forces within the liquid.

$$Lp = \frac{\rho_L \sigma\, d_0}{\mu_L^2} \tag{IV-49}$$

The density ratio, $\left(\frac{\rho_L}{\rho_G}\right)$, denotes the ratio of the liquid density to the air density, while the viscosity ratio, $\left(\frac{\mu_L}{\mu_G}\right)$, denotes the ratio of the liquid viscosity to the air viscosity. In addition, the spatial factor is represented as the normalized length scale, $\left(\frac{X}{d_0}\right)$. Also, implicit within the array of parameters mentioned here is the Reynolds number (*Re*), which represents the ratio of the liquid inertial forces to the viscous forces.

$$Re = \frac{\rho_L \, d_0 V}{\mu_L} \tag{IV-50}$$

The following relationship holds for the Reynolds number:

$$Re = \sqrt{We \cdot Lp \cdot \frac{\rho_L}{\rho_G}} \tag{IV-51}$$

Therefore, we may also use *Re* instead of *Lp* as a term in the dimensionless equation.

MULTIPLE LINEAR REGRESSION MODELING

The model developed is of the form

$$\frac{D}{d_0} = A(\mathrm{Re})^B (We)^C \left(\frac{\rho_L}{\rho_G}\right)^D \left(\frac{\mu_L}{\mu_G}\right)^E \left(\frac{X}{d_0}\right)^F \tag{IV-52}$$

In order to obtain the value of the constants *A* through *F*, the model is first converted into a multivariate linear form by taking its natural logarithm.

$$\ln\left(\frac{D}{d_0}\right) = \ln(A) + B\ln(\mathrm{Re}) + C\ln(We) + D\ln\left(\frac{\rho_L}{\rho_G}\right) + E\ln\left(\frac{\mu_L}{\mu_G}\right) + F\ln\left(\frac{X}{d_0}\right) \tag{IV-53}$$

Multiple linear regression of equation (IV-53) will now give us the values of the constants *A* through *F*.

Before accepting equation (IV-52) or its variation equation (IV-53) as the true form of the model for regression it is first necessary to analyze if any of the dimensionless parameters are redundant or do not significantly contribute to the correlations developed. The statistical analysis of the regression process for different combinations of the above set of five dependant variables is performed using SAS®. Complete details of the programs and the resulting statistical output have been provided in Appendix H.

The first criterion that is often used is the adjusted R-square, which adjusts the R-square of each model to account for the number of variables in the model. Since models with different numbers of independent variables are to be compared, the adjusted R-square is the appropriate criterion here rather than R-square. Referring to Table IV-3, we observe that the adjusted R-square reaches a maximum value of 0.7669 for the complete model with all five variables.

Table IV-3. Statistical comparison of various models for the BDO

Number in Model	R-Square	Adjusted R-Square	C(p)	MSE	SSE	Variables in Model
1	0.3842	0.3755	121.2246	0.11074	7.86257	X2
1	0.2152	0.2042	173.4123	0.14112	10.01964	X1
1	0.0205	0.0067	233.5705	0.17614	12.50616	X3
1	0.0202	0.0064	233.6619	0.17620	12.50994	X5
1	0.0020	-0.0120	239.2667	0.17946	12.74161	X4
2	0.7585	0.7516	7.6084	0.04405	30.8379	X2 X5
2	0.4736	0.4585	95.6023	0.09601	6.72085	X1 X5
2	0.4192	0.4026	112.4003	0.10593	7.41516	X1 X2
2	0.4002	0.3831	118.2678	0.10940	7.65768	X2 X3
2	0.3865	0.3690	122.4929	0.11189	7.83232	X2 X4
2	0.3179	0.2984	143.6940	0.12441	8.70863	X1 X3
3	0.7641	0.7538	7.8766	0.04366	3.01221	X2 X3 X5
3	0.7637	0.7534	7.9941	0.04373	3.01707	X1 X2 X5
3	0.7594	0.7489	9.3279	0.04452	3.07220	X2 X4 X5
3	0.6539	0.6388	41.9127	0.06404	4.41903	X1 X3 X5
3	0.6391	0.6234	46.4708	0.06677	4.60743	X1 X4 X5
3	0.4657	0.4424	100.0510	0.09887	6.82206	X1 X2 X4
4	0.7740	0.7607	6.8157	0.04244	2.88570	X2 X3 X4 X5
4	0.7679	0.7543	8.6894	0.04358	2.96314	X1 X2 X4 X5
4	0.7645	0.7507	9.7375	0.04421	3.00646	X1 X2 X3 X5
4	0.6565	0.6363	43.0931	0.06449	4.38515	X1 X3 X4 X5
4	0.5066	0.4775	89.4179	0.09265	6.29990	X1 X2 X3 X4
5	0.7831	0.7669	6.0000	0.04133	2.76931	X1 X2 X3 X4 X5

A second criterion often used in the evaluation of competing models is based on the Cp statistic developed by Mallows. When a regression model with p independent variables contains only random differences from a true model, the average value of Cp is p + 1, the number of parameters. A value of Cp near p+1 indicates that the model bias is small. In other words, there is no significant underfitting or overfitting of the model. Thus, in evaluating many alternative regression models our goal is to find models whose Cp is close to or below p + 1. From Table IV-3, we can see that only the full model with all five variables fulfills this criterion.

Other significant observations deal with the Mean Square Error (MSE) and the Sum of Square Errors (SSE). The most desirable model is the one with the smallest MSE and SSE. The five parameter model satisfies these criteria too.

The statistical analysis on the BDO data indicates the superiority of the five parameter model over the other alternatives. Similar observations can be made from the statistical analysis of all data from all the other fluids.

With the five parameter model being the choice, regression analysis is carried out to obtain the constants *A* through *F* in equations IV-52 and IV-53. The results of the regression analysis are shown in Table IV-4. Again more details about the regression analysis are located in Appendix H.

Table IV-4. Correlation parameters for six heat transfer coefficients based on equation IV-52

Heat Transfer Fluid		AAR	MTP	DTA	DAA	BDO	WMO
Constant	A	3.9270 E+34	4.6072 E+04	1.7233 E-01	1.0169 E+43	1.3741 E+49	8.7716 E+31
Re	*B*	-0.5271	0.4926	1.8879	1.1555	0.4373	0.3994
Wb	*C*	-0.3239	-1.2249	-1.9157	-1.5272	-1.1216	-1.1148
$\left(\frac{\rho_L}{\rho_G}\right)$	*D*	-11.2582	-1.7504	-2.5911	-16.3310	-16.8878	-11.4291
$\left(\frac{\mu_L}{\mu_G}\right)$	*E*	-0.2026	0.6624	1.8939	1.6372	0.8711	0.5006
$\left(\frac{X}{d_0}\right)$	*F*	-0.1746	-0.5262	-0.2462	-0.5974	-0.2931	-0.5787

CORRELATIONS AND PREDICTIONS

The correlations for all fluids show good agreement with the data. The coefficient of multiple regression was above 80% for the mean droplet diameters and most of the values predicted from the correlation are within the total measurement uncertainty, as shown in Figure IV-10.

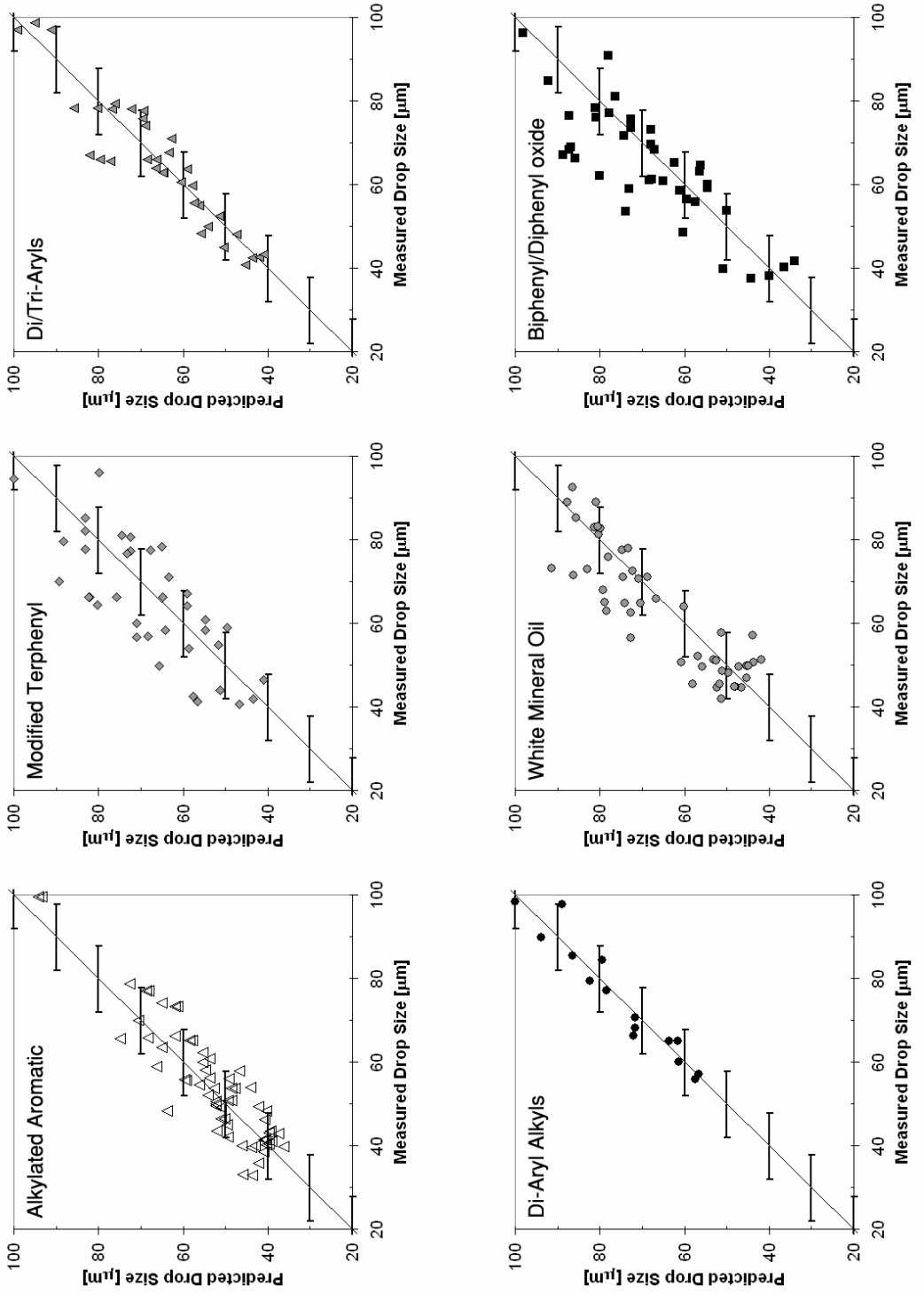

Figure IV-10. Correlation results: Predicted mean droplet diameters for six tested fluids (x-error bars indicate ± 8 µm)

The correlation validation is performed on the basis of the basic parameters that are described by the dimensionless groups. All of the obtained equations are expanded in terms of the basic parameters, and the exponent on each parameter is examined for its significance.

$$D = a\left(\rho_G\right)^b\left(\mu_G\right)^c\left(\rho_L\right)^d\left(\mu_L\right)^e(\sigma)^f(V)^g(X)^h\left(d_0\right)^i \qquad \text{(IV-54)}$$

The parameters a through *i* for equation IV-54 are tabulated for the six fluids tested in Table IV-5. The exponent for liquid viscosity is positive, which means that higher viscosities result in larger aerosol mean droplet diameters and also larger aerosol formation distances. Therefore, while a higher viscosity hinders atomization, under conditions where atomization does occur, the mean droplet diameters will be larger.

The exponent for surface tension is positive, which indicates that, while higher surface tension can produce larger droplets, it also hinders aerosol formation (Tabata et al., 1985). All exponents of liquid density are negative, which means that more dense fluids will produce smaller droplets while atomizing much closer to the orifice. This behavior can be rationalized by the fact that denser liquids have a higher kinetic energy and consequently smaller droplets develop. Liquid velocity always has a negative exponent. Higher velocities are caused by higher injection pressures and result in smaller droplets as well as shorter aerosol formation distances (Tabata et al., 1985). The smaller orifice size constricts the liquid stream to a greater extent, resulting in smaller droplets and hence confirms the positive exponent. These correlations have a good agreement with the experiments and their implications can be rationalized by theory.

Table IV-5. Correlation parameters for six heat transfer coefficients based on equation IV-54

Heat Transfer Fluid		AAR	MTP	DTA	DAA	BDO	WMO
Liquid	Density (*d*)	-12.1092	-2.4827	-2.6189	-16.7027	-17.6100	-12.1066
	Viscosity (*e*)	0.3245	0.1698	0.0060	0.4818	0.4716	0.0633
	Surface tension (*f*)	0.3239	1.2249	1.9157	1.5272	1.1216	1.1148
Nozzle	Velocity (*g*)	-1.1750	-1.9572	-1.9436	-1.8989	-1.8438	-1.7923
	Orifice diameter (*i*)	0.3235	0.7939	1.2184	1.2257	0.8565	0.6156
Distance from the orifice (*h*)		-0.1746	-0.5262	-0.2462	-0.5974	-0.5787	-0.2931

VERIFICATION

In addition to validating the correlations based on the physical significance of the exponents, additional data will be collected at conditions not previously tested and compared to the correlation predictions. This will confirm the robustness of the correlations and provide an effective evaluation of the correlation performance.

All the HTFs were re-tested at arbitrary conditions within the range of the correlations and the measured drop sizes compare favorably against the correlation

predictions as indicated by the values in Table IV-6 and Figure IV-11. All fluids show a percentage absolute error of under 10% and a percentage bias between +2% and –5%.

Table IV-6. Verification of correlation performance

Heat Transfer Fluid	Percentage Absolute Error	Percentage Bias
Alkylated Aromatic (AAR)	9.46	-0.85
Modified Terphenyl (MTP)	7.42	-1.66
Di/Tri- Aryl (DTA)	8.00	1.83
Di Aryl Alkyls (DAA)	8.67	0.03
White Mineral Oil (WMO)	9.52	2.21
Bi phenyl/Di phenyl Oxide (BDO)	7.80	4.88

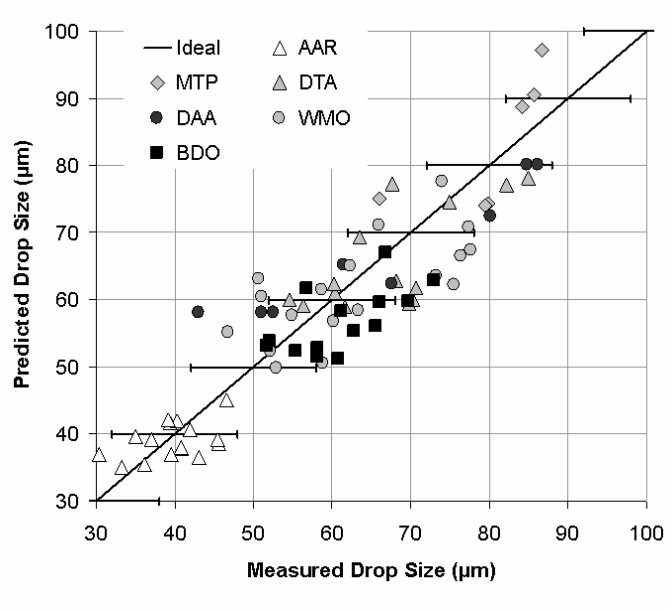

Figure IV-11. Verification of correlation performance

SUMMARY OF CHAPTER IV

This chapter deals with how the raw data and observations from the experimental part of the research are transformed into useful predictive correlations. These correlations have performed well in three levels of validation. The first is purely statistical and showed that the correlations were a good fit for the data for the purpose of predicting aerosol drop sizes. The second layer of validation showed that the correlations did not contradict laws of nature, where the trends observed with respect to the individual properties were verifiable in theory. The third and final layer demonstrated that the correlations were able to closely predict the aerosol drop diameters under conditions previously untested.

CHAPTER V

COROLLARIES AND CONSEQUENCES

The devastating consequences of aerosol/mist explosions have been detailed in Chapters I and II. Heat transfer fluids are particularly susceptible to these hazards, because they are utilized under high pressures and below their flash points, making them more prone to leaking as aerosols. However, there is a critical need during design stages for a perception of explosion risks associated with the selection of heat transfer fluids. This chapter discusses a novel scheme to integrate the knowledge of heat-transfer fluid aerosol formation from leaks in process equipment into the selection of heat transfer fluids during the design process.

In addition the problem of aerosol explosions is compounded by a serious dearth of knowledge about such hazards. Laboratory studies are crucial for design criteria to reduce or eliminate aerosol explosion hazards from the workplace. Experimental proof of the greater severity of heterogeneous aerosol mixture explosions and enhanced propagation criteria will create invaluable awareness about the potential hazards and information for heat transfer equipment design criteria to reduce these hazards.

Part of this chapter is reprinted from "Incorporating aerosol formation, flammability and explosion information into HTF selection" by Krishna, K., Rogers, W.J., and Mannan, M.S., (2003). *Journal of Hazardous Materials, in press,* Copyright (2003), with permission from Elsevier

This chapter also discusses the experimental design of a laboratory apparatus that will establish the relationships among aerosol droplet sizes, process conditions, enhanced flame speeds, and flammability limits. Visualization and other optical techniques required are introduced. Knowledge of combustion modeling will also help guide the design. The minimum ignition energies necessary for aerosol explosions also will make possible design constraints to reduce aerosol explosion hazards. The ultimate goal is to reduce or eliminate hazards caused by aerosols and make handling and utilization of such fluids safer.

EXISTING HTF SELECTION CRITERIA, SHORTCOMINGS, AND REQUIRED IMPROVEMENTS

Existing elementary screening employed in heat-transfer fluid selection are flash point, fire point, and autoignition temperature. Chapter II provides the details of these three criteria and their testing methods. The absence of design criteria to incorporate aerosol flammability and explosion into the selection of heat transfer fluids (HTFs) is alarming. Hence, an indicator that can relate the degree of hazard of a particular HTF, to other selection criteria is necessary to integrate aerosol hazards into the design of processes. The Sauter Mean Diameter (SMD) can provide an effective index to characterize the aerosol or mist.

SMD as a Criterion

The mean drop diameter is the most common quantity that represents a set of droplets in a spray. Depending on the requirement, several different expressions of the mean drop diameter are available. The general definition that describes all forms of the mean diameter is:

$$D_{pq} = \sqrt[p-q]{\frac{\sum_{i=1}^{m} D_i^p \Delta n_i}{\sum_{i=1}^{m} D_i^q \Delta n_i}} \qquad \text{(V-1)}$$

By using different values of p and q, we can generate a host of mean droplet diameters, each of which can yield different information about the spray system. Bayvel and Orzechowski (1993) have provided the commonly used mean diameters based on equation V-1 and their applications, as shown in Table IV-1 of Chapter IV.

Studies on the atomization of leaking HTF have related the SMD of a leaking aerosol to the operating conditions and the fluid properties (Krishna et al, 2001). Utilizing the models to predict the SMD that would result under certain operating conditions and with certain HTFs can help to assess the hazard posed. As discussed earlier, smaller droplet sizes are ignited faster and combust more vigorously than larger droplets, indicating that they pose a greater mist explosion hazard. Krishna et al. also provide rules that will help in the design process: the higher density HTFs will form smaller droplets on leaking, higher viscosity HTFs are less likely to form aerosol, HTFs with the higher surface tension will form larger droplets on leaking, and higher

operating pressures will produce aerosols closer to the leak and with smaller droplet sizes.

The SMD also represents a distribution with which the fraction of the droplets below 20 microns in a given release can be estimated. It is understood that for a given distribution of droplet sizes, this fraction decreases with increases in the SMD. It therefore appears prudent to use SMD as an index of the hazard associated with a particular aerosol release.

Selection Methodology

From discussions thus far, the main parameters for heat transfer fluid selection are (Singh, 1981, Cuthbert, 1994): temperature range, operating pressure, heat transfer coefficient, economics, maintenance, limitations on materials of construction, and hazard potential.

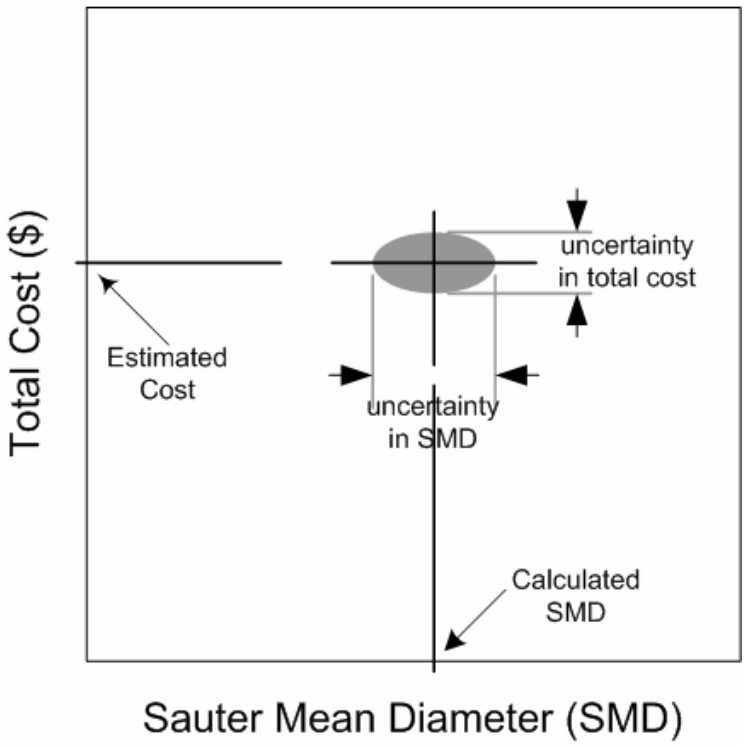

Figure V-1. Plotting SMD versus total cost

The hazard potential can be sub-divided into vapor and mist hazards. Operating the system below the flash point of the HTF reduces the vapor hazard. The SMD, which is calculated for various HTFs using correlations, can be plotted against any other parameter and analyzed. Consider the case where after several HTFs have been short-listed for selection, based on initial screening of the temperature range, heat transfer coefficient, and flash point. The developed correlations can be used to estimate the SMD under the given conditions. The SMD and the total cost of the HTF system are both plotted as shown in Figure V-1 for one HTF. The uncertainty in the SMD includes the uncertainties in the correlation prediction, temperature range of operation, and

operating pressure. The procedure is repeated for the short-listed fluids and the resulting plot, as illustrated for four HTFs in Figure V-2, is then analyzed. A range of HTFs must be utilized at operating pressures that yield the required range of temperature utility.

Based on this comparison, we can see that fluids with high operating pressures and low aerosol SMDs pose the highest risk. Hence the ideal fluid would be one that operates at a low pressure and on leaking would produce a high SMD aerosol. The plot can therefore be divided into different hazard levels, an example of which is shown in Figure V-2.

Comparing the plots in Figure V-2, we see that HTFs A & D both operate at higher hazard as a result of lower SMD, whereas HTFs B, C, and E are relatively less hazardous. While D offers a very economical choice, its hazard potential is relatively high. Conversely, E has the lowest hazard potential but the highest cost. According to the classification, B and C provide us with the most attractive options. Additionally, other considerations also can be applied to determine the most appropriate fluid.

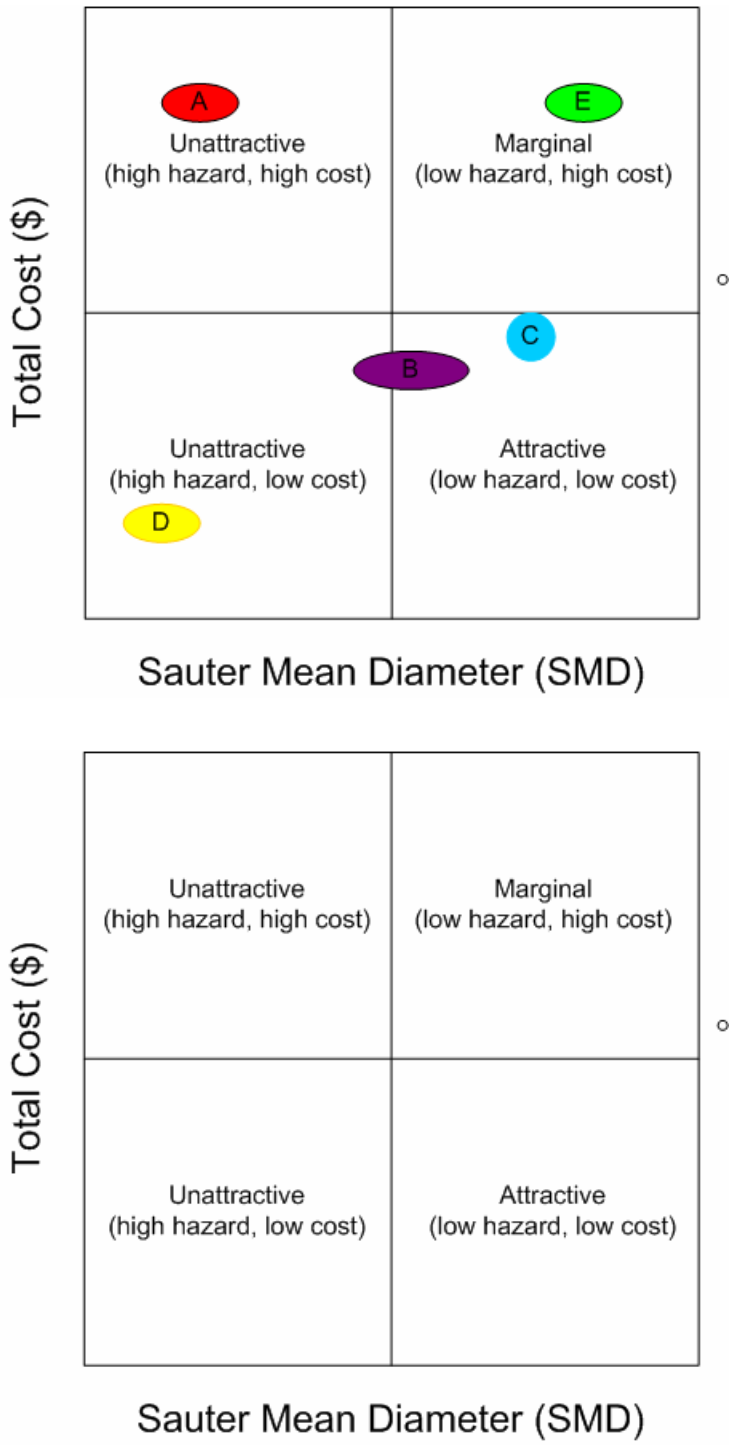

Figure V-2. Comparison of five heat transfer fluids and possible hazard levels for HTF selection

Inferences and Significance

With a simple application of available data, the potential hazards due to aerosol leaks can be factored into the selection of heat transfer fluids in the design process. Additionally, recommendations may be made to alter the design of the heat transfer process if low or moderate hazard levels are not attainable. One recommendation could be the addition of minute quantities of additives to the HTF to increase the surface tension that results in higher SMDs. Any degradation of the fluid during plant operations over time can be translated into an altered hazard level, which may necessitate a replacement of the fluid. The hazard level can therefore be monitored throughout the life of the process.

The proposed scheme will ensure that product selection based on hazard analysis becomes part of the seamless flow of design and development of safer chemical processes. It also demands that links between fire and explosion hazards, requirements (and associated design outputs), are based on verifiable and validated data. By integrating the hazard analysis with the design process, monitoring of the hazard can be achieved throughout the life of the process, and every instance of process alteration thereby becomes an effective tool for management of change. Finally, such methods can be integrated into the design curriculum thereby making safety second nature.

The chemical industry utilizes different process fluids that vary widely in their properties. These fluids do not necessarily take part in chemical reactions to form a

desired product, but their specific properties are utilized for “services” as fuels, lubricants, heat transfer fluids, or other such functions.

FUTURE DIRECTION: FLAME PROPAGATION STUDIES

Heavy hydrocarbons (HHCs), such as gear oils, pump oils, heat transfer fluids (HTFs), and lubricants, are widely used and can form flammable and highly hazardous aerosols when they leak under pressure. Though aerosol explosion hazards have been widely documented, knowledge about their formation and flammability behavior is limited. This research correlated measurements of HTF aerosol formation behavior to fluid properties and conditions, and the correlations must be extended to aerosol flammability and combustion behavior.

The problem of aerosol explosions is compounded by a serious dearth of knowledge about such hazards. Laboratory studies are crucial for design criteria to reduce or eliminate aerosol explosion hazards from the workplace. Experimental proof of the greater severity of heterogeneous aerosol mixture explosions and enhanced propagation criteria will create invaluable awareness about the potential hazards and information for heat transfer equipment design criteria to reduce these hazards.

This section discusses the proposed experimental design of a laboratory apparatus that will establish the relationships between aerosol droplet sizes, process conditions, enhanced flame speeds, and flammability limits. Visualization and other optical techniques required are introduced. Knowledge of combustion modeling will

also help guide the design. The minimum ignition energies necessary for aerosol explosions also will make possible design constraints to reduce aerosol explosion hazards.

As described in Chapter II the hazards associated with aerosols of heavy hydrocarbons are of critical concern in the process industries. Existing theory suggests that aerosol explosions can be more energetic compared to homogenous vapor-air mixtures because of higher enthalpy concentrations in the liquid aerosol phase. In addition, with aerosols there can be significantly enhanced burning velocities in the heterogeneous mixture, as discussed below. Chapter II also introduces Eichhorn's (1955) views and Polymeropoulos' (1984) theories on enhanced flame propagation speeds through monodisperse aerosols. The emphasis is definitely on the proposed critical droplet size range.

It is therefore essential that this proposed transition range be studied experimentally to verify and understand the mechanism of aerosol explosions. HHCs are generally very low volatility liquids with high boiling points, and therefore with $\Omega \rightarrow 0$, and should make possible a more easily observable flame speed enhancement than high volatility liquids.

Identifying the transition range for various industrial fluids would help develop strategies to prevent the critical droplet sizes from being generated for industrial safety or to enhance explosion energy by augmenting the droplets in this range. Aerosol drop sizes generated through leaks in process systems are closely related to the operating

conditions and the fluid and thermal properties. Using correlations developed in previous chapters to predict HHC aerosol formation behavior as a function of atomization conditions, guidelines for selection of HHCs or similar hydrocarbon fluids and their operation conditions can be established (Sukmarg et al., 2002, Krishna et al., 2003).

In Chapters II and IV functional relationships between the operating conditions and the drop-size distributions of the resulting aerosols were established and have made possible the development of predictive models to relate aerosol droplet sizes and formation distances to bulk liquid pressures, temperatures, fluid properties, orifice sizes, and ambient conditions (Krishna et al., 2003). Figure IV-8 shows the droplet size correlations measured for six fluids using a Malvern laser diffraction particle analyzing technique. The developed predictive correlations will be used to determine under what operating conditions a HTF will generate a significant proportion of aerosol droplets in its transition range for enhanced flame propagation.

Experimental Objectives

Future research is critical for understanding mechanisms underlying the flammability and combustion of aerosols and for relating this behavior to the atomization characteristics. Objectives include measurement of minimum ignition energies of heat transfer fluid aerosols in air and measurement of combustion propagation velocities in aerosol-air mixtures as functions of air-to-fuel concentration

ratio, droplet size, and the vapor fuel to liquid fuel concentration ratio, test a theoretical region of enhanced flame velocities, and model the laminar combustion propagation behavior. This understanding will make possible development of explosion models to incorporate multiphase effects of fuels. This information also will greatly improve the safety of operations with industrial fluids.

Experimental Apparatus, Tools, and Techniques

Aerosol combustion apparatus: The aerosol combustion apparatus is presented in Figure V-3. The ignition system will employ both burning wire as well as spark ignition. Minimum ignition energy tests will employ burning wire ignition, which allow precise control of ignition energy, and flame propagation tests will employ an ignition system consisting of spark electrodes with a fixed spark gap connected to a power supply to allow ramping of the ignition energy. The ignition energy will be governed by the potential difference across the spark gap.

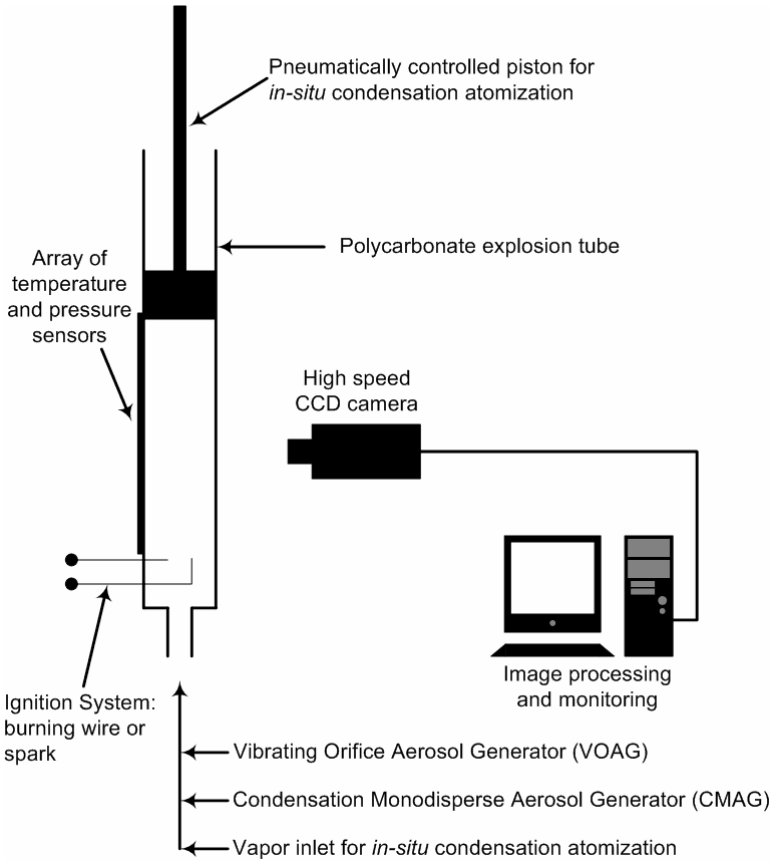

Figure V-3. Schematic of the proposed apparatus

Combustion cell: The aerosol combustion cell will be a vertical combustion cylinder/ shock tube made of transparent polycarbonate for laser access, optical monitoring, and video visualization. Also, the tube will be provided with an inlet for aerosol/vapor and will include a piston to create in-*situ* mono-disperse droplets using the condensation atomization process (Cameron and Bowen, 2001). The cell will be designed for combustion tests at atmospheric pressure and will be provided with a safety rupture

disk. For safety of operation, the combustion cell and associated equipment will be surrounded by Lexan® polycarbonate panels.

Atomization: Atomization of a liquid is the process by which aerosol can be produced, such as with a liquid forced under pressure through a leak in an industrial process. Upon exiting the leak structure, the liquid stream is destabilized by friction forces between the air and the liquid surface. These aerodynamic forces cause disturbances in the surface of the stream, overcome the surface energy of the stream, and break up the stream. This separation of the liquid stream results in the formation of non-spherical segments known as ligaments, which break-up further until they are small enough to form stable spherical droplets with a wide range size distribution (Bayvel and Orzechowski, 1993, Lefebvre, 1989).

Mono-disperse droplets for characterization of critical sizes**:** To study the effect of aerosol drop-size on the flammability characteristics, generation of a mono-disperse spray with a narrow size distribution is of utmost importance. Several methods of aerosol generation are available.

The Vibrating Orifice Aerosol Generator (VOAG) is an accurate source of mono-disperse particles in the range from 1 to 200 micrometers. Using a variety of solutes and solvents, the generator creates solid or liquid aerosol particles uniform in size, shape, density, and surface characteristics. The VOAG generates uniform particles by

controlling the breakup of a liquid jet. It delivers a consistent volume of liquid using a constant-flow syringe pump. Because of its consistency and accuracy for particle sizes of pure liquids above 5 microns, it is an effective aerosol-generation standard for this research. Included with the VOAG is a neutralizer to remove significant electrostatic charges formed from formation of drops below about 30 micrometers. Such charges can greatly reduce aerosol drop transport for the smaller drop sizes.

The Condensation Mono-disperse Aerosol Generator (CMAG) is a condensation-type instrument that produces high-concentration, mono-disperse aerosol particles. It is well suited for applications requiring mono-disperse particles in various concentrations. The CMAG generates liquid or solid particles from a variety of oils, waxes, and other materials, in concentrations greater than 106 particles per cubic centimeter. It generates mono-disperse particles in the range from 0.1 to 8 micrometers and operates at a flow rate of 4 liters per minute. This atomizer is required for particle sizes below ~ 5 microns, in which the vibrating orifice atomizer is not practical for the tests with pure liquids required in this research. Although the critical range for aerosol flame propagation enhancement is theorized to be above 5 microns, this hypothesis has not been tested for heavy hydrocarbons for which the critical size could be below 5 microns. In order to measure the enhanced propagation phenomenon for a variety of fluids, a CMAG that is capable of generating mono-disperse aerosol within the 1 to 8 micron range also will be utilized (Lefebvre, 1989) by introducing vaporized fuel into the shock tube and by controlling the expansion rate and expansion ratio of the pneumatically controlled piston to induce aerosol formation (Cameron and Bowen,

2001). As discussed above, this flame speed enhancement should become much more pronounced with heavy, low volatility fluids for which the critical droplet size range could be near 5 microns or less.

Schlieren imaging: The combustion or flame front will be visualized by a Schlieren imaging technique, and the subsequent flame propagation images will be recorded by a high-speed CCD camera (Montaser et al., 2000). The Schlieren technique, essentially consisting of a parallel "back-lighting", detects the refractive index variation across the flame front and converts it into illumination light intensity variation to visualize the flame front.

Aerosol visualization and measurement apparatus: The laser of the proposed equipment generates a light sheet with well-defined geometrical characteristics and intensity distribution for Particle Imaging Velocimetry (PIV) measurements. The integrated light sheet optics is compact, modular, and easy to set up and adjust. The standard models include in a single unit a focal distance adjustment to set the light sheet thickness in the illumination plane, and a further adjustment that controls the light sheet angle. The copper vapor laser system generates up to 10,000 pulses per second, with a 25 nano-second flash duration. The speed of this laser system is required for visualization of rapid droplet vaporization and combustion at the flame propagation front to verify propagation velocity enhancement for critical droplet diameters. The Photron Ultima

camera with 500 to 4,000 fps is expected to provide sufficient imaging speed and resolution for droplet measurements down to about 1 micron. The system also has pulse-on-demand capability for easy synchronization and ultra-thin light sheet generation through a fiber optic light delivery capability. The included software incorporates hardware control, image acquisition and storage, on-line analysis, off-line and batch analysis, and visualization.

High-speed video recording: High-speed, particle imaging velocimetry (PIV) will include cinematographic digital recording of the flame propagation with a sufficiently high flame rate (500 to 4,000 fps with the proposed apparatus) and sufficiently short shutter opening to freeze the flame image with minimal blur for sufficient resolution for droplets down to 1 micron to provide a visualization of the droplets as they disappear with the arrival of the combustion front. The recorded images will be processed using software in a PC platform for calculating the flame propagation speed (Figure V-4). The laminar burning velocities will be compared with the theoretical predictions to test the hypothesized transition aerosol droplet size region for each tested fluid (Polymeropoulos, 1984).

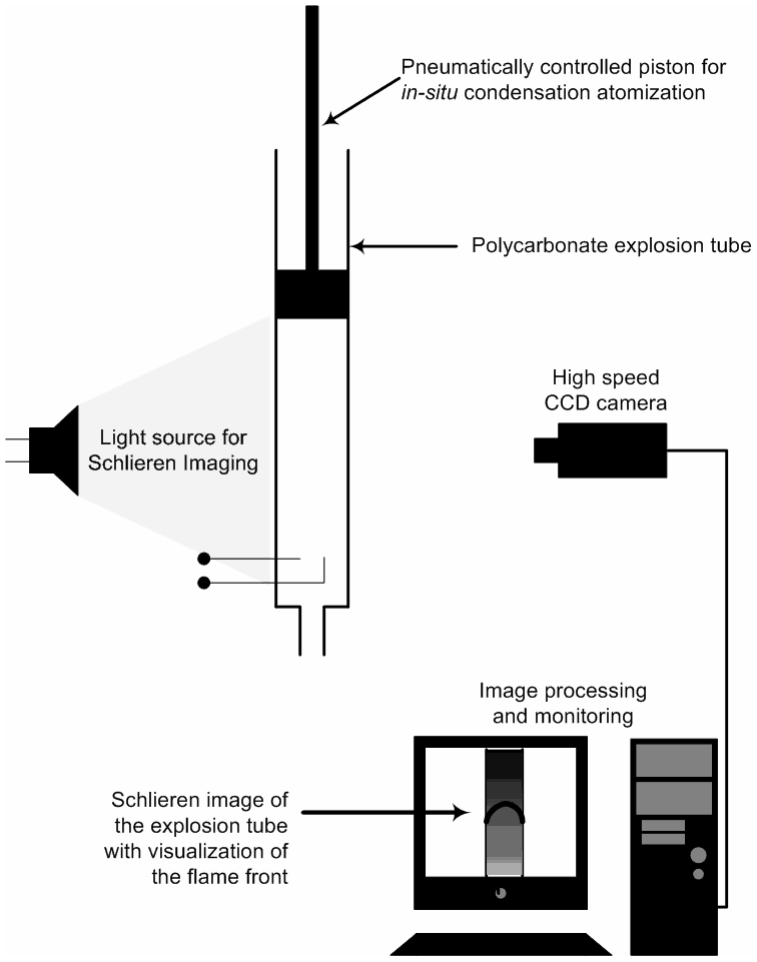

Figure V-4. Apparatus configured for Schlieren visualization

Test fluids: Pure fluids as well as mixtures will be experimentally tested. Pure fluids with well-characterized properties will provide a basis for modeling combustion behavior in terms of known properties. Pure fluids will be selected from a variety of organic classes such as paraffins, olefins, and aromatics. Measurements will then be extended to binary and tertiary mixtures of the previously tested pure fluids. Finally,

complex blends that represent industrial fluids, such as heat transfer fluids, pump oils, gear oils, and machining fluids, will be tested. A Table of test fluids for aerosol combustion measurements is shown below.

Table V-1. Proposed test fluids

Test fluid	Formula
Long chain paraffin	$C_{15}H_{32}$
Long chain paraffin	$C_{20}H_{42}$
Alkylated aromatic	$C_6H_5C_{13}H_{27}$
Alkylated aromatic	$C_6H_5C_{17}H_{35}$
Alkylated aromatic	$C_6H_5C_{20}H_{41}$
Blend of alkylated aromatics	$C_6H_5C_nH_{2n+1}$ N between 13 and 20

Experimental methods: The experimental procedure starts with introduction of an aerosol into the combustion chamber. A repeatable method of atomization and homogeneous mixing will be developed for the experiments. The CMAG will be used to generate monodisperse droplets in the range of 1 to 8 microns and the VOAG will be used for monodisperse aerosols from 5 to 30 microns. This total range of 1 to 30 microns should be adequate to test theories of enhanced flame speed in aerosols (Polymeropoulos, 1984, Lin and Sheu, 1991, Bowen and Cameron, 1999). The PIV method makes possible visualization of velocity flow, so turbulent eddies and relative

quiescence of the mixture prior to ignition can be determined. Laser sheet imaging will be used to monitor aerosol droplet sizes. The images are then processed by PIV software to determine the area and perimeter of the individual droplets. From the areas and perimeters, the diameter, and a shape factor (perfect sphere = 1) are calculated. Results from individual droplets are combined to provide diameter distributions and to calculate aerosol statistics such as the Sauter mean diameter, monodispersity, and volume percentiles.

The value of Ω is calculated from the determined amounts of vapor and liquid fractions in the combustion cell. The liquid amount is based on the droplet size distribution and liquid density, and the vapor fraction can be determined from the equilibrium vapor pressure. The droplet size distribution and the total volume concentration of droplets determined from the laser sheet imaging are used to estimate the total mass of aerosol in the test chamber.

The aerosol at a controlled fuel-to-air ratio is ignited using either burning wire or spark ignition. Spark ignition will be used initially because it can easily provide a very high-energy discharge. However, the burning wire will provide a more accurate measurement of minimum ignition energies, which is expected to be greater for aerosols of larger mean diameters.

After ignition of the aerosol has been achieved, the laser sheet that illuminates a cross section of the flow takes pairs of images. By comparing the position of the combustion or flame front in consecutive images, the droplet imaging system

automatically calculates the flame propagation velocity. The velocity information is presented as a series of evenly distributed vectors that are used to identify turbulent and laminar regions in the flame for further analysis and combustion modeling.

The flame propagation velocities obtained in the aerosol air mixtures are compared to flame propagation velocities in the vapor-air mixtures, which are obtained from flame ignition and propagation tests on vapor-air mixtures at various concentrations. The amount of vapor in these tests is calculated from a precisely weighed amount of liquid injected into the combustion cell and completely vaporized.

It is important to note that challenges in the above experiment include production of a homogeneous, monodisperse spray and an accurate estimation of the vapor amount in the combustion chamber. While the aerosol generators are capable of generating monodisperse aerosols, coalescence in the combustion chamber will alter the aerosol droplet size distribution, which must be carefully monitored. Additionally, replicas of the experiments must be performed to ensure consistent and reproducible results and to estimate experimental uncertainties.

Analyzing the relation between the aerosol mean droplet diameter and the flame propagation velocity will help identify the transition droplet size region described by Polymeropoulos (1984) and subsequent authors (Lin and Sheu, 1991, Greenberg et al., 1998, Ju et al., 1998). Additionally, studies using the various fluids identified above will help characterize the effect of fluid volatility (vapor pressure) and equivalence ratio

(ratio of the actual to the stoichiometric fuel to air ratio) on the flame propagation velocity.

Combustion Propagation Modeling

There is some, but not definitive, experimental evidence that when a flame-front propagates through an aerosol mixture of air, fuel vapor and fuel droplets, it can be accelerated beyond the laminar flame speed. It has also been shown that liquid droplets affect the combustion behavior of volatile mixtures. Specifically, the flammability limits of droplet clouds in air are found to decrease significantly as the droplet size increases (Williams, 1988). Although various explanations have been advanced for the observed behavior, complete understanding of the physical mechanisms underlying this counter-intuitive behavior remains elusive. Simple one-dimensional computational models have been constructed that reproduce some of the observed behavior, but the quantitative agreement has been quite inadequate (Eshwaran & Pope, 1988).

In conjunction with a comprehensive series of experiments using the proposed instrumentation, we propose an analytical and computational study to develop a fundamental understanding of the physical phenomena and construct quantitatively accurate models to represent the observed explosion behavior. The various physical processes contributing to flame propagation in aerosol mixtures will first be studied in isolation. While some of the phenomena such as the burning of individual droplets are well understood, several others including the augmentation of flame surface area due to

wrinkling caused by the presence of droplets and effect of thermal expansion of the gas due to the burning droplet are relatively unexplored. Even less is known about the effect of turbulence on aerosol combustions and overall flame propagation speed.

Based on the experimental findings of the first part of the study, a model of a one-dimensional reacting flow will be constructed to study the combined effects of all the individual processes on flame propagation. As in previous works (Polymeropoulos, 1984), with the one-dimensional model, it will be assumed that the flame-front propagating through the aerosol mixture can be treated as planar (Weber et al., 1985). This approximation will be tested by visualization of velocity flow using the proposed instrumentation with which turbulent eddies can be measured prior to ignition. This planar simplification is reasonable if the droplet size is small compared to the flow length scale and the conditions for ignition of droplets in a spray are satisfied.

A one-dimensional flame propagation equation can then be written as in the case of a homogeneous well-stirred reactor. The reaction rate of the gas-gas mixture and gas-liquid mixture will be added linearly to yield the overall reaction rate of the aerosol mixture. When all the ignition criteria are satisfied, the total heat release will be a sum of the heat release from the gas-gas and gas-liquid reactions. If the evaporation timescale is very small compared to the gas-gas reaction timescale, then all the droplets evaporate before the reaction is complete and the homogeneous gas-phase laminar flame speed is obtained. Otherwise, as with the heavier fluids to be tested initially, the droplet combustion characteristics modify the flame speed in the aerosol mixture. In

this analysis, the size and properties of the droplets appear only indirectly via the gas-liquid ignition, reaction-rate, and heat-release characteristics.

An accurate assessment of the droplet size on aerosol combustion can be obtained only by complete three-dimensional simulation (Girimaji, 1994, Yu et al., 2003). In the subsequent part of the study we will consider combustion in a periodic computational cube with the air, fuel vapor, and fuel droplets initially segregated and distributed in a random isotropic fashion. With time, diffusion and evaporation will lead to reaction. The effective flame propagation rate can be deduced from the heat release rate or the fuel depletion rate. In this study, more complete and accurate models for diffusion and evaporation can be employed. A major advantage of this approach is that it permits fractal analysis of the flame surface. Thus the surface-area enhancement as a function of droplet size can be analyzed. In addition, the effect of turbulence will also be investigated in a subsequent study by introducing a background turbulent velocity field in the computations.

SUMMARY OF CHAPTER V

Heavy hydrocarbons are used in almost every chemical process and manufacturing industry and the workforce employed by the industry is very large. This workforce is constantly exposed to the potential hazards of aerosol explosions, for which there exists a serious dearth of knowledge. The proposed laboratory studies are crucial for development of models that clearly predict the special combustion behavior

of two-phase as distinct from vapor explosions and also to reduce aerosol explosion hazards from the workplace. Experimental proof of the greater severity of heterogeneous aerosol mixture explosions and enhanced propagation criteria will create awareness about the potential hazards and information for heat transfer equipment design criteria to reduce these hazards. The minimum ignition energies necessary for aerosol explosions also will make possible design constraints to reduce aerosol explosion hazards. A goal is to reduce or eliminate hazards caused by aerosols and improve industrial and occupational safety.

CHAPTER VI

CONCLUSIONS

This dissertation has presented research on a critical topic in chemical plant safety: aerosol formation. While the chemical industry does recognize the potential hazards of aerosol explosions, the belief that process fluids like heat transfer fluids have the ability to form aerosols upon leaking is lacking. As a result, aerosol explosion hazards are generally ignored.

In the process of studying aerosol formation, an effective system to pursue this objective experimentally has been designed, evaluated and implemented. Aerosol releases from leaking heat transfer fluids have been observed at temperatures well below their flash points. This extends the potential flammability limit below the fluid's flash point, forcing industry to pay more attention to aerosol flammability.

The fluids were tested at temperatures and pressures that are common in industry applications. Pressure had a more direct influence on the atomization. Higher injection pressures increased the liquid velocity, which hastened the atomization and also made it more severe, i.e., it resulted in smaller droplet sizes and shorter aerosol formation distances. Temperature indirectly affected the atomization through the liquid properties. At higher temperatures, liquids have lower densities, lower viscosities, and

lower surface tensions, resulting in lower droplet sizes. The orifice size tortured the leaking fluid stream: lower orifice diameters resulted in lower droplet sizes.

While this research has characterized the dependence of aerosol droplet diameter distributions on the operating conditions and the leak size, the most important conclusion for process safety is that significant quantities of aerosol are formed from HTFs at conditions well below their flash points. However, there are threshold conditions below which significant amounts of aerosols were not formed in the tested ranges. Operating conditions and leak size also had a significant effect on the mean droplet diameter, atomization distance, and the amount of aerosol generated.

Correlations developed here help define a source term for leaking fluids forming aerosols. During the design process the engineer must consider the following additional design criteria: the HTF with the higher density will form smaller droplets on leaking; the HTF with the higher viscosity is less likely to form aerosol; the HTF with the higher surface tension will form larger droplets on leaking; higher operating pressures will produce aerosols closer to the leak and smaller mean droplet diameters.

Using the correlations described here to define source terms for leaks forming aerosols will help optimize existing dispersion models by relating the dispersion to the operating conditions of the process. The study of aerosol combustion as a function of drop size distributions, concentrations, and fluid properties will facilitate the development of correlations for the upper and lower explosive limits of HTF aerosol/air mixtures. Such studies are currently being planned and will provide a better

understanding of aerosol hazards. This information will make possible a more comprehensive understand of aerosol explosions and thereby improve process safety.

With a simple application of available data, the potential hazards due to aerosol leaks can be factored into the selection of heat transfer fluids in the design process. Additionally, recommendations may be made to alter the design of the heat transfer process if low or moderate hazard levels are not attainable. One recommendation could be the addition of minute quantities of additives to the HTF to increase the surface tension and result in higher SMDs. Any degradation of the fluid during plant operations over time can be translated into an altered hazard level, which may necessitate a replacement of the fluid. The hazard level can therefore be monitored throughout the life of the process.

The proposed scheme will ensure that product selection based on hazard analysis becomes part of the seamless flow of design and development of safer chemical processes. It also demands that links between fire and explosion hazards, requirements (and associated design outputs), are based on verifiable and validated data. By integrating the hazard analysis with the design process, monitoring of the hazard can be achieved throughout the life of the process, and every instance of process alteration thereby becomes an effective tool for management of change. Finally, such methods can be integrated into the design curriculum thereby making safety second nature.

REFERENCES

Abbas, M.A., & Latham, J. (1967). The instability of evaporating charged drops. *Journal of Fluid Mechanics, 30*(4), 663-670.

Albrecht, A.R., & Seifert, W.F. (1971). Accident prevention in high temperature heat transfer fluid systems. *Loss Prevention, 4*, 67-88.

Annamalai, K., Ryan, W., & Chandra, S. (1993). Evaporation of multicomponent drop arrays. *Journal of Heat Transfer, 115*, 707-716.

Asihmin, V.I., Geller, Z.I., & Skobel'cyn, Y.A. (1961). Discharge of a real fluid from cylindrical orifices. *Oil Industry, 9*, 135-172.

Bailey, A.G. (1988). *Electrostatic Spraying of Liquid*s. Taunton, Somerset, UK: Research Studies Press Ltd.

Ballal, D.R., & Lefebvre, A.H. (1978). Ignition and quenching of quiescent fuel mists. *Proceedings of the Royal Society of London, Series A, Mathematical and Physical Sciences, 364*, 277-294.

Ballal, D.R., & Lefebvre, A.H. (1981). Flame propagation in heterogeneous mixtures of fuel droplets, fuel vapor, and air. *Proceedings of the Eighteenth Symposium (Int.) on Combustion, Waterloo, Ontario, Canada*, 321-328.

Barth, H.G. (1984). Particle and droplet sizing using Fraunhofer diffraction. In (pp. 135-172). *Modern Methods of Particle Size Analysis*, New York: Wiley & Son.

Bayvel, L. & Orzechowski, Z. (1993). *Liquid Atomization*. Washington D.C.: Taylor & Francis.

Bowen, P.J., & Cameron, L.R.J. (1999). Hydrocarbon aerosol explosion hazards: a review. *Transactions of the IChemE, 77*B, 22 – 30.

Bowen, P.J., & Shirvill, L.C. (1994). Combustion hazards posed by the pressurized atomization of high flash point liquid. *Journal of Loss Prevention in the Process Industries, 7(3)*, 233-241.

Bowen, P.J., Bull, D.C., Prothero, A., & Rowson, J.J. (1997). Deflagration of hydrocarbon aerosol fuels. *Combustion Science & Technology, 130*, 25-47.

Britton, L.G. (1999). A*voiding Static Ignition Hazards in Chemical Operations*. New York: Center for Chemical Process Safety, AIChE.

Burgoyne, J.H. (1957). Mist and spray explosions. *Chemical Engineering Progress, 53*(3), 121-124.

Burgoyne, J.H., & Cohen, L. (1954). The effect of droplet size on flame propagation of liquid aerosols. *Proceedings of the Royal Society of London, Series A, Mathematical and Physical Sciences, 225*, 375-392.

Burgoyne, J.H., & Richardson, J.F. (1949). The inflammability of oil mists. *Fuel, 28*, 2-6.

Cameron, L.R.J., & Bowen, P.J. (2001). Novel cloud chamber design for 'transition range' aerosol combustion studies. *Transactions of the IChemE, 79*(B), 197-205.

Chabay, I., & Bright, D. (1979). Measuring aerosol particles. *CHEMTECH, 9*(11), 694-699.

Chan, K-K., & Jou, C-S. (1988). An experimental and theoretical investigation of the transition phenomenon in fuel spray deflagration. 1. The experiment. *Fuel, 67*, 1223-1227.

Chan, K-K., & Jou, C-S. (1989). An experimental and theoretical investigation of the transition phenomenon in fuel spray deflagration. 2. The model. *Fuel, 68*, 139-144.

Chen, J.L., Dobashi, R. & Hirano, T. (1996). Mechanisms of flame propagation through combustible particle clouds. *Journal of Loss Prevention in the Process Industries, 9(3)*, 225-229.

Crowl, D.A., & Louvar, J.F. (1990). *Chemical Process Safety: Fundamentals with Applications*. Englewood Cliffs, NJ: Prentice Hall.

Cuthbert, J. (1994). Choose the right heat-transfer fluid. *Chemical Engineering Progress, July*, 29-37.

Eichhorn, J. (1955). Careful! Mists can explode. *Petroleum Refiner, 34(11)*, 194-196.

Elkotb, M.M. (1982). Fuel atomization for spray modeling. *Progress in Energy and Combustion Science, 8*, 61-91.

Eswaran, V., & Pope, S.B. (1988). Direct Numerical Simulations of the turbulent mixing of a passive scalar. *Physics of Fluids, 31*, 506 – 520.

Factory Mutual Engineering Corporation. (1974). *Accident Prevention Manual for Industrial Operations*, Chicago, IL: National Safety Council.

Faeth, G.M. (1983). Evaporation and combustion of sprays. *Progress in Energy and Combustion Science, 9(1-2)*, 1-76.

Faeth, G.M. (1990). Structure and atomization properties of dense turbulent sprays. *Proceedings of the Tewnty-third Symposium (Int.) on Combustion, Orleans, France*, 1345-1352.

Febo, H.L., & Valiulis, J.V. (1995). Heat transfer fluid mist explosion potential an important consideration for users. *Proceedings of the AIChE Loss Prevention Symposium, Norwood, MA.* Paper 4F.

Febo, H.L., & Valiulis, J.V. (1996). Recognize the potential for heat-transfer-fluid mist explosions. *Chemical Engineering Progress, March*, 52-55.

Felton, P.G. (1981). *Measurement of particle/droplet size distributions by a laser diffraction technique*. Department of Chemical Engineering and Fuel Technology Report, University of Sheffield, Sheffield, UK.

Felton, P.G., Hamidi, A.A., & Aigal, A.K. (1985). Measurement of drop size distribution in dense sprays by laser diffraction. *Proceedings of the ICLASS 85, London, England,* (July 8-10), IVA/4/1.

Fuchs, H.C.G. (1997). Understand thermal fluid analysis techniques. *Chemical Engineering Progress, December,* 39-44.

Fuhr, J.C. (1992). Prevent fires in thermal oil heat-transfer systems. *Chemical Engineering Progress, May*, 42-44.

Girimaji, S.S. (1994). Modeling turbulent scalar mixing as enhanced diffusion. *Combustion Science and Technology, 97*, 85 - 98.

Greenberg, J.B., Silverman, I., & Tambour, Y. (1998). On droplet enhancement of the burning velocity of laminar premixed spray flames. *Combustion and Flame, 113* (1-2), 271-273 (1998).

Hamidi, A.A. & Swithenbank, J. (1986a). Treatment of multiple scattering of light in laser diffraction measurement techniques in dense sprays and particle fields. *Journal of the Institute of Energy, June*, 101-105.

Hamidi, A.A. & Swithenbank, J. (1986b). Vignetting in forward light scattering particle size distribution measurement techniques. *Optical Engineering, 25:10*, 11294-1298.

Hecht E. (1998). *Optics,* 3rd ed. Reading, MA: Addison Wesley.

Hirleman, E.D., & Dodge, L.G. (1985). Performance comparison of Malvern Instruments lased diffraction drop size analyzers. *Proceedings of the ICLASS 85, London, England,* (July 8-10), IVA/3/1-14.

Hiroyasu, H. (1991). Experimental and theoretical studies on the structure of fuel sprays in diesel engines. *ICLASS-91,* 17-31.

Johnson, D.W. (1991). Prediction of aerosol formation from the release of pressurized, superheated liquids to the atmosphere. *Proceedings of the International Conference and Workshop on Modeling and Mitigating the Consequences of Accidental Releases of Hazardous Materials, New Orleans, Louisiana*, (May 20-24), 1-34.

Johnson, D.W., & Woodward, J.L. (1998). *Release: A Model with Data to Predict Aerosol Rainout in Accidental Releases*. New York: Center for Chemical Process Safety, AIChE.

Ju, W.J., Dobashi, R., & Hirano, T. (1998). Dependence of flammability limits of a combustible particle cloud on particle diameter distribution. *Journal of Loss Prevention in the Process Industries, 11,* 177-185.

Kihm, K.D. & Chigier, N. (1991). Effect of shock waves on liquid atomization of a two-dimensional airblast atomizer. *Atomization and Sprays, 1*, 113-136.

Kihm, K.D., Terracina, D.P., Payne, S.E., & Caton, J.A. (1994). Synchronised droplet size measurements for coal-water slurry sprays generated from a high-pressure diesel injection system. *Journal of the Institute of Energy, 67,* 2-9.

Krishna, K., Kim, T.K., Kihm, K.D., Rogers, W.J. & Mannan, M.S. (2001). Understanding the formation of heat transfer fluid aerosols in air. *Proceedings of the 4th Annual Mary Kay O'Connor Process Safety Center Symposium – Beyond Regulatory Compliance: Making Safety Second Nature, College Station, Texas,* (October 30-31).

Krishna, K., Kim, T.K., Kihm, K.D., Rogers, W.J., & Mannan, M.S. (2003). Predictive correlations for leaking heat transfer fluid aerosols in air. *Journal of Loss Prevention in the Process Industries, 16*(1), 1-8.

Laster, W.R. & Annamalai, K. (1989). Effect of droplet interactions on ignition delay times. *National Heat Transfer Conference, 106*, 415-421.

Lefebvre, A.H. (1989). *Atomization and Sprays*, Washington D.C.: Taylor&Francis.

Lewis, B., & G. Von Elbe (1961/87) *Combustion, flames and explosions of gases*, 2/3 ed., New York: Academic Press Inc.

Lin, T.H. & Sheu, Y.Y. (1991). Theory of laminar flame propagation in near-stoichiometric dilute sprays. *Combustion and Flame, 84* (3-4), 333-342.

Malvern Instruments Ltd. (1993). *Instruction Manual (System 2600)*. Malvern Instruments Ltd, Spring Lane South, Malvern, Worcs. WR14 1 AQ, England, IM 026 (MAN 0004), Issue 2.3.

McLean, J.A., Minnich, M.G., Montaser, A., Su, J., & Lai, W. (2000). Optical Patternation: A Technique for Three-dimensional Aerosol Diagnostics. *Analytical Chemistry*, *72*, 4796-4804.

Miles, B.H., King, G.B., & Sojka, P.E. (1989). Malvern particle size measurements in media with time varying index of refraction gradients. *Proceedings of the Institute of Liquid Atomization and Spray Systems (ILASS), Irvine, California*, 156-160.

Nakayama, Y. (1961). Action of fluid in the air micrometer: first report, characteristics of small diameter nozzle and orifice. *Bulletin of the Japanese Society of Mechanical Engineers*, 4, 516-514.

Nikmo, J., Kukkonen, J., Vesala, T., & Kulmala, M. (1994). A model for mass and heat transfer in an aerosol cloud. *Journal of Hazardous Materials*, *38*, 293-311.

Oetinger, J. (2002). Prevent fires in thermal fluid systems. *Chemical Engineering Progress*, *January*, 46-48.

Ohnesorge, W. (1936). Formation of drops by nozzles and the breakup of liquid jets. *Zeitschrift für Angewandte Mathematik und Mechanik,16*, 355–358.

Orme, M. (1997). Experiments on droplet collisions, bounce, coalescence and disruption. *Progress in Energy and Combustion Science*, *23*, 65-79.

Park, B.K., Lee, J.S., & Kihm, K.D. (1996). Comparative study of twin-fluid atomization using sonic or supersonic gas jets. *Atomization and Sprays*, 6, 285-304.

Peters, J.E., & Mellor, A.M. (1980). An ignition model for quiescent fuel sprays. *Combustion and Flame*, *38*, 65-74.

Pidoll, U.V. (2001). The ignition of clouds of sprays, powders and fibers by flames and electric sparks. *Journal of Loss Prevention in the Process Industries*, *14*, 103-109.

Polymeropoulos, C.E., (1984). Flame propagation in aerosols of fuel droplets, fuel vapor and air. *Combustion Science and Technology*, *40*, 217-232.

Richer, J.R., Swithenbank, J., & Wedd, M. (1994). Transient behavior of aerosol clouds in a confined volume: an experimental and computational study. *Proceedings of the ICLASS, Palais des Congrès, Rouen, France*, (July 18-22), XI.11, 978-985.

Rosin, P., & Rammler, E. (1933). The laws governing the fineness of powdered coal. *The Institute of Fuel, October*, 29-36.

Ruff, G. A., Bernal, L.P., & Faeth, G. M. (1989). Structure of the near-injector region of non-evaporating pressure-atomized sprays. *AIAA paper*, 89-0050.

Schmidli, J., Banerjee, S., & Yadigaroglu, G. (1990). Effects of vapor/aerosol and pool formation on rupture of vessels containing superheated liquid. *Journal of Loss Prevention in the Process Industries, 3,* 104-111.

Schweitzer, P.H. (1937). Mechanism of disintegration of liquid jets. *Journal of Applied Physics*, 8, 513-521.

Sehgal, D.P.S., Sharma, S.N., & Mishra, G.J. (1999). Aerosol or IED explosion: a case report. *Forensic Science International*. *102*, 67-72.

Semião, V., Andrade, P., & da Graça Carvalho, M. (1996). Spray characterization: numerical prediction of Sauter mean diameter and droplet size distribution. *Fuel*, *75(15)*, 1707-1714.

Singh, J. (1981). Selecting heat-transfer fluids for high-temperature service. *Chemical Engineering, June 1*, 53-58.

Sommerfeld, M., & Qiu, H.H. (1998). Experimental studies of spray evaporation in turbulent flow. *International Journal of Heat and Fluid Flow, 19*, 10-22.

Spalding, D.B. (1979). *Combustion and Mass Transfer*, Oxford, UK: Pergamon Press.

Sukmarg, P., Krishna, K., Kihm, K.D., Rogers, W.J., & Mannan, M.S. (2002). Non-intrusive characterization of heat transfer fluid aerosols in air. *The Journal of Loss Prevention in the Process Industries*, *15*(1), 19-27.

Sullivan, M.V., Wolfe, J.K., & Zisman, W.A. (1947). Flammability of higher boiling liquids and their mists. *Industrial and Engineering Chemistry*. 39(12), 1607-1614.

Tabata, M., Arai, M., & Hiroyasu, H. (1985). Effect of fuel viscosity and surface tension on diesel spray drops. *Proceedings of the ICLASS 85, London, England*, (July 8-10), IIB/1/1.

The Institute of Petroleum. (1990). *Classification Code for Petroleum Installations*. Chichester, UK: Wiley.

The Institute of Petroleum. (1990). *Model Code of Safe Practice*. Chichester, UK: Wiley.

Vasserman, A.A., Kazavchinskii, Y.Z., & Rabinovich, V.A. (1966). *Thermophysical Properties of Air and Air Components.* Moscow: Academy of Sciences of the USSR.

Vincent, G.C., & Howard, W.B. (1976a). Part I: Hydrocarbon mist explosions, prevention by explosion suppression. *CEP Technical Manual*, *10*, 43-47.

Vincent, G.C., Nelson, R.C., Howard, W.B., & Russel, W.W. (1976b). Part II: Hydrocarbon mist explosions, prevention by water fog. *CEP technical manual*, *10*, 55-64.

Watson, D.J., & Tech, B. (1985). Laser diffraction measurements in transient spray conditions. *Proceedings of the ICLASS 85, London, England*, (July 8-10), VC/4/1.

Weber, R., Boysan, F., Swithenbank, J., Bolado, R., & Yule, A. (1985). Spray combustion of small and large droplets of heavy fuel oils. *Proceedings of the ICLASS 85, London, England*, (July 8-10), VIA/1/1.

Wild, P.N., & Swithenbank, J. (1986). Beam stop and vignetting effects in particle size measurements by laser diffraction. *Applied Optics*, *25:19*, 3520-3526.

Williams, F.A. (1998). *Combustion Theory*. Reading, MA: Addison-Wesley.

Wong, S.C., Liao, X.X., & Yang, J.R. (1997). A simplified theory of the ignition of single droplets under forced convection. *Combustion and Flame*, *110*, 319-334.

Woodward, J.L., & Papadourakis, A. (1995). Reassessment and reevaluation of rainout and drop size correlation for an aerosol jet. *Journal of Hazardous Materials*, *44*, 209-230.

Woodward, J.L., Cook, J., & Papadourakis, A. (1995). Modeling and validation of a dispersing aerosol jet. *Journal of Hazardous Materials*, *44*, 185-207.

Yu, H., Luo, L-S., & Girimaji, S.S. (2002) Scalar mixing and chemical reaction simulations using Lattice-Boltzman Method. *International Journal of Computational Engineering Sciences*, *3*(1), 73-87.

APPENDIX A

DEFINITIONS

Aerosol: A suspension of fine solid or liquid particles in gas

Atomization: To reduce to minute particles or to a fine spray. The action of producing an aerosol.

Autoignition temperature: The lowest temperature at which a material will ignite without an external source of ignition. Storing a substance anywhere near its autoignition temperature is a severe safety hazard. Knowing a substance's autoignition temperatures is also very useful in the event of a fire.

Drop: The quantity of fluid that falls in one spherical mass

Droplet: A tiny drop (as of a liquid)

Fire Point: The temperature at which the flame becomes self-sustained so as to continue burning the liquid. At the fire point, the flame does not need to be sustained.

Flash point: The lowest temperature at which a liquid can form an ignitable mixture in air near the surface of the liquid. The lower the flash point, the easier it is to ignite the material.

Fresnel-Kirchhoff theory: Diffraction can be defined as the resultant wave phenomena when part of its wave front has been obstructed. The parts of the wave that move beyond the obstruction interfere to create the diffraction pattern. Huygens' principle can explain the important features of this theory. This principle states that the propagation of a light wave can be predicted by assuming that each section of the wave front acts as another source that spreads out in all directions. The mathematical form used to quantify Huygens' principle is known as the Fresnel-Kirchhoff formula. Fraunhofer diffraction is the resultant diffraction pattern when the distance from the object to the source and the object to the image are so great that the incoming and outgoing waves are planar. Fresnel diffraction is the opposite of Fraunhofer diffraction in that the curvature of the incoming and outgoing waves is important. The condition that differentiates between the two types of diffraction is as follows:

Hazard: A source of danger or risk

Heat transfer fluids: Non-toxic and non-fouling, these thermal oils are designed for rugged, indirect heating and cooling service in non-pressurized high-temperature closed-loop heat transfer systems, temperature control units, thermal fluid heaters, process temperature controllers, and heat exchangers. Also called Thermal Fluids, Hot Oils and Diathermic Oils

Ignition: The process or means (as an electric spark) of igniting a fuel mixture

Minimum Ignition Energy: The minimum ignition energy (MIE) of an aerosol cloud is the lowest energy value of a high-voltage capacitor discharge required to ignite the most readily ignitable aerosol/air mixture at atmospheric pressure and room temperature. The aerosol concentration and the ignition delay are systematically varied until a minimum value of the ignition energy is found

Mist: A cloud of small particles or objects suggestive of a mist; a suspension of a finely divided liquid in a gas; a fine spray

Particle: A minute quantity or fragment. May be solid of liquid

Plane wave: Wave in which wave fronts are parallel to a plane normal to the direction of propagation.

Risk: Probability of loss or injury

Spray: (N) A jet of vapor or finely divided liquid; (V) to disperse or apply as a spray

APPENDIX B

SUMMARY OF FLUID PROPERTIES

Heat Transfer Fluid	AAR	MTP	DTA	DAA	WMO	BDO
Appearance	Clear, yellow liquid	Clear, pale yellow liquid	Light amber to brown liquid	Clear colorless liquid	Bright, clear, colorless	Clear, water white liquid
Composition	Synthetic hydrocarbon mixture of alkylated aromatics	Modified terphenyl	Mixture of di- and tri-aryl compounds	Diaryl alkyl	White mineral oil	Biphenyl/diphenyl oxide eutectic mixture
Recommended operating range	-25 °C To 290 °C	0 °C To 345 °C	29 °C To 371 °C	0 °C To 350 °C	-25 °C To 315 °C	Liquid: 12 °C to 400 °C Vapor: 260 °C to 400 °C
Average Molecular Weight	320	252	204.6	236.4	350	166
Pour Point	-54 °C	-32 °C	NA	NA	-40 °C	NA
Crystal Point	NA	NA	4 °C	NA	NA	12 °C
Flash Point	177 °C†	184 °C†	124 °C†	194°C‡	171 °C†	124 °C†
Fire Point†	218 °C	212 °C	128 °C	206 °C	196 °C	127 °C
Boiling Point	351 °Cℑ	359 °Cℑ	288 °Cℑ	353 °Cℑ	349 °Cℜ	257 °Cℑ
Autoignition Temperatureℵ	343 °C	374 °C	584 °C	385 °C	366 °C	621 °C

† ASTM D-92: Cleveland Open Cup (COC)
‡ ASTM D-93: Pensky Martens Closed Cup (PMCC)
ℑ Normal Boiling Point
ℜ Atmospheric Boiling Point (10%) ASTM D1160
ℵ ASTM E 659-78: The old ASTM procedure, D-2155-66 has been withdrawn by the testing society and replaced by ASTM E 659-78
NA Data not available

APPENDIX C

AEROSOL CHARACTERIZATION DATA

Heat Transfer Fluid	Orifice diameter	Axial Distance	Air temp	Nozzle temp	Pressure transducer readings		Obscu-ration	*Log Diff.*	SMD
	mm	cm	°C	°C	Vin	Vout			μm
AAR	0.38	41	16.8	108.4	10.2219	0.0230	0.6262	5.165	71.13
AAR	0.38	36	16.8	110.5	10.2219	0.0234	0.6594	5.180	67.07
AAR	0.38	31	16.8	110.4	10.2220	0.0234	0.6173	5.248	72.98
AAR	0.38	26	16.8	109.8	10.2220	0.0239	0.6022	5.385	77.78
AAR	0.38	21	16.8	111.4	10.2220	0.0235	0.6177	5.126	122.43
AAR	0.38	41	16.8	112.9	10.2220	0.0377	0.8176	4.438	42.25
AAR	0.38	36	16.8	113.1	10.2220	0.0382	0.8170	4.600	40.40
AAR	0.38	31	16.8	111.8	10.2220	0.0385	0.7560	4.790	36.81
AAR	0.38	26	16.8	112.1	10.2220	0.0383	0.7572	5.097	41.49
AAR	0.38	41	16.6	105.9	10.2117	0.0216	0.6116	5.007	67.93
AAR	0.38	36	16.6	106.4	10.2118	0.0217	0.6243	5.097	67.89
AAR	0.38	31	16.6	107.2	10.2118	0.0213	0.6117	5.290	72.93
AAR	0.38	26	16.6	107.8	10.2118	0.0218	0.5998	5.594	84.43
AAR	0.38	21	16.6	108.6	10.2117	0.0217	0.6342	4.968	112.48
AAR	0.38	41	16.6	110.8	10.2118	0.0385	0.7875	4.274	39.74
AAR	0.38	41	16.6	112.3	10.2118	0.0367	0.7935	4.569	42.83
AAR	0.38	36	16.6	119.9	10.2118	0.0360	0.7722	4.737	43.62
AAR	0.38	41	15.0	118.8	10.0449	0.0205	0.5640	4.089	67.23
AAR	0.38	36	15.0	116.2	10.0446	0.0206	0.4958	4.084	54.60
AAR	0.38	41	15.0	116.7	10.0446	0.0212	0.5590	4.026	61.30
AAR	0.38	31	15.0	116.2	10.0448	0.0206	0.6101	4.168	71.15
AAR	0.38	31	15.0	117.2	10.0447	0.0207	0.6119	4.158	73.46
AAR	0.21	41	18.7	123.1	10.0280	0.0213	0.0463	4.100	251.51
AAR	0.21	41	18.5	121.1	10.0280	0.0358	0.1400	5.095	134.21
AAR	0.21	36	18.3	119.7	10.0280	0.0358	0.0415	4.876	146.44

Heat Transfer Fluid	Orifice diameter	Axial Distance	Air temp	Nozzle temp	Pressure transducer readings		Obscu-ration	*Log Diff.*	SMD
	mm	cm	°C	°C	Vin	Vout			μm
AAR	0.21	31	18.0	120.8	10.0276	0.0358	0.0843	4.638	240.69
AAR	0.58	41	17.8	120.3	10.0601	0.0208	0.6827	4.114	48.41
AAR	0.58	36	17.8	119.6	10.0566	0.0202	0.7980	5.205	58.95
AAR	0.58	31	17.7	117.8	10.0426	0.0216	0.8195	5.280	63.50
AAR	0.58	26	17.6	119.1	10.0395	0.0210	0.8130	5.226	65.89
AAR	0.58	21	17.5	119.2	10.0503	0.0212	0.8101	5.487	69.95
AAR	0.58	16	17.4	119.2	10.0529	0.0219	0.8159	5.531	78.71
AAR	0.38	41	18.8	121.5	10.2000	0.0350	0.6099	3.906	41.02
AAR	0.38	36	18.8	120.2	10.2002	0.0352	0.6966	3.863	40.40
AAR	0.38	31	18.8	120.1	10.1672	0.0351	0.6607	4.102	38.55
AAR	0.38	26	18.8	120.2	10.1465	0.0351	0.6973	4.313	35.84
AAR	0.38	21	18.8	120.3	10.1499	0.0352	0.6880	4.390	32.85
AAR	0.38	16	18.8	120.2	10.1460	0.0350	0.6889	4.587	33.04
AAR	0.38	11	18.8	120.4	10.0562	0.0351	0.6459	4.860	37.23
AAR	0.38	6	18.8	120.6	10.0508	0.0351	0.5955	5.123	55.94
AAR	0.38	41	18.9	119.8	10.0596	0.0210	0.4055	4.704	53.71
AAR	0.38	36	18.9	119.3	10.0597	0.0211	0.4591	4.852	56.19
AAR	0.38	31	18.9	118.2	10.0597	0.0210	0.3854	4.733	46.73
AAR	0.38	26	18.9	120.0	10.0600	0.0211	0.4111	4.828	47.65
AAR	0.38	21	18.9	120.3	10.0600	0.0210	0.5174	4.926	106.34
AAR	0.38	41	18.7	121.8	10.0588	0.0110	0.3002	5.099	118.21
AAR	0.38	36	18.7	122.1	10.0588	0.0109	0.1778	5.420	77.85
AAR	0.38	31	18.7	122.1	10.0588	0.0109	0.1926	5.349	95.75
AAR	0.38	26	18.7	123.1	10.0591	0.0109	0.1943	5.333	113.71
AAR	0.38	21	18.7	123.4	10.0591	0.0110	0.1406	5.485	64.55
AAR	0.38	16	18.7	122.8	10.0593	0.0110	0.1976	5.235	112.93
AAR	0.38	11	18.7	121.9	10.0592	0.0109	0.1757	5.232	124.86
AAR	0.38	40	19.2	80.3	10.0564	0.0349	0.7101	3.950	54.91
AAR	0.38	36	19.2	80.3	10.0564	0.0346	0.6690	3.901	53.00
AAR	0.38	31	19.2	81.6	10.0564	0.0345	0.7092	4.206	49.47
AAR	0.38	26	19.2	81.0	10.0565	0.0345	0.6849	4.363	51.29
AAR	0.38	21	19.2	81.4	10.0565	0.0348	0.5099	4.224	33.03
AAR	0.38	16	19.2	81.4	10.0565	0.0348	0.2065	4.863	49.27
AAR	0.38	11	19.2	81.4	10.0565	0.0345	0.5218	5.272	59.16

Heat Transfer Fluid	Orifice diameter	Axial Distance	Air temp	Nozzle temp	Pressure transducer readings		Obscu-ration	*Log Diff.*	SMD
	mm	cm	°C	°C	Vin	Vout			μm
AAR	0.38	6	19.2	80.9	10.0565	0.0344	0.5022	5.592	74.88
AAR	0.38	36	17.2	80.6	10.2612	0.0263	0.3302	5.771	69.11
AAR	0.38	31	17.2	81.5	10.2612	0.0257	0.2383	5.942	62.23
AAR	0.38	26	17.2	83.1	10.2613	0.0257	0.3138	5.685	84.07
AAR	0.38	21	17.2	83.7	10.2615	0.0259	0.1963	5.791	61.76
AAR	0.38	16	17.2	85.0	10.2613	0.0259	0.1533	5.631	56.11
AAR	0.21	1	19.0	78.7	10.2314	0.0214	0.0797	4.175	217.79
AAR	0.21	6	19.0	79.0	10.2317	0.0214	0.0387	4.571	183.02
AAR	0.21	11	19.0	79.3	10.2316	0.0214	0.0586	4.255	220.44
AAR	0.21	16	19.0	79.7	10.2315	0.0215	0.0257	4.939	136.06
AAR	0.38	11	19.0	80.8	10.0490	0.0210	0.4974	4.474	150.56
AAR	0.38	16	19.0	81.0	10.0494	0.0218	0.3369	5.161	71.75
AAR	0.38	16	19.0	82.0	10.0495	0.0217	0.4754	4.488	118.23
AAR	0.38	21	19.0	81.8	10.0496	0.0208	0.2444	4.847	59.83
AAR	0.38	21	19.0	81.6	10.0498	0.0213	0.3016	4.692	53.71
AAR	0.38	26	19.0	80.3	10.0499	0.0213	0.3124	4.255	54.74
AAR	0.38	31	19.0	80.3	10.0500	0.0210	0.3400	4.583	63.98
AAR	0.38	36	19.0	80.0	10.0500	0.0210	0.1559	4.664	85.47
AAR	0.38	36	19.0	82.0	10.0500	0.0212	0.3262	3.913	49.49
AAR	0.38	41	19.0	81.8	10.0500	0.0212	0.3476	3.922	44.97
AAR	0.38	41	15.3	118.8	10.0449	0.0205	0.5640	5.035	75.32
AAR	0.38	36	15.3	116.2	10.0446	0.0206	0.4958	4.915	59.94
AAR	0.38	41	15.3	116.7	10.0446	0.0212	0.5590	4.993	72.59
AAR	0.38	31	15.3	116.2	10.0448	0.0206	0.6101	5.110	89.95
AAR	0.38	31	15.3	117.2	10.0447	0.0207	0.6119	4.896	103.86
AAR	0.58	41	15.3	117.5	10.0446	0.0208	0.8218	4.404	48.19
AAR	0.58	36	15.3	117.6	10.0447	0.0215	0.8417	4.684	50.83
AAR	0.58	31	15.3	118.2	10.0448	0.0216	0.8275	4.991	57.33
MTP	0.38	41	17.6	95.2	10.2609	0.0299	0.5219	4.898	76.99
MTP	0.38	36	17.6	99.1	10.2609	0.0303	0.5332	5.145	79.48
MTP	0.38	31	17.6	100.5	10.2608	0.0302	0.5634	4.995	96.25
MTP	0.38	26	17.6	102.0	10.2608	0.0304	0.5286	5.367	84.03

Heat Transfer Fluid	Orifice diameter	Axial Distance	Air temp	Nozzle temp	Pressure transducer readings		Obscu-ration	*Log Diff.*	SMD
	mm	cm	°C	°C	Vin	Vout			μm
MTP	0.38	21	17.6	103.7	10.2607	0.0303	0.4121	5.416	64.23
MTP	0.38	21	17.6	103.9	10.2606	0.0306	0.5442	4.102	113.07
MTP	0.38	31	17.6	104.9	10.2607	0.0304	0.5752	4.835	108.06
MTP	0.38	41	17.2	114.1	10.2129	0.0231	0.4545	4.457	107.89
MTP	0.38	36	17.2	113.4	10.2130	0.0235	0.4525	4.233	111.43
MTP	0.38	31	17.2	113.1	10.2131	0.0235	0.4089	5.063	111.94
MTP	0.38	26	17.2	113.5	10.2131	0.0235	0.3391	5.067	106.86
MTP	0.38	21	17.2	114.7	10.2131	0.0233	0.5093	4.630	153.89
MTP	0.38	41	17.2	113.5	10.2132	0.0241	0.2672	4.908	60.15
MTP	0.38	36	17.2	115.2	10.2132	0.0241	0.2951	5.159	69.02
MTP	0.38	31	17.2	114.9	10.2132	0.0241	0.3033	5.333	73.19
MTP	0.38	26	17.2	114.4	10.2131	0.0241	0.2815	5.433	75.05
MTP	0.38	21	17.2	113.8	10.2131	0.0241	0.3248	5.300	94.40
MTP	0.38	16	17.2	113.7	10.2131	0.0241	0.3482	5.113	111.84
MTP	0.38	11	17.2	113.5	10.2130	0.0240	0.3539	5.133	149.97
MTP	0.38	41	16.1	96.0	10.0630	0.0215	0.4289	4.994	98.34
MTP	0.38	36	16.1	97.2	10.0620	0.0219	0.3499	5.093	74.26
MTP	0.38	31	16.1	96.5	10.0619	0.0219	0.3727	5.042	101.14
MTP	0.38	26	16.1	96.2	10.0619	0.0219	0.4358	4.650	126.50
MTP	0.38	21	16.1	95.2	10.0615	0.0219	0.4301	4.567	144.66
MTP	0.38	41	16.8	117.8	10.0492	0.0111	0.1276	4.404	149.01
MTP	0.38	36	16.8	116.3	10.0493	0.0112	0.1934	3.775	201.21
MTP	0.21	41	16.8	117.3	10.0490	0.0212	0.2672	5.087	65.45
MTP	0.21	36	16.8	123.2	10.0489	0.0212	0.2596	5.287	63.58
MTP	0.21	31	16.8	122.2	10.0490	0.0212	0.2171	5.273	64.44
MTP	0.21	26	16.8	119.4	10.0490	0.0212	0.2645	5.517	74.14
MTP	0.21	21	16.8	122.5	10.0491	0.0212	0.2841	5.704	78.35
MTP	0.21	16	16.8	121.4	10.0491	0.0212	0.2308	5.527	121.92
MTP	0.21	11	16.8	122.7	10.0491	0.0212	0.2225	6.194	87.66
MTP	0.21	31	16.8	123.1	10.0491	0.0212	0.2579	4.853	55.58
MTP	0.58	41	16.8	120.2	10.0490	0.0214	0.7071	5.095	75.64
MTP	0.58	36	16.8	120.4	10.0494	0.0218	0.7226	5.289	95.22
MTP	0.58	31	16.8	122.4	10.0491	0.0217	0.7027	5.335	98.03

Heat Transfer Fluid	Orifice diameter	Axial Distance	Air temp	Nozzle temp	Pressure transducer readings		Obscu-ration	*Log Diff.*	SMD
	mm	cm	°C	°C	Vin	Vout			μm
MTP	0.58	26	16.8	121.4	10.0491	0.0214	0.7153	5.033	114.20
MTP	0.38	41	16.8	117.3	10.0499	0.0209	0.4402	5.122	76.96
MTP	0.38	36	16.8	119.5	10.0496	0.0209	0.4216	4.910	110.33
MTP	0.38	31	16.8	119.9	10.0499	0.0209			
MTP	0.38	31	16.8	118.2	10.0495	0.0210	0.4459	4.628	114.63
MTP	0.38	26	16.8	117.1	10.0493	0.0209	0.4415	4.487	121.05
MTP	0.38	41	16.8	116.8	10.0491	0.0210	0.3661	5.108	85.53
MTP	0.38	36	16.8	116.6	10.0490	0.0210	0.4332	5.082	119.63
MTP	0.38	41	16.8	118.3	10.0490	0.0353	0.5657	4.559	51.57
MTP	0.38	36	16.8	118.4	10.0490	0.0353	0.4855	4.455	41.01
MTP	0.38	31	16.8	119.1	10.0493	0.0355	0.5907	4.867	60.23
MTP	0.38	26	16.8	119.1	10.0496	0.0354	0.6415	5.134	82.50
MTP	0.38	21	16.8	118.4	10.0495	0.0355	0.4860	5.157	56.60
MTP	0.38	16	16.8	118.9	10.0491	0.0348	0.4497	5.073	62.99
MTP	0.38	11	16.8	118.6	10.0492	0.0354	0.6244	4.442	142.05
MTP	0.38	26	16.8	118.9	10.0490	0.0351	0.6350	4.974	84.74
MTP	0.38	36	16.8	118.6	10.0493	0.0353	0.6258	4.826	63.66
DTA	0.38	38	17.7	70.1	10.2315	0.0203	0.3348	4.851	115.74
DTA	0.38	41	17.6	69.3	10.2315	0.0203	0.3360	4.487	109.61
DTA	0.38	36	17.7	69.6	10.2315	0.0203	0.3513	4.414	121.64
DTA	0.38	31	17.9	69.4	10.2317	0.0202	0.3577	4.387	131.08
DTA	0.38	31	17.2	70.1	10.2319	0.0358	0.6033	4.928	75.79
DTA	0.38	41	17.4	69.4	10.2320	0.0361	0.6049	4.817	62.85
DTA	0.38	36	17.6	69.9	10.2321	0.0361	0.6133	4.864	66.12
DTA	0.38	31	17.9	70.3	10.2322	0.0359	0.6254	4.891	74.16
DTA	0.38	26	17.1	69.7	10.2324	0.0360	0.6192	5.396	78.12
DTA	0.38	21	16.8	69.9	10.2325	0.0359	0.6043	6.339	78.82
DTA	0.38	16	17.4	70.1	10.2327	0.0355	0.5592	4.814	138.70
DTA	0.38	21	18.1	70.2	10.2331	0.0357	0.5915	6.271	79.35
DTA	0.38	41	17.3	69.6	10.2333	0.0124	0.1581	4.393	194.89
DTA	0.21	41	17.5	69.4	10.2338	0.0212	0.2332	5.088	65.71
DTA	0.21	36	17.3	70.4	10.2341	0.0211	0.2524	5.244	66.09
DTA	0.21	31	18.1	71.1	10.2343	0.0212	0.2302	5.204	59.43

Heat Transfer Fluid	Orifice diameter	Axial Distance	Air temp	Nozzle temp	Pressure transducer readings		Obscu-ration	*Log Diff.*	SMD
	mm	cm	°C	°C	Vin	Vout			μm
DTA	0.21	26	17.3	70.6	10.2344	0.0212	0.2428	5.403	78.26
DTA	0.21	21	16.8	70.2	10.2346	0.0212	0.2549	5.121	97.06
DTA	0.21	16	17.9	71.0	10.2349	0.0212	0.2811	5.134	113.87
DTA	0.21	31	17.6	70.5	10.2347	0.0212	0.2367	5.219	67.12
DTA	0.76	41	18.2	70.8	10.2355	0.0147	0.5966	4.413	154.59
DTA	0.76	41	18.8	71.8	10.2358	0.0197	0.6691	4.800	125.57
DTA	0.38	41	19.0	51.9	10.2365	0.0210	0.2818	4.114	76.37
DTA	0.38	41	18.4	50.6	10.2366	0.0209	0.3556	4.018	108.68
DTA	0.38	36	17.7	49.1	10.2369	0.0212	0.3487	3.892	108.10
DTA	0.38	31	17.7	49.4	10.2368	0.0211	0.3629	3.656	118.62
DTA	0.21	41	17.9	47.8	10.2314	0.0221	0.1404	4.930	112.95
DTA	0.21	36	17.4	49.6	10.2315	0.0221	0.1610	4.959	115.74
DTA	0.21	31	17.8	50.5	10.2313	0.0220	0.1503	5.172	115.74
DTA	0.21	26	17.8	49.9	10.2312	0.0219	0.1598	4.765	118.86
DTA	0.21	41	18.5	50.1	10.2309	0.0360	0.3380	3.776	52.51
DTA	0.21	36	20.4	51.0	10.2310	0.0365	0.3380	3.759	52.48
DTA	0.21	31	18.9	50.0	10.2308	0.0366	0.3548	4.068	50.04
DTA	0.21	26	19.4	49.8	10.2308	0.0367	0.3321	4.076	54.93
DTA	0.21	21	20.1	50.0	10.2307	0.0366	0.3334	4.353	63.70
DTA	0.21	16	20.5	50.2	10.2306	0.0366	0.3409	4.044	70.94
DTA	0.21	11	20.4	49.9	10.2309	0.0365	0.3413	4.538	77.79
DTA	0.21	6	20.0	50.4	10.2307	0.0366	0.3659	5.993	78.34
DTA	0.21	1	20.7	49.9	10.2305	0.0364	0.3931	4.297	113.98
DTA	0.21	41	18.8	70.9	10.2305	0.0360	0.3611	3.882	43.38
DTA	0.21	36	18.7	70.6	10.2305	0.0364	0.3862	4.240	42.66
DTA	0.21	31	19.6	68.0	10.2306	0.0365	0.3732	4.393	42.55
DTA	0.21	26	19.3	29.4	10.2307	0.0365	0.4279	4.757	40.84
DTA	0.21	21	202.0	69.8	10.2306	0.0365	0.4135	4.995	48.18
DTA	0.21	16	20.2	70.3	10.2306	0.0365	0.4113	5.091	44.98
DTA	0.21	11	19.7	70.0	10.2307	0.0365	0.4186	5.231	48.30
DTA	0.21	6	19.7	70.0	10.2307	0.0364	0.5148	5.426	62.82
DTA	0.21	1	19.2	70.3	10.2307	0.0366	0.5803	5.803	105.98
DTA	0.21	41	19.6	70.1	10.2308	0.0111	0.0681	4.719	183.16

Heat Transfer Fluid	Orifice diameter	Axial Distance	Air temp	Nozzle temp	Pressure transducer readings		Obscu-ration	*Log Diff.*	SMD
	mm	cm	°C	°C	Vin	Vout			μm
DTA	0.38	41	18.2	84.2	10.2327	0.0215	0.4213	4.711	97.06
DTA	0.38	36	18.6	87.3	10.2328	0.0216	0.4319	4.483	101.18
DTA	0.38	31	18.8	88.9	10.2332	0.0215	0.4279	4.368	118.17
DTA	0.38	26	18.8	89.0	10.2332	0.0216	0.4364	4.413	115.75
DTA	0.38	21	18.7	89.1	10.2331	0.0217	0.4220	4.595	98.75
DTA	0.21	41	18.5	88.9	10.2337	0.0226	0.2723	5.249	55.63
DTA	0.21	26	18.4	90.8	10.2337	0.0227	0.2781	5.561	67.68
DTA	0.21	21	18.3	90.6	10.2337	0.0228	0.3191	5.614	64.03
DTA	0.21	16	19.2	91.9	10.2341	0.0227	0.3150	5.535	66.12
DTA	0.21	11	19.0	92.7	10.2340	0.0228	0.3630	5.380	104.92
DTA	0.21	36	19.2	91.4	10.2341	0.0227	0.2678	5.443	59.78
DTA	0.21	31	18.9	90.5	10.2341	0.0227	0.2775	5.502	60.71
DAA	0.76	40.5	17.0	110.2	10.2251	0.0196	0.7486	4.860	109.88
DAA	0.76	36	17.0	111.1	10.2251	0.0198	0.7214	4.967	126.12
DAA	0.76	31	16.7	111.7	10.2253	0.0201	0.6346	5.311	93.10
DAA	0.76	26	16.8	112.1	10.2253	0.0193	0.6712	5.230	149.83
DAA	0.76	31	16.9	111.9	10.2252	0.0202	0.6951	4.999	106.74
DAA	0.76	36	17.2	111.7	10.2254	0.0201	0.6437	5.050	69.09
DAA	0.38	41	15.7	133.1	10.2193	0.0212	0.4749	4.857	99.77
DAA	0.38	36	15.5	135.3	10.2193	0.0213	0.4162	4.648	122.31
DAA	0.38	31	15.5	135.0	10.2194	0.0215	0.5033	4.496	108.52
DAA	0.38	26	15.2	134.6	10.2193	0.0214	0.5053	4.231	145.52
DAA	0.38	41	15.5	114.6	10.2194	0.0284	0.5556	5.037	82.15
DAA	0.38	63	15.7	113.0	10.2194	0.0282	0.5237	5.012	86.48
DAA	0.38	31	15.6	112.6	10.2194	0.0287	0.4884	5.023	63.56
DAA	0.38	31	15.6	112.0	10.2194	0.0283	0.5636	4.715	113.21
DAA	0.38	26	15.6	111.3	10.2194	0.0286	0.5379	4.711	105.63
DAA	0.38	21	15.6	110.4	10.2193	0.0284	0.5425	4.619	127.32
DAA	0.38	31	15.9	110.1	10.2193	0.0284	0.5429	5.381	95.75
DAA	0.58	41	16.2	110.6	10.2195	0.0215	0.7044	5.241	84.08
DAA	0.58	36	15.8	110.7	10.2195	0.0210	0.6681	5.316	83.26
DAA	0.38	41	17.5	90.0	10.2161	0.0218	0.4217	4.728	98.45

Heat Transfer Fluid	Orifice diameter	Axial Distance	Air temp	Nozzle temp	Pressure transducer readings		Obscu-ration	*Log Diff.*	SMD
	mm	cm	°C	°C	Vin	Vout			μm
DAA	0.38	36	17.3	90.6	10.2161	0.0221	0.4332	5.027	111.94
DAA	0.38	31	17.6	91.3	10.2162	0.0220	0.4470	4.403	118.43
DAA	0.38	26	17.4	91.0	10.2162	0.0220	0.4481	4.340	121.75
DAA	0.21	71	17.0	110.2	10.2165	0.0225	0.2601	4.778	57.22
DAA	0.21	36	16.6	110.4	10.2165	0.0229	0.2970	5.155	60.24
DAA	0.21	31	17.4	110.9	10.2164	0.0231	0.2821	5.271	65.31
DAA	0.21	26	17.0	111.4	10.2166	0.0231	0.3169	5.410	66.39
DAA	0.21	21	16.9	111.2	10.2166	0.0231	0.3145	5.517	79.57
DAA	0.21	16	16.7	111.4	10.2165	0.0231	0.3419	5.113	107.77
DAA	0.21	11	16.7	111.5	10.2166	0.0230	0.2822	6.103	72.41
DAA	0.58	41	17.1	112.4	10.2167	0.0222	0.6691	5.084	66.84
DAA	0.58	36	16.9	112.1	10.2167	0.0230	0.7342	5.306	80.02
DAA	0.38	41	18.3	108.0	10.2188	0.0108	0.2110	4.394	199.87
DAA	0.38	41	18.3	109.2	10.2188	0.0220	0.4404	5.063	97.82
DAA	0.38	36	18.2	109.0	10.2188	0.0227	0.4389	4.823	89.99
DAA	0.38	31	17.1	107.9	10.2188	0.0227	0.4913	4.577	94.77
DAA	0.38	26	17.0	108.5	10.2188	0.0228	0.5125	4.546	141.65
DAA	0.38	41	17.6	110.2	10.2187	0.0357	0.6285	4.937	56.07
DAA	0.38	36	17.6	109.9	10.2188	0.0361	0.6669	5.123	65.12
DAA	0.38	31	16.5	108.3	10.2188	0.0361	0.6088	5.225	68.37
DAA	0.38	21	17.2	108.1	10.2188	0.0363	0.6326	5.735	85.72
DAA	0.38	16	16.9	107.9	10.2188	0.0363	0.6675	4.624	117.75
DAA	0.38	26	16.5	107.8	10.2188	0.0362	0.6121	5.568	84.49
DAA	0.38	26	16.7	108.2	10.2187	0.0363	0.5604	5.273	77.38
DAA	0.38	31	16.5	108.0	10.2187	0.0362	0.6001	5.179	70.81
WMO	0.38	41	19.2	84.8	10.2358	0.0222	0.5126	4.034	64.94
WMO	0.38	41	19.4	87.5	10.2360	0.0221	0.5691	4.482	74.47
WMO	0.38	36	19.4	87.7	10.2361	0.0219	0.5751	4.625	78.71
WMO	0.38	31	19.6	88.2	10.2361	0.0218	0.5656	4.716	87.47
WMO	0.38	26	19.3	88.3	10.2361	0.0220	0.5214	4.761	79.06
WMO	0.38	21	19.3	88.8	10.2361	0.0217	0.5533	7.840	91.80
WMO	0.38	16	19.4	89.0	10.2362	0.0219	0.5726	4.560	115.88
WMO	0.38	26	19.3	88.8	10.2363	0.0220	0.6035	4.956	96.15

Heat Transfer Fluid	Orifice diameter	Axial Distance	Air temp	Nozzle temp	Pressure transducer readings		Obscu-ration	*Log Diff.*	SMD
	mm	cm	°C	°C	Vin	Vout			μm
WMO	0.21	41	19.2	90.4	10.2365	0.0226	0.3093	4.604	70.42
WMO	0.21	36	20.0	92.0	10.2365	0.0225	0.3037	4.710	69.72
WMO	0.21	31	20.3	90.1	10.2366	0.0225	0.3384	4.891	61.60
WMO	0.21	26	20.2	90.0	10.2365	0.0225	0.3314	5.008	68.70
WMO	0.21	21	20.6	90.6	10.2366	0.0223	0.2671	4.991	71.43
WMO	0.21	16	20.3	90.2	10.2366	0.0224	0.3435	5.031	110.93
WMO	0.21	11	20.5	90.8	10.2366	0.0223	0.3537	4.886	137.32
WMO	0.21	41	20.1	106.3	10.2363	0.0220	0.2828	4.791	69.72
WMO	0.21	36	20.5	106.7	10.2363	0.0219	0.3230	4.841	82.76
WMO	0.21	31	20.0	108.7	10.2362	0.0218	0.3321	5.047	79.80
WMO	0.21	26	21.0	111.4	10.2362	0.0217	0.3133	5.100	69.72
WMO	0.21	21	20.6	109.8	10.2362	0.0218	0.3408	5.287	88.51
WMO	0.21	16	20.6	110.5	10.2362	0.0218	0.3593	5.111	89.33
WMO	0.21	11	20.6	110.9	10.2362	0.0219	0.3683	5.045	105.19
WMO	0.21	6	20.6	111.1	10.2364	0.0217	0.3256	5.027	118.70
WMO	0.21	41	21.0	110.7	10.2362	0.0218	0.2984	4.756	74.81
WMO	0.21	26	20.2	110.2	10.2363	0.0217	0.3329	5.138	89.09
WMO	0.38	41	20.7	109.2	10.2363	0.0210	0.4841	4.469	90.69
WMO	0.38	36	21.5	108.3	10.2363	0.0212	0.4889	4.756	117.88
WMO	0.38	31	21.9	109.1	10.2363	0.0210	0.4914	4.578	116.27
WMO	0.38	26	21.7	108.9	10.2363	0.0211	0.4993	4.210	120.91
WMO	0.38	41	21.9	110.1	10.2361	0.0107	0.2928	4.026	203.07
WMO	0.21	41	22.1	107.3	10.2362	0.0112	0.1565	5.110	156.99
WMO	0.21	36	21.6	111.7	10.2361	0.0351	0.4311	4.142	57.39
WMO	0.21	41	22.0	108.1	10.2346	0.0358	0.4883	4.335	49.27
WMO	0.21	36	21.7	109.8	10.2347	0.0359	0.5151	4.480	49.68
WMO	0.21	31	21.8	111.0	10.2348	0.0359	0.5392	4.796	47.02
WMO	0.21	26	21.6	111.0	10.2349	0.0360	0.5235	4.837	45.79
WMO	0.21	21	21.6	110.8	10.2351	0.0359	0.5655	5.065	46.06
WMO	0.21	16	21.4	112.2	10.2352	0.0357	0.4750	5.009	39.56
WMO	0.21	11	21.5	111.8	10.2354	0.0357	0.4946	5.226	34.76
WMO	0.21	6	21.1	110.9	10.2355	0.0360	0.4706	5.719	44.30
WMO	0.21	1	21.3	111.0	10.2355	0.0360	0.3932	6.326	37.54

Heat Transfer Fluid	Orifice diameter	Axial Distance	Air temp	Nozzle temp	Pressure transducer readings		Obscu-ration	*Log Diff.*	SMD
	mm	cm	°C	°C	Vin	Vout			μm
WMO	0.38	41	19.7	89.8	10.2342	0.0210	0.5491	4.812	73.00
WMO	0.38	36	20.1	90.7	10.2342	0.0211	0.5623	4.754	83.64
WMO	0.38	31	20.0	91.0	10.2342	0.0212	0.5776	4.941	95.93
WMO	0.38	26	20.4	91.1	10.2342	0.0211	0.5712	4.698	102.03
WMO	0.38	21	20.0	90.4	10.2342	0.0211	0.5405	4.803	108.62
WMO	0.38	16	19.9	90.4	10.2342	0.0211	0.5152	4.876	139.98
WMO	0.38	41	21.8	107.6	10.2342	0.0348	0.7744	4.595	48.83
WMO	0.38	36	21.6	108.2	10.2343	0.0350	0.7077	4.433	40.77
WMO	0.38	31	21.5	108.8	10.2341	0.0348	0.7578	4.876	51.87
WMO	0.38	26	21.8	109.2	10.2341	0.0350	0.7878	5.041	57.18
WMO	0.38	21	21.4	109.1	10.2342	0.0350	0.7783	5.019	62.06
WMO	0.38	16	21.5	108.4	10.2342	0.0353	0.7045	5.267	59.64
WMO	0.38	11	21.3	109.0	10.2342	0.0352	0.6870	5.428	73.87
WMO	0.38	6	21.2	109.3	10.2342	0.0352	0.7160	5.342	112.58
WMO	0.38	36	21.4	109.4	10.2344	0.0351	0.7408	4.670	44.60
WMO	0.21	41	21.9	124.8	10.2362	0.0217	0.3314	4.918	77.22
WMO	0.21	36	21.2	127.3	10.2363	0.0218	0.3653	5.071	97.82
WMO	0.21	31	21.7	128.5	10.2366	0.0218	0.3575	5.237	97.82
WMO	0.21	26	21.6	129.6	10.2366	0.0218	0.3496	5.111	105.24
WMO	0.21	21	21.7	130.0	10.2368	0.0218	0.3836	5.269	93.75
WMO	0.21	16	21.5	129.9	10.2369	0.0218	0.4099	5.038	95.11
WMO	0.21	11	21.5	129.8	10.2370	0.0218	0.3531	4.980	100.72
WMO	0.21	6	21.4	130.3	10.2372	0.0218	0.4477	5.096	143.86
WMO	0.38	41	21.5	125.6	10.2377	0.0210	0.5352	4.278	136.74
WMO	0.38	36	21.5	127.2	10.2377	0.0212	0.5432	3.965	134.47
BDO	0.21	41	17.6	50.3	10.2403	0.0212	0.2138	5.426	66.76
BDO	0.21	36	17.9	49.7	10.2400	0.0214	0.1967	5.435	70.41
BDO	0.21	31	17.0	48.9	10.2400	0.0214	0.2201	5.678	78.85
BDO	0.21	26	17.5	50.1	10.2399	0.0213	0.2254	5.453	95.16
BDO	0.21	21	17.7	50.6	10.2402	0.0213	0.2266	5.569	111.69
BDO	0.21	16	17.3	50.3	10.2400	0.0213	0.2434	5.407	139.28
BDO	0.21	11	18.0	51.1	10.2401	0.0213	0.1880	5.194	131.08
BDO	0.38	41	17.6	49.2	10.2401	0.2040	0.3502	4.407	114.86

Heat Transfer Fluid	Orifice diameter	Axial Distance	Air temp	Nozzle temp	Pressure transducer readings		Obscu-ration	*Log Diff.*	SMD
	mm	cm	°C	°C	Vin	Vout			μm
BDO	0.38	36	17.5	49.9	10.2402	0.2160	0.3602	4.317	119.19
BDO	0.38	41	17.9	69.4	10.2400	0.0221	0.3898	5.122	81.59
BDO	0.38	36	17.8	69.2	10.2401	0.0216	0.3976	4.568	127.32
BDO	0.76	41	17.9	71.7	10.2401	0.0213	0.7483	5.623	88.35
BDO	0.76	36	17.6	72.2	10.2398	0.0217	0.7577	5.705	89.42
BDO	0.76	31	17.9	71.5	10.2399	0.0216	0.7289	6.078	79.96
BDO	0.76	26	18.0	72.1	10.2398	0.0209	0.7409	4.767	119.84
BDO	0.38	41	18.4	69.2	10.2396	0.0233	0.3761	5.022	87.04
BDO	0.38	36	18.6	69.3	10.2395	0.0218	0.4033	4.841	99.99
BDO	0.38	31	17.6	68.9	10.2395	0.0218	0.3924	4.562	111.40
BDO	0.38	41	18.3	69.6	10.2395	0.0105	0.1263	4.612	199.87
BDO	0.38	31	19.4	68.8	10.2357	0.0348	0.6279	5.060	68.81
BDO	0.38	41	18.8	68.8	10.2357	0.0351	0.6532	5.052	55.25
BDO	0.38	36	19.6	69.9	10.2357	0.0353	0.6491	5.079	63.25
BDO	0.38	31	19.2	70.4	10.2357	0.0353	0.6286	5.122	64.68
BDO	0.38	26	19.5	70.6	10.2357	0.3550	0.6190	5.041	70.27
BDO	0.38	21	19.2	70.4	10.2357	0.0355	0.6135	5.336	83.67
BDO	0.38	16	19.7	70.7	10.2355	0.0353	0.6051	4.561	116.82
BDO	0.38	41	19.6	71.6	10.2355	0.0344	0.6320	5.042	56.48
BDO	0.38	36	19.0	71.2	10.2354	0.0352	0.6184	5.031	57.34
BDO	0.38	31	19.2	71.2	10.2354	0.0352	0.6296	5.176	60.29
BDO	0.38	26	18.7	71.0	10.2355	0.0354	0.6014	5.121	64.75
BDO	0.38	21	18.7	70.8	10.2354	0.0354	0.6083	5.604	87.54
BDO	0.38	16	19.0	71.2	10.2353	0.0355	0.6301	4.861	108.80
BDO	0.21	41	18.9	68.9	10.2353	0.0354	0.3985	4.717	41.81
BDO	0.21	36	19.1	70.0	10.2353	0.0359	0.4063	5.007	41.26
BDO	0.21	31	19.4	70.7	10.2353	0.0361	0.4160	5.193	41.26
BDO	0.21	26	20.1	70.5	10.2353	0.0361	0.4077	5.310	45.67
BDO	0.21	21	19.4	70.9	10.2352	0.0359	0.4015	5.413	54.19
BDO	0.21	16	19.0	70.8	10.2352	0.0359	0.3966	5.567	58.63
BDO	0.21	11	18.7	70.7	10.2353	0.0359	0.3368	5.747	59.60
BDO	0.21	6	18.5	70.8	10.2354	0.0359	0.3746	5.385	139.17

Heat Transfer Fluid	Orifice diameter	Axial Distance	Air temp	Nozzle temp	Pressure transducer readings		Obscu-ration	*Log Diff.*	SMD
	mm	cm	°C	°C	Vin	Vout			μm
BDO	0.21	41	19.6	72.1	10.2354	0.0216	0.2250	5.592	66.39
BDO	0.21	36	19.1	71.9	10.2353	0.0218	0.2295	5.630	68.59
BDO	0.21	31	19.4	72.0	10.2353	0.0219	0.2323	5.713	73.85
BDO	0.21	26	19.5	70.6	10.2354	0.0219	0.2187	5.381	107.69
BDO	0.21	21	19.5	70.7	10.2353	0.0218	0.2323	5.157	105.95
BDO	0.21	41	19.5	71.4	10.2353	0.0107	0.6592	5.121	208.74
BDO	0.21	41	19.5	87.5	10.2352	0.0216	0.2234	5.555	77.31
BDO	0.21	36	18.5	87.2	10.2351	0.0216	0.2049	5.561	69.38
BDO	0.21	31	19.5	88.7	10.2353	0.0216	0.2183	5.221	98.34
BDO	0.21	26	19.0	89.6	10.2353	0.0215	0.2220	5.017	111.40
BDO	0.21	21	19.9	90.6	10.2353	0.0216	0.2262	4.790	116.95
BDO	0.38	41	20.2	90.7	10.2353	0.0209	0.4272	4.709	100.63
BDO	0.38	36	19.8	91.0	10.2353	0.0210	0.3996	4.644	96.07
BDO	0.38	31	20.0	91.2	10.2354	0.0209	0.4316	4.381	118.17

APPENDIX D

PRESSURE TRANSDUCER CALIBRATION

Table D-1. Calibration data for the Sensotek pressure transducer

V_{out}	V_{in}	V_{out}/V_{in}	Pressure (psig)	Atmospheric Pressure (psia)	Pressure (psia)
0.005	10.103	0.000	60.000	14.149	74.149
0.009	10.109	0.001	110.000	14.149	124.149
0.012	10.159	0.001	160.000	14.149	174.149
0.016	10.300	0.002	210.000	14.149	224.149
0.019	10.256	0.002	260.000	14.149	274.149
0.023	10.296	0.002	310.000	14.149	324.149
0.027	10.295	0.003	360.000	14.149	374.149
0.030	10.294	0.003	410.000	14.149	424.149
0.034	10.294	0.003	460.000	14.149	474.149
0.038	10.293	0.004	510.000	14.149	524.149
0.041	10.292	0.004	560.000	14.149	574.149
0.038	10.293	0.004	520.000	14.149	534.149
0.035	10.292	0.003	470.000	14.149	484.149
0.031	10.292	0.003	420.000	14.149	434.149
0.024	10.293	0.002	320.000	14.149	334.149
0.020	10.293	0.002	270.000	14.149	284.149
0.017	10.293	0.002	220.000	14.149	234.149
0.013	10.293	0.001	170.000	14.149	184.149
0.009	10.295	0.001	120.000	14.149	134.149
0.006	10.296	0.001	70.000	14.149	84.149

V_{out}	V_{in}	V_{out}/V_{in}	Pressure (psig)	Atmospheric Pressure (psia)	Pressure (psia)
0.003	10.296	0.000	30.000	14.149	44.149
0.005	10.296	0.000	60.000	14.149	74.149
0.009	10.297	0.001	110.000	14.149	124.149
0.012	10.297	0.001	160.000	14.149	174.149
0.016	10.298	0.002	210.000	14.149	224.149
0.020	10.299	0.002	260.000	14.149	274.149
0.023	10.300	0.002	310.000	14.149	324.149
0.027	10.299	0.003	360.000	14.149	374.149
0.030	10.299	0.003	410.000	14.149	424.149
0.034	10.299	0.003	460.000	14.149	474.149
0.038	10.296	0.004	510.000	14.149	524.149
0.041	10.297	0.004	560.000	14.149	574.149

The atmospheric pressure at College Station, Texas on September 03, 2000 was 28.8 inches of mercury.

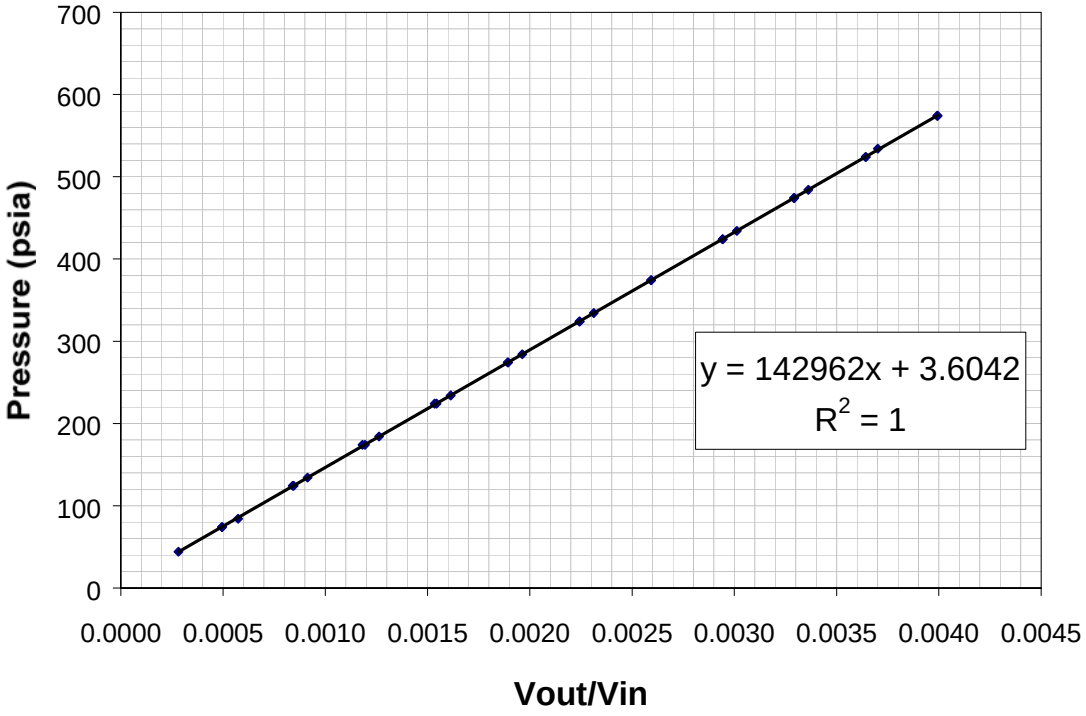

Figure D-1 Calibration of the Sensotek pressure transducer

(TJE/0713-18TJA: #595564)

APPENDIX E

THERMOCOUPLE CALIBRATION

The thermocouples were all factory calibrated by Omega and reported maximum departures of + 1.5 °C and –1.11 °C over a temperature range of 0 °C to 419 °C (Table E-1). Hence the total uncertainty associated with the temperature data is taken as + 1.5 °C and -1.11 °C.

Table E-1. Temperature calibration of thermocouples

Thermocouple location	Temperature reading (°C)	Departure (°C)	Actual temperature (°C)
Nozzle	0	0.06	-0.06
	100	0.17	99.83
	232	1.11	230.89
	419	1.44	417.56
Fluid cell	0	0.06	-0.06
	100	0.17	99.83
	232	1.11	230.89
	419	1.44	417.56
Air	0	0.11	-0.11
	100	1.11	98.89
	232	-1.11	233.11
	419	1.50	417.50

APPENDIX F

EXPERIMENTAL PROCEDURE

1. Depressurize the Fluid Cell by opening the valve at the vent line.
2. Check the spring in the pressure relief valve for the correct range of working pressure.
3. Fill HTF into the glass storage with the desired amount.
4. Open the valve at the fill line and wait until all HTF is transferred into the Fluid Cell, then close the valve.
5. Attach the test nozzle. Adjust the nozzle so that the spray is straight and the center of the spray passes through the laser beam.
6. Replace the insulation, both on the Fluid Cell and the spray line.
7. Turn on the temperature control box connected to the heater strip to heat the system. Initially, the set temperature can be adjusted to a much higher level than the required temperature to accelerate the heating process. Decrease the set temperature when the temperature of HTF is close to the required test temperature.
8. Ensure that room ventilation is working at all times.

9. Pressurize the Fluid Cell to the test pressure and wait until the pressure gauge on fluid cell comes to equilibrium.
10. Check the focal length of lens $L_{2.}$ In this case 300 mm is selected (refer to instructions in Malvern Laser manual).
11. The Malvern Laser must be aligned on a daily basis. The reticle will be placed at the focal lens, $L_{2.}$ Move the reticle until the laser beam just passes through the glass part and not the particle part. Measure the particle size distribution by using the set zero mode (F3). Then move the reticle again so the laser beam will pass through to the particle part. By setting the independent model, measure the particle size distribution using the measured sample and analyze (F5). The exact particle size distribution for D(v,0.5) should be 46.5 micron. If the error is greater than 5%, the alignment of the detector must be adjusted.
12. If the error is greater than 5%, clean the reticle and lens using lens cleaning fluid and lens tissues.
13. Turn the knobs (both x and y direction) in the Malvern's detector box until the synchronizer reaches the maximum value, to ensure that the lasers alignment is good.
14. Repeat (11) again. If the error is still greater than 5%, keep adjusting.
15. Ensure that the printer is online. All data must be backed up by a hard copy of the results.

16. Turn on the exhaust system. The exhaust system must be turned on during the measurements to ensure that aerosol does not accumulate in the laboratory.
17. Now the system is ready to make measurements. Turn off all the lights in the room and measure the background (F3).
18. Open the spray valve to a certain position (this position needs to be fixed throughout every measurement). Wait until the spray is steady for about 10 seconds. Ensure that the temperature and pressure are at the required setting. Measure the droplet size distribution with the F5 mode. The measurement is set to 500 sweeps per one time measurement. This step will take about 5 seconds.
19. Write down the temperature and pressure data on the data sheet.
20. Close the spray valve and turn on the light.
21. During this time Malvern software will calculate the size distribution.
22. Write down the value of Sauter mean diameter, volume concentration, obscuration, and *Log Diff*.
23. Save data on disk.
24. For the next measurement, go back to (17).
25. Ensure that the nitrogen cylinder valve is closed, the residual nitrogen in the system is vented, and all power supplies switched off during shut down.
26. Drain the Mist Separator every day after all the measurements, but not after more than 10 measurements.

27. Change the filter in the Mist Separator on a monthly basis.

28. Clean all equipment before testing another fluid.

APPENDIX G

HEAT TRANSFER FLUID PHYSICAL PROPERTIES

In order to analyze the experimental data, HTF physical properties of density, viscosity, and surface tension as functions of temperature, were needed. Some data were obtained from the manufacturers, but in cases where data were insufficient, measurements were made to obtain them. Correlations were then fit to the data to allow interpolation of the data for the dimensionless modeling.

Correlations of density and viscosity variation with temperature, derived from data provided by the manufacturers, are shown in Figures G-1 and G-2, respectively. Surface tension of the six HTFs was measured using a Fisher Surface Tensiomat, Model 21, which operates according to the ASTM D-971 and D1331 methods. In all cases the error listed is given by

$$Error, \% = \frac{predicted\ value - actual\ value}{actual\ value} \times 100 \qquad \text{(III-16)}$$

Part of this appendix is reprinted from "Predictive correlations for leaking heat transfer fluid aerosols in air" by Krishna, K., Kim, T.K., Kihm, K.D., Rogers, W.J., and Mannan, M.S., (2003). *Journal of Loss Prevention in the Process Industries, 16* (1), 1-8, Copyright 2003, with permission from Elsevier

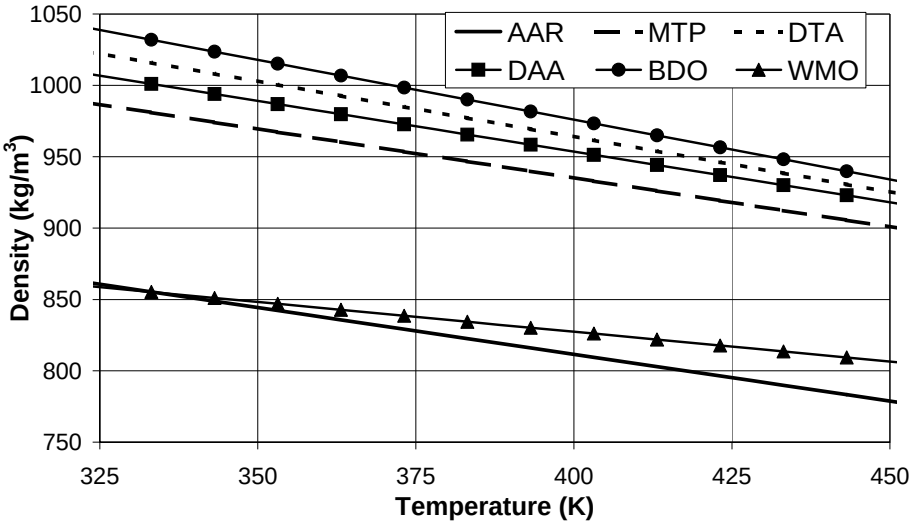

Figure G-1. Variation of density with temperature for the six HTFs

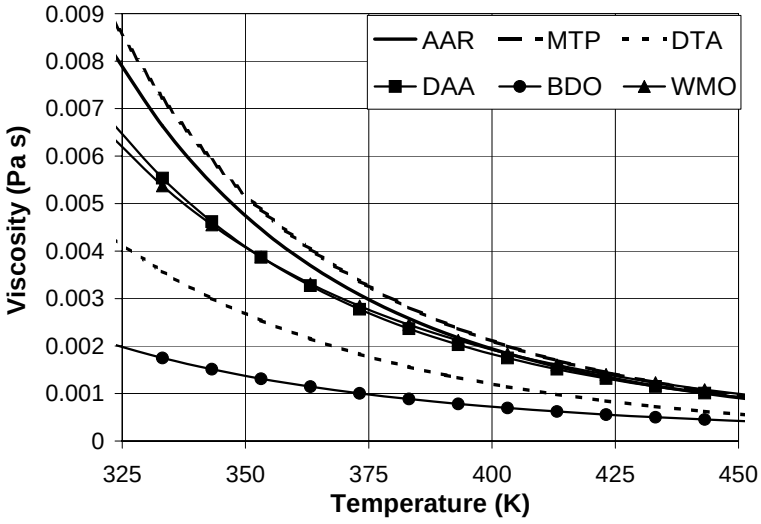

Figure G-2. Variation of viscosity with temperature for the six HTFs

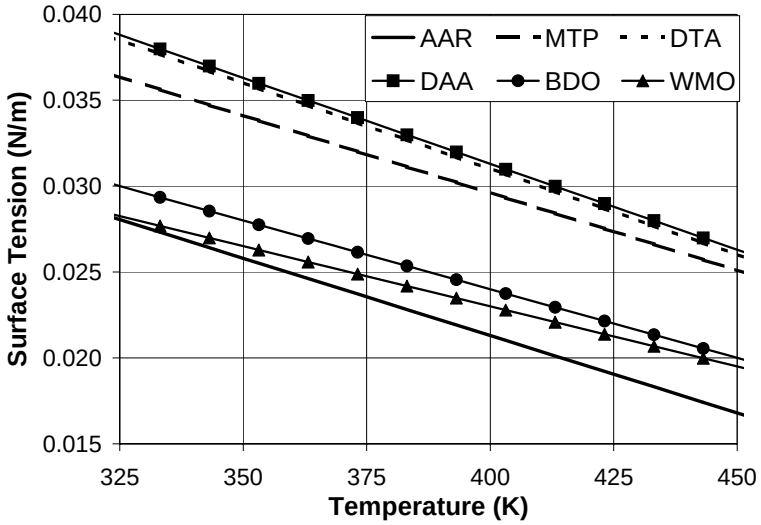

Figure G-3. Variation of surface tension with temperature for the six HTFs

The overall error for surface tension measurements of –3.5% to –6.5% consists of the error due to calibration (± 1.5%) and the maximum error obtained from verification with water (-5.5%). Figure G-3 displays a correlation of surface tension with temperature for the six HTFs. Additionally, Tables G-1, G-2, and G-3 provides the correlation equations and the error of correlation predictions.

Table G-1. Fluid Density – Temperature (K) Correlations

Heat Transfer Fluid	Density (kg/m^3)		
	$\rho = a(T) + b$		
	a	b	Error, %
AAR	-0.6544	1073.3	-0.1, +0.2
MTP	-0.6857	1209.4	±0.06
DTA	-0.7748	1274.0	0.00
DAA	-0.7103	1237.7	±0.05
BDO	-0.8379	1311.1	±0.05
WMO	-0.4169	994.15	-0.1, +0.2

Table G-2. Fluid Viscosity – Temperature (K) Correlations

Heat Transfer Fluid	Viscosity (Pa s)			
	$\mu = x(T)^y + z$			
	x	*y*	*z*	***Error, %***
AAR	$2e^{15}$	-6.9315	0.0001	-8.0, +3.0
MTP	$7e^{14}$	-6.7336	0.0	±5.8
DTA	$8e^{11}$	-5.6838	-0.0001	-7.0, +3.0
DAA	$3e^{13}$	-6.2399	0.00009	-9.5, +2.5
BDO	$2e^{10}$	-5.1838	0.00007	-8.5, +2.2
WMO	$8e^{11}$	-5.6182	0.0	-2.9, +1.9

Table G-3. Fluid Surface Tension – Temperature (K) Correlations

Heat Transfer Fluid	Surface Tension (N/m)		
	$\sigma = m(T) + n$		
	m	*n*	***Error, %***
AAR	-0.00009	0.0573	-6.8, -1.5
MTP	-0.00009	0.0656	-2.8, +3.6
DTA	-0.0001	0.0710	-3.9, +0.7
DAA	-0.0001	0.0713	-1.0, 0.0
BDO	-0.00008	0.056	-4.3, +0.4
WMO	-0.00007	0.051	-6.8, +2.9

APPENDIX H

REGRESSION ANALYSIS

ALKYLATED AROMATIC (AAR)

SAS Program

```
OPTIONS LS=20 PS=75 NOCENTER NODATE;
DATA ATOMIZE;
TITLE 'SMD AS A FUNCTION OF DIMENSIONLESS ATOMIZATION PARAMETERS';
* X1 = natural log of Reynolds Number;
* X2 = natural log of Weber Number;
* X3 = natural log of Density Ratio (fluid/air);
* X4 = natural log of Viscosity Ratio (fluid/air);
* X5 = natural log of Normalized Axial Distance (Y/orifice dia);
* Y = natural log of Diameter Ratio (SMD/orifice);
INPUT X1-X5 Y;
CARDS;
8.984405226    4.208140022    6.510031912    4.834142743    6.853688058    -1.911432448
8.990165763    4.205667036    6.509631088    4.825720158    6.983741186    -1.956572049
9.002417814    4.246967942    6.510112058    4.835828955    6.042757841    -1.574401041
8.985699069    4.21353045     6.510112058    4.835828955    6.314691557    -1.692390552
8.979689366    4.204315099    6.510192197    4.837515731    6.528265657    -1.752184568
8.972690629    4.226889605    6.511233423    4.859495293    6.704156324    -1.789131347
8.966848574    4.164626352    6.509791437    4.829087498    6.853688058    -1.863481626
8.993377516    4.198129234    6.509230102    4.817311684    6.983741186    -2.060464849
8.297637029    3.97209825     6.539489278    5.503415341    6.853688058    -2.038400624
8.316658275    4.016746909    6.53964491     5.50722915     6.983741186    -2.134175652
9.485091721    4.413321852    6.4852006      4.344279512    6.042757841    -1.632598804
9.485091721    4.413321852    6.4852006      4.344279512    6.314691557    -1.747944065
9.487587663    4.41351366     6.485036258    4.341246785    6.528265657    -1.918935162
9.471487711    4.376518953    6.48487189     4.338216229    6.704156324    -1.919832104
9.442337299    4.39312987     6.48741657     4.385434039    6.853688058    -1.94013737
9.45402104     4.389770894    6.48651436     4.368619544    6.983741186    -1.845160246
9.255435959    4.725035762    6.509310312    4.818992251    6.042757841    -2.442452304
9.259794261    4.730962724    6.509230102    4.817311684    6.314691557    -2.448219508
9.256870075    4.727903994    6.509310312    4.818992251    6.528265657    -2.361106665
9.254086009    4.725126814    6.509390516    4.820673381    6.704156324    -2.288215153
9.255625335    4.725414515    6.509310312    4.818992251    6.853688058    -2.241341468
9.274002409    4.726005458    6.508267081    4.797188839    6.983741186    -2.2261115
8.02906741     3.325637102    6.521982547    5.093452101    3.863232841    -0.747150912
8.027437768    3.328380114    6.522140928    5.096997258    5.65499231     -1.003302109
8.020398089    3.323314167    6.522378453    5.102319374    6.261128114    -1.051456112
8.07734504     3.33871761     6.519762577    5.044064485    6.635821563    -1.167962367
8.148915033    3.408203849    6.517776287    5.000352523    6.907755279    -1.395671523
8.130168513    3.403016657    6.51865074     5.019541288    7.121329379    -1.573657175
8.108022456    3.400072443    6.519762577    5.044064485    7.297220046    -1.510239199
8.045866864    3.383277093    6.522615921    5.107646749    7.44675178     -1.41665539
8.090738417    3.392222167    6.520476676    5.059889369    7.576804908    -1.363508327
8.290488813    3.744298795    6.519206813    5.031788708    3.863232841    -1.162617619
```

```
8.287068736    3.743368129    6.519365634    5.035293178    5.65499231     -1.284253636
8.307914683    3.746742919    6.518332846    5.012555476    6.261128114    -1.606822289
8.298366444    3.751199749    6.518968534    5.026536344    6.635821563    -1.659228577
8.290153145    3.746581541    6.519286227    5.033540654    6.907755279    -1.670047653
8.262764234    3.715484016    6.519921309    5.047577065    7.121329379    -1.6567292
8.28672194     3.745631264    6.519445035    5.037046281    7.297220046    -1.624793301
8.260334538    3.719526582    6.520159362    5.052850284    7.44675178     -1.653987082
8.174255083    3.646077096    6.522774201    5.111201255    7.576804908    -1.621896147
8.036910587    3.341323457    6.521982547    5.093452101    3.863232841    -0.747150912
8.035280945    3.344066469    6.522140928    5.096997258    5.65499231     -1.003302109
8.028241266    3.339000521    6.522378453    5.102319374    6.261128114    -1.051456112
8.085188217    3.354403965    6.519762577    5.044064485    6.635821563    -1.167962367
8.148915033    3.408203849    6.517776287    5.000352523    6.907755279    -1.395671523
8.130168513    3.403016657    6.51865074     5.019541288    7.121329379    -1.573657175
8.092518269    3.36906407     6.519762577    5.044064485    7.297220046    -1.510239199
8.030362678    3.35226872     6.522615921    5.107646749    7.44675178     -1.41665539
8.075234231    3.361213794    6.520476676    5.059889369    7.576804908    -1.363508327
8.290488813    3.744298795    6.519206813    5.031788708    3.863232841    -1.162617619
8.287068736    3.743368129    6.519365634    5.035293178    5.65499231     -1.284253636
8.307914683    3.746742919    6.518332846    5.012555476    6.261128114    -1.606822289
8.298366444    3.751199749    6.518968534    5.026536344    6.635821563    -1.659228577
8.290153145    3.746581541    6.519286227    5.033540654    6.907755279    -1.670047653
8.262764234    3.715484016    6.519921309    5.047577065    7.121329379    -1.6567292
8.28672194     3.745631264    6.519445035    5.037046281    7.297220046    -1.624793301
8.260334538    3.719526582    6.520159362    5.052850284    7.44675178     -1.653987082
8.174255083    3.646077096    6.522774201    5.111201255    7.576804908    -1.621896147
9.124902636    4.662503248    6.51490908     4.938039601    5.668064392    -1.912500824
9.118042098    4.637263984    6.514589994    4.931161793    6.042757841    -1.881453868
9.110138814    4.653183104    6.515467237    4.950097785    6.314691557    -1.953411901
9.104889816    4.654261216    6.515786044    4.957000771    6.528265657    -2.042450032
9.111233604    4.661158103    6.515626653    4.953548132    6.704156324    -2.104597419
9.112924202    4.661645932    6.515546948    4.951822672    6.853688058    -2.174562266
9.087390847    4.601907016    6.515307795    4.946649728    6.983741186    -2.060464849
9.008278407    4.300887569    6.511313473    4.861189991    6.314691557    -1.807567978
9.01050848     4.294065951    6.510993236    4.854414597    6.528265657    -1.831923785
9.003345815    4.288199977    6.511233423    4.859495293    6.704156324    -2.026549526
9.001128921    4.283766188    6.511233423    4.859495293    6.853688058    -2.043871208
8.970114986    4.207645951    6.51083308     4.851030297    6.983741186    -2.014245342
9.144085253    4.770420034    6.516821464    4.979498852    6.983741186    -2.257813016
9.144982105    4.728655105    6.515626653    4.953548132    6.983741186    -2.182932461
9.261611477    4.745763583    6.509550904    4.824037335    6.853688058    -2.164655492
PROC PRINT;
PROC REG; MODEL Y=X1-X5/SELECTION=RSQUARE ADJRSQ CP SSE MSE BEST=6;
PROC REG; MODEL Y=X1-X5/VIF;
PROC CORR; VAR X1-X5 Y;
```

Statistical comparison of various models for the AAR

Number in Model	R-Square	Adjusted R-Square	C(p)	MSE	SSE	Variables in Model
1	0.7456	0.742	132.1853	0.03934	2.79295	X2
1	0.5942	0.5885	251.8953	0.06274	4.45481	X1
1	0.1793	0.1677	579.9984	0.1269	9.00969	X5
1	0.1158	0.1034	630.2001	0.13671	9.70662	X4
1	0.1133	0.1009	632.1558	0.1371	9.73377	X3
2	0.8969	0.894	14.4932	0.01616	1.13133	X2 X5
2	0.7655	0.7588	118.4372	0.03678	2.57432	X2 X4
2	0.7646	0.7579	119.1299	0.03691	2.58394	X2 X3
2	0.7605	0.7537	122.3601	0.03755	2.62878	X1 X2
2	0.751	0.7439	129.9072	0.03905	2.73356	X1 X5
2	0.7502	0.7431	130.5226	0.03917	2.7421	X1 X4
3	0.9138	0.91	3.1883	0.01372	0.94662	X2 X4 X5
3	0.9132	0.9094	3.6711	0.01382	0.95332	X2 X3 X5
3	0.9114	0.9075	5.0734	0.0141	0.97279	X1 X2 X5
3	0.8925	0.8878	20.0466	0.01711	1.18066	X1 X4 X5
3	0.8921	0.8874	20.3414	0.01717	1.18475	X1 X3 X5
3	0.7681	0.758	118.3883	0.0369	2.54588	X2 X3 X4
4	0.9152	0.9102	4.0539	0.01369	0.93087	X2 X3 X4 X5
4	0.9138	0.9087	5.1818	0.01392	0.94653	X1 X2 X4 X5
4	0.9132	0.9081	5.6683	0.01402	0.95328	X1 X2 X3 X5
4	0.8925	0.8862	21.9985	0.01735	1.17999	X1 X3 X4 X5
4	0.7683	0.7546	120.2617	0.03741	2.54412	X1 X2 X3 X4
5	0.9153	0.909	6	0.01388	0.93012	X1 X2 X3 X4 X5

Regression results for the five parameter model for AAR

Source	Degrees of Freedom	Sum of Squares	Mean Square
Model	5	10.04789	2.00958
Error	67	0.93012	0.01388
Corrected Total	72	10.97801	

Root MSE	0.11782
Dependent Mean	-1.70663
Coeff of Varience	-6.90391
R-square	0.9153
Adjusted R-Square	0.9090

Variable	Parameter Estimate
Intercept	79.6558
X1	-0.5271
X2	-0.3239
X3	-11.2582
X4	-0.2026
X5	-0.1746

MODIFIED TERPHENYL (MTP)

SAS Program

```
OPTIONS LS=20 PS=75 NOCENTER NODATE;
DATA ATOMIZE;
TITLE 'SMD AS A FUNCTION OF DIMENSIONLESS ATOMIZATION PARAMETERS';
* X1 = natural log of Reynolds Number;
* X2 = natural log of Weber Number;
* X3 = natural log of Density Ratio (fluid/air);
* X4 = natural log of Viscosity Ratio (fluid/air);
* X5 = natural log of Normalized Axial Distance (Y/orifice dia);
* Y = natural log of Diameter Ratio (SMD/orifice);
INPUT X1-X5 Y;
CARDS;
8.589051412    3.592602918    6.690663579    5.262440473    6.983741186    -1.439473088
8.574288929    3.597324421    6.692126391    5.281829376    6.983741186    -1.389668468
8.557334154    3.589566001    6.692027694    5.29693459     6.853688058    -1.222208239
8.542880173    3.585533192    6.693274336    5.310951627    6.704156324    -1.182451668
8.542156291    3.581560944    6.692529793    5.309687624    6.528265657    -1.064363429
8.530532415    3.57363788     6.693561116    5.318251912    6.314691557    -0.962817013
8.525837441    3.57740201     6.693511454    5.325839998    6.042757841    -0.926939333
8.530855314    3.565018245    6.693009678    5.313055833    5.668064392    -0.68658978
8.811548675    4.14831337     6.690744822    5.326254041    6.983741186    -1.778323817
8.833513445    4.134875651    6.692557025    5.292735465    6.853688058    -1.678336803
8.838966759    4.149306144    6.692292418    5.294834742    6.704156324    -1.5887327
8.837498387    4.147042461    6.691619358    5.295394731    6.528265657    -1.545969042
8.837146686    4.149527653    6.691691107    5.297214623    6.314691557    -1.494465841
8.842539907    4.15075158     6.691475844    5.291756422    6.314691557    -1.533330062
8.841447825    4.145045499    6.691740666    5.289657971    6.042757841    -1.030904453
8.841299394    4.151120383    6.69188419     5.293295297    5.668064392    -0.925278368
8.003448842    3.215905547    6.695516044    5.377220762    7.576804908    -1.342323045
8.020301656    3.223746542    6.694943714    5.362500494    7.44675178     -1.282535127
8.030331031    3.231236015    6.694320952    5.355432365    7.297220046    -1.360162599
8.041289988    3.233491948    6.69422784     5.344145296    7.121329379    -1.28099099
8.058016885    3.241240058    6.693654772    5.329497079    6.907755279    -1.309686116
7.684241403    1.931512921    6.670238958    5.009527214    7.576804908    0.228273229
7.665917431    1.905613805    6.668756088    5.016167594    7.44675178     0.281484335
7.592874948    1.857636548    6.670054652    5.073034844    7.297220046    0.458449036
8.634581441    3.077921091    6.663174027    4.916937668    6.983741186    -0.81365102
8.648298882    3.105015143    6.663514858    4.916654703    6.853688058    -0.780598846
8.647165395    3.094449226    6.665751617    4.911241987    6.704156324    -0.737099068
8.646900939    3.070294613    6.665168142    4.89752269     6.528265657    -0.53205822
8.647278369    3.06152652     6.665628945    4.891820579    6.314691557    -0.377530005
9.02649691     3.735616792    6.662830831    4.842923329    6.983741186    -1.586158365
9.013650077    3.744326306    6.664387657    4.86278167     6.853688058    -1.564540025
8.997042203    3.732660729    6.663879247    4.875570684    6.704156324    -1.289932103
8.989348848    3.734570031    6.664657322    4.885541192    6.528265657    -1.140174689
8.993668651    3.73178835     6.664025287    4.878986588    6.314691557    -1.049295947
8.991219043    3.726209208    6.664705212    4.878421856    6.042757841    -0.842441252
8.990452242    3.722077654    6.66429229     4.876996014    5.668064392    -0.708848755
8.99471741     3.718866439    6.664000169    4.87016767     5.061928588    -0.399299941
8.221680104    2.875070037    6.666699039    4.933595634    7.576804908    -1.307747277
8.22825859     2.843896602    6.6624685      4.908638505    7.44675178     -1.15261602
8.229337047    2.839806143    6.662663579    4.904925636    7.297220046    -1.15261602
8.225496046    2.838371513    6.6624685      4.908638505    7.297220046    -1.15261602
8.235092179    2.83906112     6.665847836    4.896958117    7.121329379    -1.098041023
8.232318069    2.831815683    6.667545053    4.895548077    6.907755279    -1.092630217
8.230411624    2.83095253     6.667618006    4.897261462    6.635821563    -0.765103623
8.241907097    2.835920832    6.667519306    4.88670592     6.261128114    -0.541284831
8.264948212    2.838289082    6.666084874    4.86137163     5.65499231     -0.538180507
9.713262975    4.372596899    6.67041608     4.815527813    6.290594005    -2.046515905
```

```
9.714841474    4.365487237    6.668773974    4.809876595    6.160540877    -1.851174297
9.705339329    4.350398646    6.667834012    4.812411765    6.011009143    -1.867050327
9.697660298    4.340717579    6.671090048    4.814967196    5.835118477    -1.884394284
9.720853532    4.396837388    6.670298473    4.82089276     5.621544376    -1.911343468
9.298127966    4.244533438    6.670298473    4.82089276     6.983741186    -1.86500951
9.228093698    4.21891133     6.675915238    4.8868146      6.853688058    -1.830938078
9.220908364    4.22258438     6.676016548    4.89737871     6.704156324    -1.733838189
9.231678838    4.217577687    6.675359971    4.881958245    6.528265657    -1.580134636
9.23125776     4.222964537    6.67516944     4.88566192     6.314691557    -1.592606672
9.22176613     4.213164097    6.675051728    4.891080799    6.314691557    -1.601835307
9.176534966    4.230189115    6.680100989    4.952825879    6.314691557    -1.550672603
9.226621533    4.217649938    6.674232303    4.888214769    6.042757841    -1.190208322
9.219660788    4.219156063    6.673923073    4.897344488    5.668064392    -0.83005268
8.416270476    3.383410808    6.682399216    4.999416188    7.576804908    -1.510670512
8.441462242    3.392362198    6.680710435    4.975631661    7.44675178     -1.610152453
8.450989039    3.397435206    6.67933854     4.967797972    7.297220046    -1.643339464
8.452891962    3.397910037    6.679602073    4.965784943    7.121329379    -1.561782178
8.445275401    3.395334652    6.67922029     4.973280218    6.907755279    -1.598074154
8.483234752    3.413172415    6.676081814    4.940073995    6.907755279    -1.627214023
8.480060617    3.405813704    6.677092255    4.939233424    6.635821563    -1.440298092
8.466502321    3.402554576    6.677674499    4.953054801    6.261128114    -1.183703433
9.149150461    3.733300099    6.665543037    4.696021008    6.983741186    -1.376239815
9.176279111    3.713766541    6.663965235    4.652603078    6.853688058    -1.246990189
9.176775313    3.73198994     6.664070494    4.662813692    6.704156324    -1.196631397
9.209475279    3.749611558    6.662817125    4.634715664    6.528265657    -1.138201491
9.193056928    3.736078346    6.663670336    4.645990975    6.314691557    -0.947360544
9.193960329    3.74069469     6.663744069    4.647643392    6.042757841    -0.737924355
9.19792644     3.737394398    6.663449104    4.641036155    5.668064392    -0.512230118
8.377646405    2.883253587    6.66811478     4.754530811    7.576804908    -1.15261602
8.473000422    2.926300718    6.663954473    4.668064709    7.297220046    -1.251596982
PROC PRINT;
PROC REG; MODEL Y=X1-X5/SELECTION=RSQUARE ADJRSQ CP SSE MSE BEST=6;
PROC REG; MODEL Y=X1-X5/VIF;
PROC CORR; VAR X1-X5 Y;
```

Statistical comparison of various models for the MTP

Number in Model	R-Square	Adjusted R-Square	C(p)	MSE	SSE	Variables in Model
1	0.4790	0.4720	104.6399	0.1318	9.88555	X2
1	0.2614	0.2516	178.8047	0.1868	14.01277	X1
1	0.0686	0.0562	244.5347	0.2356	17.67061	X3
1	0.0060	-0.0072	265.8771	0.2514	18.8583	X5
1	0.0018	-0.0115	267.3325	0.2525	18.93929	X4
2	0.7765	0.7704	5.2108	0.0573	4.24108	X2 X5
2	0.5109	0.4976	95.7634	0.1254	9.28028	X1 X2
2	0.4948	0.4812	101.2345	0.1295	9.58474	X1 X5
2	0.4902	0.4764	102.8203	0.1307	9.67299	X2 X3
2	0.4808	0.4668	106.0013	0.1331	9.85001	X2 X4
2	0.4172	0.4014	127.7100	0.1494	11.05809	X1 X3
3	0.7787	0.7696	6.4605	0.0575	4.19933	X2 X4 X5
3	0.7771	0.7679	7.0068	0.0579	4.22973	X2 X3 X5
3	0.7766	0.7674	7.1607	0.0581	4.23829	X1 X2 X5
3	0.6915	0.6789	36.1614	0.0802	5.85217	X1 X3 X5
3	0.6451	0.6305	52.0026	0.0922	6.73372	X1 X4 X5
3	0.5677	0.5499	78.3921	0.1124	8.20228	X1 X2 X4
4	0.7916	0.7800	4.0493	0.0549	3.95385	X1 X2 X4 X5
4	0.7829	0.7709	7.0086	0.0572	4.11853	X1 X2 X3 X5
4	0.7820	0.7699	7.3203	0.0574	4.13588	X2 X3 X4 X5
4	0.6962	0.6793	36.5826	0.0801	5.76431	X1 X3 X4 X5
4	0.5716	0.5478	79.0542	0.1129	8.12783	X1 X2 X3 X4
5	0.7917	0.7771	6.0000	0.0557	3.95111	X1 X2 X3 X4 X5

Regression results for the five parameter model for MTP

Source	Degrees of Freedom	Sum of Squares	Mean Square
Model	5	15.02163	3.00433
Error	71	3.95111	0.05565
Corrected Total	76	18.97273	

Root MSE	0.23590
Dependent Mean	-1.19157
Coeff of Varience	-19.79757
R-square	0.7917
Adjusted R-Square	0.7771

Variable	Parameter Estimate
Intercept	10.73799
X1	0.49259
X2	-1.22490
X3	-1.75035
X4	0.66236
X5	-0.52619

DI/TRI- ARYL (DTA)

SAS Program

```
OPTIONS LS=20 PS=75 NOCENTER NODATE;
DATA ATOMIZE;
TITLE 'SMD AS A FUNCTION OF DIMENSIONLESS ATOMIZATION PARAMETERS';
* X1 = natural log of Reynolds Number;
* X2 = natural log of Weber Number;
* X3 = natural log of Density Ratio (fluid/air);
* X4 = natural log of Viscosity Ratio (fluid/air);
* X5 = natural log of Normalized Axial Distance (Y/orifice dia);
* Y = natural log of Diameter Ratio (SMD/orifice);
INPUT X1-X5 Y;
CARDS;
8.747760834    3.391363912    6.725126028    5.129407511    6.704156324    -1.064363429
8.75377221     3.397909596    6.724284973    5.126469285    6.853688058    -1.13910539
8.762344346    3.399656227    6.723900741    5.117705033    6.907755279    -1.188824957
8.748624765    3.397206458    6.724171563    5.132017027    6.983741186    -1.243242641
9.065115234    4.014453918    6.720955275    5.123778199    6.314691557    -1.581925147
9.064531478    4.018412107    6.722143089    5.126427344    6.528265657    -1.581925147
9.071984477    4.012095427    6.72443441     5.113631848    6.704156324    -1.633946331
9.067975667    4.017419487    6.723710572    5.121494767    6.853688058    -1.74869998
9.059405062    4.016371763    6.723406633    5.130832825    6.983741186    -1.799420318
9.067146737    4.010981587    6.722180162    5.11913116     6.704156324    -1.612204895
9.06736978     4.005255547    6.725198211    5.114813772    6.314691557    -1.566302806
8.494076471    2.879894343    6.722908747    5.127610024    6.983741186    -0.667735956
8.029745867    2.499168283    6.723896153    5.101381007    6.635821563    -0.612050084
8.016056183    2.500165585    6.7207247      5.118521705    6.907755279    -0.771778187
8.022916455    2.499862008    6.722140134    5.110090071    7.121329379    -0.987070914
8.021189214    2.498449319    6.723249369    5.110984854    7.297220046    -1.140625469
8.017050989    2.494280126    6.722293904    5.113591329    7.44675178     -1.156090081
8.002379981    2.495041209    6.723750749    5.1305476      7.576804908    -1.16185641
8.419389507    3.36862117     6.739685783    5.488380581    6.704156324    -1.164246146
8.416454028    3.372522771    6.739912729    5.493880804    6.853688058    -1.257114528
8.435957848    3.360349532    6.741181327    5.464425885    6.983741186    -1.251763468
7.600007476    2.306308571    6.739651184    5.478937331    7.121329379    -0.569161201
7.618720258    2.324243315    6.739196964    5.467961804    7.297220046    -0.595761235
7.599327836    2.316083282    6.738502464    5.485571392    7.44675178     -0.595761235
7.566968366    2.308375519    6.741582974    5.517191175    7.576804908    -0.620162288
7.924041985    2.944459588    6.749569186    5.470707999    3.863232841    -0.611084536
7.93579076     2.954097427    6.746805674    5.463540839    5.65499231     -0.986049202
7.925424291    2.948245652    6.748547735    5.471556176    6.261128114    -0.993094642
7.932213827    2.951734444    6.748661251    5.46578365     6.635821563    -1.085273081
7.928625151    2.952419022    6.747449551    5.47057473     6.907755279    -1.192922968
7.926429189    2.956919631    6.745211028    5.476219417    7.121329379    -1.341047883
7.928620155    2.956509498    6.743349084    5.47397754     7.297220046    -1.434284845
7.945112719    2.951915347    6.747714841    5.451446305    7.44675178     -1.386675386
7.921957728    2.941305319    6.741902822    5.473284482    7.576804908    -1.386103903
8.342913526    3.142560607    6.72889105     5.109935512    3.863232841    -0.683857134
8.334972694    3.134201768    6.730830461    5.113772942    5.65499231     -1.206834037
8.336374986    3.13700635     6.730830461    5.113772942    6.261128114    -1.46967597
8.341520153    3.136359139    6.732305771    5.107101444    6.635821563    -1.540889584
8.332951474    3.134611707    6.732690063    5.115862269    6.907755279    -1.472163534
8.326085303    3.136277935    6.729924666    5.125427406    7.121329379    -1.637445537
8.302032121    3.130384933    6.732024858    5.149172213    7.297220046    -1.596427676
8.345259934    3.139740437    6.726948662    5.106103165    7.44675178     -1.593845818
8.3447451      3.129150353    6.727060546    5.100569653    7.576804908    -1.577109025
9.12516168     3.552615922    6.713042297    4.789036791    6.528265657    -1.18873856
9.121095961    3.547432544    6.713120289    4.790732531    6.704156324    -1.168046987
9.096981935    3.547141502    6.713682038    4.818467763    6.853688058    -1.323270144
9.042955418    3.532464525    6.714721771    4.872434056    6.983741186    -1.364841909
```

```
9.129220662    3.558129014    6.712621717    4.787625477    6.983741186    -1.347579849
8.487964777    2.784681839    6.712147061    4.738833158    6.635821563    -1.155636258
8.454813777    2.75961045     6.710079519    4.763360883    6.907755279    -1.187755807
8.455856269    2.755477126    6.710266377    4.759693672    7.121329379    -1.132316815
8.450863528    2.752591906    6.712214164    4.763346853    7.297220046    -1.240999102
8.465728725    2.75487014     6.71253784     4.747278358    7.44675178     -1.256436374
8.422118753    2.743569951    6.712092187    4.791585288    7.576804908    -1.328384907
PROC PRINT;
PROC REG; MODEL Y=X1-X5/SELECTION=RSQUARE ADJRSQ CP SSE MSE BEST=6;
PROC REG; MODEL Y=X1-X5/VIF;
PROC CORR; VAR X1-X5 Y;
```

Statistical comparison of various models for DTA

Number in Model	R-Square	Adjusted R-Square	C(p)	MSE	SSE	Variables in Model
1	0.4768	0.4668	257.9936	0.0569	2.9583	X2
1	0.3440	0.3314	336.1617	0.0713	3.7092	X1
1	0.0734	0.0556	495.4661	0.1008	5.2393	X4
1	0.0570	0.0389	505.1247	0.1025	5.3321	X5
1	0.0495	0.0312	509.5777	0.1034	5.3748	X3
2	0.6499	0.6362	158.0897	0.0388	1.9795	X2 X5
2	0.4957	0.4760	248.8494	0.0559	2.8513	X2 X4
2	0.4829	0.4627	256.3887	0.0573	2.9237	X2 X3
2	0.4774	0.4569	259.6301	0.0579	2.9548	X1 X2
2	0.4359	0.4138	284.0841	0.0625	3.1897	X1 X5
2	0.3872	0.3632	312.7575	0.0679	3.4651	X1 X3
3	0.6629	0.6427	152.4188	0.0381	1.9059	X1 X2 X5
3	0.6586	0.6381	155.0076	0.0386	1.9307	X1 X2 X4
3	0.6569	0.6363	155.9643	0.0388	1.9399	X2 X4 X5
3	0.6504	0.6295	159.7836	0.0395	1.9766	X2 X3 X5
3	0.6003	0.5763	189.2917	0.0452	2.2600	X1 X2 X3
3	0.5414	0.5139	223.9802	0.0519	2.5932	X1 X3 X5
4	0.9180	0.9113	4.2570	0.0095	0.4635	X1 X2 X4 X5
4	0.7713	0.7526	90.6254	0.0264	1.2931	X2 X3 X4 X5
4	0.7474	0.7268	104.7102	0.0292	1.4284	X1 X2 X3 X5
4	0.6760	0.6495	146.7495	0.0374	1.8322	X1 X2 X3 X4
4	0.6385	0.6090	168.7970	0.0417	2.0440	X1 X3 X4 X5
5	0.9185	0.9100	6.0000	0.0096	0.4611	X1 X2 X3 X4 X5

Regression results for the five parameter model for DTA

Source	Degrees of Freedom	Sum of Squares	Mean Square
Model	5	5.19344	1.03869
Error	18	0.46105	0.00961
Corrected Total	53	5.65449	

Root MSE	0.09801
Dependent Mean	-1.21481
Coeff of Varience	-8.06757
R-square	0.9185
Adjusted R-Square	0.9100

Variable	Parameter Estimate
Intercept	-1.75837
X1	1.88787
X2	-1.91571
X3	-2.59108
X4	1.89390
X5	-0.24621

DI ARYL ALKYL (DAA)

SAS Program

```
OPTIONS LS=20 PS=75 NOCENTER NODATE;
DATA ATOMIZE;
TITLE 'SMD AS A FUNCTION OF DIMENSIONLESS ATOMIZATION PARAMETERS';
* X1 = natural log of Reynolds Number;
* X2 = natural log of Weber Number;
* X3 = natural log of Density Ratio (fluid/air);
* X4 = natural log of Viscosity Ratio (fluid/air);
* X5 = natural log of Normalized Axial Distance (Y/orifice dia);
* Y = natural log of Diameter Ratio (SMD/orifice);
INPUT X1-X5 Y;
CARDS;
8.993059363    3.712608198    6.68030279     4.93902072     6.704156324    -1.388718349
9.009974585    3.713045725    6.683277177    4.918565663    6.853688058    -1.4404727
8.996805902    3.680996104    6.683473316    4.915138713    6.983741186    -1.357042198
9.237602311    4.195955828    6.680500349    4.9355817      6.314691557    -1.489085082
9.239146593    4.198072726    6.678703341    4.935433851    6.528265657    -1.591442903
9.237856042    4.193487788    6.67793962     4.934430185    6.704156324    -1.715237121
9.262406931    4.195846362    6.680553863    4.906150105    6.853688058    -1.763939531
9.261303758    4.185618333    6.680333161    4.901450981    6.983741186    -1.913570343
9.231571237    4.194399852    6.678306916    4.94231279     6.528265657    -1.503538069
9.234657357    4.19517605     6.678160014    4.939158221    6.704156324    -1.680171019
8.696743375    3.591175372    6.693672643    5.212120871    6.528265657    -1.138201491
8.701628915    3.591588066    6.694143081    5.206556124    6.704156324    -1.165849184
8.692578999    3.594767624    6.693618568    5.21907287     6.853688058    -1.153179635
8.675690416    3.577702457    6.694741999    5.228518522    6.983741186    -1.350622448
8.344983546    2.917155825    6.676349625    4.885269182    6.635821563    -0.667108204
8.341931988    2.915682765    6.677186669    4.887817797    6.907755279    -0.970470393
8.344978478    2.916111206    6.677384108    4.884412039    7.121329379    -1.151561088
8.337368586    2.91282173     6.679129889    4.891074418    7.297220046    -1.170722258
8.325227704    2.904633063    6.676740691    4.901175865    7.44675178     -1.248770947
8.31308699     2.884314279    6.6782674      4.903163066    7.576804908    -1.300204043
9.355960746    3.764049323    6.653928937    4.5410424      6.528265657    -0.959857719
9.364006553    3.769491171    6.654669072    4.534401328    6.704156324    -1.253236765
9.363376591    3.761035136    6.654444219    4.530071149    6.853688058    -1.133612447
9.329902015    3.746390214    6.656784611    4.561351948    6.983741186    -
1.337303716PROC PRINT;
PROC REG; MODEL Y=X1-X5/SELECTION=RSQUARE ADJRSQ CP SSE MSE BEST=6;
PROC REG; MODEL Y=X1-X5/VIF;
PROC CORR; VAR X1-X5 Y;
```

Statistical comparison of various models for DAA

Number in Model	R-Square	Adjusted R-Square	C(p)	MSE	SSE	Variables in Model
1	0.5360	0.5149	132.7978	0.0390	0.8584	X2
1	0.3096	0.2782	207.3761	0.0581	1.2774	X1
1	0.0260	-0.0183	300.7693	0.0819	1.8021	X3
1	0.0126	-0.0322	305.1555	0.0830	1.8267	X4
1	0.0030	-0.0423	308.3268	0.0838	1.8446	X5
2	0.8348	0.8190	36.4171	0.0146	0.3057	X2 X5
2	0.5973	0.5589	114.6321	0.0355	0.7451	X1 X2
2	0.5756	0.5352	121.7571	0.0374	0.7852	X2 X3
2	0.5562	0.5140	128.1402	0.0391	0.8210	X2 X4
2	0.5175	0.4715	140.9071	0.0425	0.8927	X1 X3
2	0.4660	0.4151	157.8636	0.0471	0.9880	X1 X4
3	0.9007	0.8858	16.7120	0.0092	0.1838	X1 X2 X5
3	0.8761	0.8575	24.7970	0.0115	0.2292	X2 X3 X5
3	0.8676	0.8477	27.6046	0.0123	0.2450	X2 X4 X5
3	0.7628	0.7273	62.1061	0.0219	0.4388	X1 X3 X5
3	0.7335	0.6935	71.7740	0.0247	0.4931	X1 X4 X5
3	0.6660	0.6159	93.9794	0.0309	0.6179	X1 X2 X4
4	0.9320	0.9176	8.4061	0.0066	0.1259	X1 X2 X4 X5
4	0.9109	0.8922	15.3355	0.0087	0.1648	X1 X2 X3 X5
4	0.8888	0.8653	22.6327	0.0108	0.2058	X2 X3 X4 X5
4	0.7673	0.7183	62.6419	0.0227	0.4306	X1 X3 X4 X5
4	0.7424	0.6882	70.8281	0.0251	0.4766	X1 X2 X3 X4
5	0.9453	0.9302	6.0000	0.0056	0.1011	X1 X2 X3 X4 X5

Regression results for the five parameter model for DAA

Source	Degrees of Freedom	Sum of Squares	Mean Square
Model	5	1.74900	0.34980
Error	18	0.10112	0.00562
Corrected Total	23	1.85013	

Root MSE	0.07495
Dependent Mean	-1.32683
Coeff of Varience	-5.64906
R-square	0.9453
Adjusted R-Square	0.9302

Variable	Parameter Estimate
Intercept	-99.02791
X1	1.15548
X2	-1.52721
X3	-16.33095
X4	1.63724
X5	-0.59472

WHITE MINERAL OIL (WMO)

SAS Program

```
OPTIONS LS=20 PS=75 NOCENTER NODATE;
DATA ATOMIZE;
TITLE 'SMD AS A FUNCTION OF DIMENSIONLESS ATOMIZATION PARAMETERS';
* X1 = natural log of Reynolds Number;
* X2 = natural log of Weber Number;
* X3 = natural log of Density Ratio (fluid/air);
* X4 = natural log of Viscosity Ratio (fluid/air);
* X5 = natural log of Normalized Axial Distance (Y/orifice dia);
* Y = natural log of Diameter Ratio (SMD/orifice);
INPUT X1-X5 Y;
CARDS;
7.765815489    3.015488711    6.568238417    5.264076669    7.576804908    -1.059391576
7.805171294    3.031270976    6.567101506    5.228341316    7.44675178     -1.079510187
7.806041599    3.027226636    6.56733883     5.224964811    7.297220046    -1.017032302
7.81788998     3.036645798    6.567763636    5.216671141    7.121329379    -0.857460436
7.837716086    3.040007596    6.565389492    5.196470547    6.907755279    -0.641730084
7.342808672    2.114389543    6.567586119    5.23270978     7.576804908    0.366493253
8.08780799     3.603679741    6.565517484    5.232839899    7.576804908    -1.300204043
8.094623357    3.611858037    6.56541857     5.229741484    7.44675178     -1.433086523
8.091088875    3.609904697    6.565854297    5.232559708    7.297220046    -1.438089034
8.071723996    3.597819969    6.567022004    5.247517318    7.121329379    -1.467194579
8.073760767    3.594024767    6.566537117    5.243137523    6.907755279    -1.407274825
8.09189867     3.592120386    6.565844759    5.221442613    6.635821563    -1.526103924
8.473564231    3.958172505    6.566267374    5.333288593    6.983741186    -1.795133576
8.495271684    3.99356879     6.565781738    5.328840288    6.853688058    -1.717873326
8.531294183    3.998735638    6.564935372    5.290869096    6.704156324    -1.648890231
8.528975776    4.004813111    6.565470428    5.296852551    6.528265657    -1.411450239
8.531245042    4.003088666    6.563294977    5.29383938     6.314691557    -1.27324767
8.549191456    4.009381346    6.564828587    5.2765194      6.042757841    -1.075872802
8.391321871    3.974715588    6.568742081    5.435698392    5.668064392    -0.890122956
8.863213797    4.557660969    6.563732798    5.231143615    6.983741186    -2.139526835
8.854605936    4.505432766    6.562752128    5.211326128    6.853688058    -2.201311866
8.874992581    4.541456875    6.561977808    5.208802037    6.704156324    -2.14042149
8.493275049    3.347950308    6.56449361     4.960092863    6.983741186    -1.153179635
8.505851914    3.368302113    6.564059492    4.957416333    6.853688058    -1.155767607
8.520129079    3.363220538    6.563745004    4.937968129    6.704156324    -1.143967569
8.52260304     3.355398884    6.563495344    4.930612538    6.528265657    -0.978866269
8.504528956    3.342251422    6.563944687    4.943859544    6.314691557    -0.923222597
8.527930462    3.347878115    6.56347994     4.920052465    6.042757841    -0.768438038
8.870564389    4.059649537    6.562976363    4.935581763    6.983741186    -1.681018716
8.887997972    4.05121666     6.56212718     4.910624993    6.853688058    -1.587187303
8.875872978    4.055422405    6.559611709    4.927802478    6.704156324    -1.540181918
8.863752544    4.053692745    6.563126144    4.93999743     6.528265657    -1.518683549
8.8734659      4.059676803    6.563545281    4.932082886    6.314691557    -1.492122823
8.8734659      4.06001114     6.563210945    4.93236136     6.042757841    -1.202395102
8.872500709    4.055528561    6.563161008    4.930891012    5.668064392    -1.09283951
9.099746687    4.578894646    6.556974985    4.972432139    6.983741186    -2.13506553
9.114164499    4.559009537    6.556026845    4.944392733    6.853688058    -2.053055883
9.134579264    4.582304597    6.555340377    4.934377868    6.704156324    -2.002090713
9.137478813    4.574167626    6.553691827    4.92669032     6.528265657    -1.983557364
9.140386439    4.574220099    6.554266556    4.923195829    6.314691557    -1.777078293
9.134464261    4.560845107    6.553204446    4.922571452    6.042757841    -1.749153803
9.140372196    4.571648832    6.554216592    4.921729701    5.668064392    -1.904515687
8.280001163    3.704490982    6.559924627    5.071214387    7.576804908    -1.407274825
8.355222943    3.735882173    6.556623666    5.003220819    7.44675178     -1.420392977
8.396730007    3.750842772    6.556338742    4.963842731    7.297220046    -1.436886147
8.412889767    3.751209569    6.554341073    4.945794864    7.121329379    -1.542669736
8.417807194    3.75116454     6.553803854    4.940190283    6.907755279    -1.526323006
```

```
8.429234109    3.747860066    6.55397925     4.924942844    6.635821563    -1.438691021
8.454996652    3.767906349    6.554391005    4.906528659    6.261128114    -1.420195913
8.425950987    3.751476919    6.554179073    4.930812715    5.65499231     -1.171490248
8.113049456    3.179360328    6.555227487    4.96173056     5.65499231     -0.51161959
8.112307224    3.162498163    6.554928052    4.952879515    6.261128114    -0.751785681
8.143156638    3.193534529    6.554328913    4.935219147    6.635821563    -1.052410505
8.122353575    3.16724417     6.554628528    4.944042391    6.907755279    -1.073919676
8.128558391    3.158420836    6.557646542    4.930948437    7.121329379    -1.167962367
8.17158958     3.19046626     6.557269288    4.899624409    7.297220046    -1.208267729
8.141747848    3.17715601     6.557496694    4.926543157    7.44675178     -1.173489788
8.151295221    3.160009481    6.557469261    4.905471372    7.576804908    -1.079510187
7.772374567    2.420082948    6.555077806    4.916492571    7.576804908    -0.430636407
7.784791756    2.439014912    6.558390875    4.912229593    7.44675178     -0.333476728
7.778027405    2.450582639    6.55922619     4.926613381    7.297220046    -0.2979569
7.788371513    2.454994966    6.559932814    4.916973117    7.121329379    -0.283247475
7.781423017    2.465893926    6.5611027      4.931093523    6.907755279    -0.485049587
7.784944702    2.461534605    6.559511808    4.924866008    6.635821563    -0.477805413
7.772831115    2.455490389    6.559525849    4.935429703    6.261128114    -0.37431257
9.347918027    4.360625623    6.562721028    4.958531005    6.290594005    -1.718753608
9.437661631    4.421069531    6.559703381    4.890089926    6.160540877    -1.666983398
8.863575616    3.396225944    6.548936568    4.55780026     6.983741186    -1.099928945
8.867659852    3.397385712    6.548784748    4.553675297    6.853688058    -1.023700129
8.86520671     3.387476165    6.549018194    4.550648296    6.704156324    -0.925411144
8.859989455    3.377376326    6.548683522    4.550927003    6.528265657    -0.870386935
8.862698622    3.37812917     6.548582285    4.548180053    6.314691557    -0.768438038
8.856066794    3.367197872    6.548632905    4.54955336     6.042757841    -0.705752612
8.850618632    3.365638731    6.548835357    4.555049948    5.668064392    -0.45786705
9.241028184    4.153803649    6.548652385    4.559454706    6.983741186    -1.582693491
9.219244951    4.152446338    6.544762878    4.585422384    6.853688058    -1.522294965
9.233268005    4.166396883    6.546862201    4.576562922    6.704156324    -1.517602663
9.217880497    4.151732092    6.545149797    4.586523918    6.528265657    -1.448841883
9.228153503    4.161534382    6.546291862    4.579881585    6.314691557    -1.190035296
9.225748062    4.156723501    6.546291862    4.579881585    6.042757841    -1.007065161
9.229173954    4.166595897    6.545670497    4.581821184    5.668064392    -0.831925396
9.508450312    4.698676724    6.548184861    4.565518524    6.983741186    -2.088960387
9.462997097    4.634242182    6.545670497    4.581821184    6.853688058    -1.879383474
PROC PRINT;
PROC REG; MODEL Y=X1-X5/SELECTION=RSQUARE ADJRSQ CP SSE MSE BEST=6;
PROC REG; MODEL Y=X1-X5/VIF;
PROC CORR; VAR X1-X5 Y;
```

Statistical comparison of various models for WMO

Number in Model	R-Square	Adjusted R-Square	C(p)	MSE	SSE	Variables in Model
1	0.7696	0.7668	102.5620	0.0607	4.9137	X2
1	0.3941	0.3866	398.5786	0.1596	12.9249	X1
1	0.0117	-0.0005	699.9331	0.2603	21.0806	X4
1	0.0015	-0.0108	707.9543	0.2629	21.2977	X3
1	0.0001	-0.0123	709.1068	0.2633	21.3289	X5
2	0.8858	0.8830	12.9823	0.0304	2.4352	X2 X5
2	0.8222	0.8177	63.1698	0.0474	3.7935	X1 X2
2	0.8024	0.7975	78.7058	0.0527	4.2139	X2 X4
2	0.7950	0.7898	84.6000	0.0547	4.3734	X2 X3
2	0.6773	0.6693	177.3276	0.0860	6.8830	X1 X4
2	0.5270	0.5152	295.7849	0.1261	10.0888	X1 X3
3	0.8994	0.8956	4.2609	0.0272	2.1451	X1 X2 X5
3	0.8963	0.8924	6.7303	0.0280	2.2119	X2 X4 X5
3	0.8951	0.8911	7.6551	0.0283	2.2369	X2 X3 X5
3	0.8257	0.8191	62.3677	0.0471	3.7176	X1 X2 X4
3	0.8222	0.8154	65.1615	0.0480	3.7933	X1 X2 X3
3	0.8025	0.7950	80.6489	0.0533	4.2124	X2 X3 X4
4	0.8999	0.8948	5.8970	0.0274	2.1352	X1 X2 X3 X5
4	0.8995	0.8943	6.2313	0.0275	2.1443	X1 X2 X4 X5
4	0.8964	0.8911	8.6395	0.0283	2.2094	X2 X3 X4 X5
4	0.8347	0.8262	57.2830	0.0452	3.5259	X1 X2 X3 X4
4	0.8241	0.8150	65.6638	0.0481	3.7527	X1 X3 X4 X5
5	0.9023	0.8960	6.0000	0.0271	2.0839	X1 X2 X3 X4 X5

Regression results for the five parameter model for WMO

Source	Degrees of Freedom	Sum of Squares	Mean Square
Model	5	19.24663	3.84933
Error	77	2.08388	0.02706
Corrected Total	82	21.33051	

Root MSE	0.16451
Dependent Mean	-1.24540
Coeff of Varience	-13.20937
R-square	0.9023
Adjusted R-Square	0.8960

Variable	Parameter Estimate
Intercept	73.55166
X1	0.43730
X2	-1.11480
X3	-11.42905
X4	0.50064
X5	-0.29306

BIPHENYL/DIPHENYL OXIDE (BDO)

SAS Program

```
OPTIONS LS=20 PS=75 NOCENTER NODATE;
DATA ATOMIZE;
TITLE 'SMD AS A FUNCTION OF DIMENSIONLESS ATOMIZATION PARAMETERS';
* X1 = natural log of Reynolds Number;
* X2 = natural log of Weber Number;
* X3 = natural log of Density Ratio (fluid/air);
* X4 = natural log of Viscosity Ratio (fluid/air);
* X5 = natural log of Normalized Axial Distance (Y/orifice dia);
* Y = natural log of Diameter Ratio (SMD/orifice);
INPUT X1-X5 Y;
CARDS;
9.167296067    3.609160129    6.766267162    4.748183309    6.983741186    -1.206519905
9.182002726    3.602541158    6.766579677    4.726943859    6.853688058    -1.20055759
9.170875287    3.605628312    6.765945022    4.741985465    6.704156324    -1.168046987
9.169357237    3.605943575    6.765344947    4.744099289    6.528265657    -1.013352445
9.16583977     3.595557277    6.765945022    4.741985465    6.314691557    -0.948650822
9.16583977     3.596237896    6.765264403    4.742550676    6.042757841    -0.705752612
9.171395664    3.59861336     6.768501768    4.736632276    6.983741186    -1.218730285
8.424003755    2.779849765    6.768537964    4.785278501    7.576804908    -1.229372016
8.434538154    2.793491638    6.767616446    4.781153407    7.44675178     -1.267200016
8.46008376     2.80455169     6.766069559    4.758062259    7.297220046    -1.216109651
8.458386927    2.803840921    6.766150039    4.759616533    7.121329379    -1.138839222
8.464177047    2.802699928    6.765066491    4.752416365    6.635821563    -0.763365292
8.466555224    2.798748399    6.765506018    4.747198211    6.261128114    -0.395868447
8.469935471    2.800844848    6.764663864    4.74466482     6.907755279    -0.961836166
8.474999274    2.801942409    6.765443661    4.739172497    7.576804908    -1.231654005
9.430515237    4.134918313    6.766947319    4.747618417    6.983741186    -1.76994648
9.449882852    4.156319102    6.765022729    4.737908223    6.853688058    -1.865519324
9.460262166    4.165400654    6.765721163    4.730878481    6.704156324    -1.828805706
9.461846514    4.163588583    6.765219827    4.728073324    6.528265657    -1.61286483
9.46197898     4.158197313    6.765398737    4.724705444    6.528265657    -1.640711342
9.461695281    4.167926863    6.766061183    4.730596075    6.314691557    -1.607334862
9.464788592    4.166133945    6.765819374    4.725965454    6.314691557    -1.577837251
9.460262166    4.166081042    6.765040775    4.731443533    6.042757841    -1.189775815
9.460336018    4.162887302    6.765640566    4.729334378    5.668064392    -0.927005829
9.123442904    3.006589305    6.75866421     4.444911701    6.983741186    -0.705752612
9.127675408    3.008068623    6.758081318    4.440865306    6.853688058    -0.599033889
9.129667674    3.016596686    6.75858238     4.443468853    6.704156324    -0.493433881
9.126265115    3.007687926    6.758163162    4.442307111    6.528265657    -0.419030386
9.526989784    3.723446642    6.758745428    4.390774706    6.983741186    -1.428542811
9.506482486    3.714090405    6.759475389    4.40961599     6.853688058    -1.270806355
9.505475628    3.709324186    6.759729765    4.407905214    6.704156324    -1.246532419
9.504804856    3.701077346    6.759147411    4.403895495    6.528265657    -1.076335943
9.503415196    3.700374424    6.759565776    4.405044966    6.314691557    -0.928070366
9.500262487    3.704067673    6.759557366    4.411047407    6.042757841    -0.734024001
9.496779065    3.694347202    6.759811749    4.409336113    5.668064392    -0.682780053
10.2229974     4.375533335    6.758529223    4.362684194    6.290594005    -2.253293801
10.18907698    4.322669308    6.758350351    4.371740802    6.160540877    -2.066785131
10.2027071     4.362217173    6.758424913    4.379115783    6.011009143    -2.053979007
8.748861041    2.860358639    6.761431752    4.450171886    7.576804908    -1.308980648
8.832714327    3.032964299    6.761595325    4.453064372    7.44675178     -1.261635547
8.791686541    2.917047109    6.760113164    4.433140864    7.297220046    -1.118960779
8.790136614    2.899695614    6.759285102    4.424793573    7.121329379    -0.95056181
8.797749051    2.902457937    6.759212149    4.417338241    6.907755279    -1.150507268
8.780124707    2.886960878    6.759530813    4.429104935    6.907755279    -1.119544125
8.77944835     2.895679594    6.75952152     4.435140887    6.907755279    -1.11068487
8.796228029    2.902512316    6.758620579    4.41933255     6.635821563    -0.508130845
9.759592321    4.226492311    6.758292762    4.413599633    6.983741186    -1.953783165
```

```
9.74831387     4.218806414    6.75844752     4.422482388    6.853688058    -1.84216673
9.758357508    4.236873828    6.760467382    4.420801951    6.704156324    -1.790865132
9.730395299    4.149173989    6.759738008    4.401906987    6.528265657    -1.694823817
9.731951051    4.153294575    6.758728926    4.402746618    6.314691557    -1.591442903
9.728834699    4.147398459    6.758392339    4.403026652    6.042757841    -1.497167117
9.769512043    4.239079953    6.75804683     4.409305382    5.668064392    -1.177399206
9.048191462    3.476859496    6.761330853    4.460864892    7.576804908    -1.613971985
9.061814677    3.48449136     6.760676668    4.449286573    7.44675178     -1.649020596
9.058798537    3.483692706    6.760503441    4.452458204    7.297220046    -1.699831626
9.070840976    3.488217599    6.759848934    4.440904979    7.121329379    -1.716917073
9.070809407    3.48638854     6.759093123    4.440023791    6.907755279    -1.657728202
9.067767343    3.483418724    6.758500544    4.442026527    6.635821563    -1.458557881
9.06930643     3.485822475    6.759174966    4.441465596    6.261128114    -1.361276598
9.722750243    3.760873187    6.743332285    4.179647823    6.983741186    -1.600530335
9.741341125    3.759728378    6.740147544    4.156879779    6.853688058    -1.371665051
9.74200643     3.774553954    6.742754713    4.16457726     6.704156324    -1.318438978
9.739740024    3.766593402    6.741576505    4.162735995    6.528265657    -1.27833722
9.741048937    3.766655686    6.741830674    4.161114751    6.314691557    -1.048019239
9.741048937    3.767330564    6.741155796    4.161675997    6.042757841    -0.945258919
9.746408364    3.764763017    6.740656377    4.153642244    5.668064392    -0.739742387
9.041179631    3.01755422     6.746769945    4.195241974    7.576804908    -1.320684985
9.052439882    3.022471916    6.745769017    4.184708764    7.44675178     -1.165515508
9.052439882    3.022471916    6.745769017    4.184708764    7.297220046    -1.052410505
9.078400682    3.045389496    6.744688336    4.16720413     7.121329379    -1.071970358
9.078620833    3.0423939      6.743511872    4.165358764    6.907755279    -0.629501915
9.066642959    3.024771951    6.744098219    4.169107858    6.635821563    -0.606183424
PROC PRINT;
PROC REG; MODEL Y=X1-X5/SELECTION=RSQUARE ADJRSQ CP SSE MSE BEST=6;
PROC REG; MODEL Y=X1-X5/VIF;
PROC CORR; VAR X1-X5 Y;
```

Statistical comparison of various models for BDO

Number in Model	R-Square	Adjusted R-Square	C(p)	MSE	SSE	Variables in Model
1	0.3842	0.3755	121.2246	0.1107	7.8626	X2
1	0.2152	0.2042	173.4123	0.1411	10.0196	X1
1	0.0205	0.0067	233.5705	0.1761	12.5062	X3
1	0.0202	0.0064	233.6619	0.1762	12.5099	X5
1	0.0020	-0.0120	239.2667	0.1795	12.7416	X4
2	0.7585	0.7516	7.6084	0.0441	3.0838	X2 X5
2	0.4736	0.4585	95.6023	0.0960	6.7209	X1 X5
2	0.4192	0.4026	112.4003	0.1059	7.4152	X1 X2
2	0.4002	0.3831	118.2678	0.1094	7.6577	X2 X3
2	0.3865	0.3690	122.4929	0.1119	7.8323	X2 X4
2	0.3179	0.2984	143.6940	0.1244	8.7086	X1 X3
3	0.7641	0.7538	7.8766	0.0437	3.0122	X2 X3 X5
3	0.7637	0.7534	7.9941	0.0437	3.0171	X1 X2 X5
3	0.7594	0.7489	9.3279	0.0445	3.0722	X2 X4 X5
3	0.6539	0.6388	41.9127	0.0640	4.4190	X1 X3 X5
3	0.6391	0.6234	46.4708	0.0668	4.6074	X1 X4 X5
3	0.4657	0.4424	100.0510	0.0989	6.8221	X1 X2 X4
4	0.7740	0.7607	6.8157	0.0424	2.8857	X2 X3 X4 X5
4	0.7679	0.7543	8.6894	0.0436	2.9631	X1 X2 X4 X5
4	0.7645	0.7507	9.7375	0.0442	3.0065	X1 X2 X3 X5
4	0.6565	0.6363	43.0931	0.0645	4.3852	X1 X3 X4 X5
4	0.5066	0.4775	89.4179	0.0927	6.2999	X1 X2 X3 X4
5	0.7831	0.7669	6.0000	0.0413	2.7693	X1 X2 X3 X4 X5

Regression results for the five parameter model for BDO

Source	Degrees of Freedom	Sum of Squares	Mean Square
Model	5	9.99796	1.99959
Error	67	2.76931	0.04133
Corrected Total	72	12.76727	

Root MSE	0.20331
Dependent Mean	-1.24694
Coeff of Varience	-16.30440
R-square	0.7831
Adjusted R-Square	0.7669

Variable	Parameter Estimate
Intercept	113.14446
X1	0.39943
X2	-1.12159
X3	-16.88784
X4	0.87107
X5	-0.57866

VITA

Name ***KIRAN KRISHNA***

Permanent Address "*Ashraya*", 411, 2nd Block, 9th Cross, R.T. Nagar, Bangalore – 560032, INDIA.

Education

Texas A&M University, College Station, Texas, U.S.A.
Doctor of Philosophy, Chemical Engineering (Dec 2003)
Master of Science, Chemical Engineering (May 2001)

R.V. College of Engineering, Bangalore University, Bangalore, India
Bachelor of Engineering, Chemical Engineering (Sep 1998)

Certification Engineer-in-training (EIT) *Texas Board of Professional Engineers*

Professional Affiliations
- American Institute of Chemical Engineers (AIChE)
- Institute of Chemical Engineers (IChemE)
- American Chemical Society (ACS)
- International Union of Pure and Applied Chemistry (IUPAC)

Academic Honors
- Omega Chi Epsilon: National Honor Society for Chemical Engineering
- Phi Lambda Upsilon: National Chemical Honor Society
- Sigma Xi: National Scientific Research Honor Society

Publications
- Sukmarg, P., Krishna, K., Kihm, K.D., Rogers, W.J., & Mannan, M.S., *Journal of Loss Prevention in the Process Industries*, 15(1), 19-27 (2002).
- Krishna, K., Kim, T.K., Kihm, K.D., Rogers, W.J., & Mannan, M.S., *Journal of Loss Prevention in the Process Industries*, 16(1), 1-8 (2003).
- Krishna K., Wang, Y., Saraf, S.R., Rogers, W.J., Baldwin, J.T., Gupta, J.P., & Mannan, M.S., *Reliability Engineering & System Safety*, 81(2), 215-224 (2003).
- Krishna, K., Rogers, W.J., & Mannan, M.S., *Journal of Hazardous Materials*, in press (2003).